Computer simulation on nano-materials:
electronic and mechanical properties

Department of Mechanical and Electro-Mechanical Engineering, National Sun Yat-sen University

Dr. Shin-Pon Ju

Email: jushin-pon@mail.nsysu.edu.tw

http://www2.nsysu.edu.tw/mel/

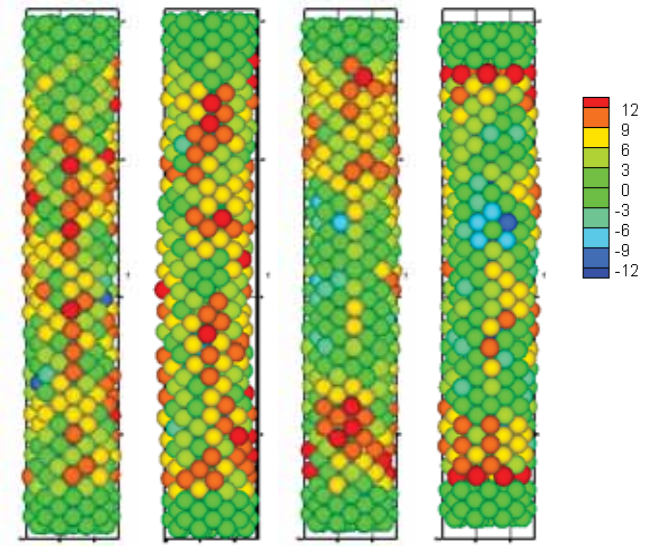

(a) 0.003% ps^{-1} (b) 0.833% ps^{-1} (c) 6.666% ps^{-1} (d) 16.666% ps^{-1}

The Scale of Things -- Nanometers and More

Things Natural

Dust mite
200 mm

Ant
~ 5 mm

Human hair
~ 10-50 mm wide

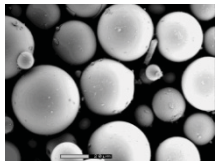

Fly ash
~ 10-20 mm

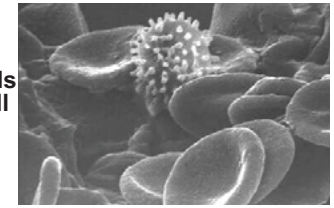

Red blood cells with white cell
~ 2-5 mm

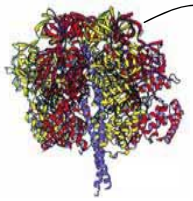

~10 nm diameter

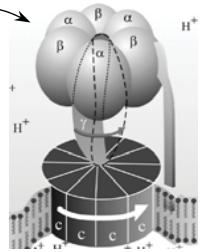

ATP synthase

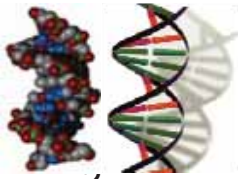

DNA
~2-1/2 nm diameter

Atoms of silicon
spacing ~tenths of nm

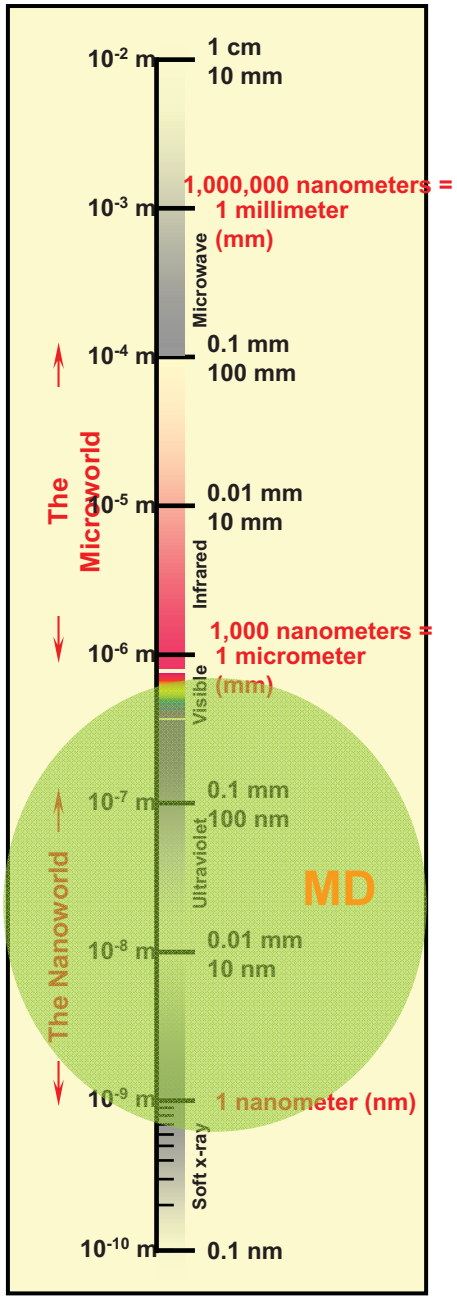

Things Manmade

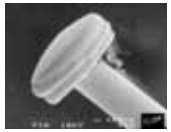

Head of a pin
1-2 mm

MicroElectroMechanical devices
10 -100 mm wide

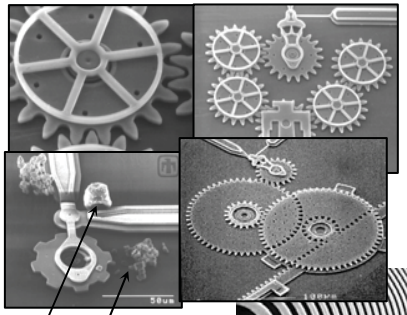

Red blood cells
Pollen grain

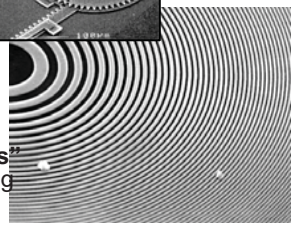

Zone plate x-ray "lens"
Outermost ring spacing ~35 nm

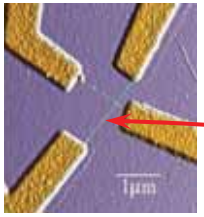

Nanotube electrode

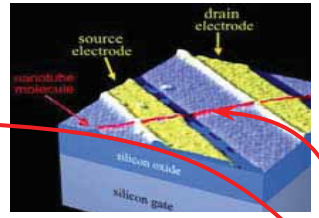

Nanotube transistor

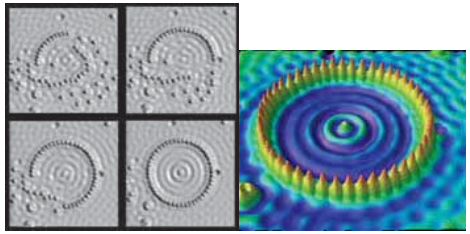

Quantum corral of 48 iron atoms on copper surface
positioned one at a time with an STM tip

21st Century Challenge

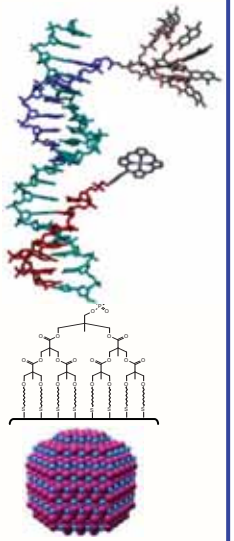

Combine nanoscale building blocks to make novel functional devices, e.g., a photosynthetic reaction center with integral semiconductor storage

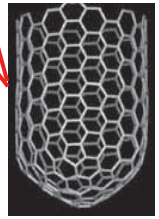

Carbon nanotube
~2 nm diameter

Office of Basic Energy Science
Office of Science, U.S. DOE
Version 03-05-02

Force and Energy at different scales

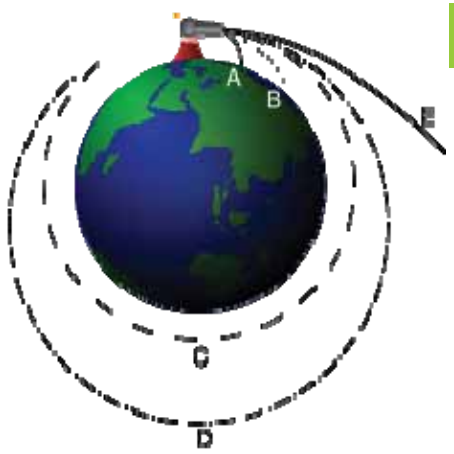

Gravitational interaction between earth and a object

$$ma = m\frac{dv}{dt} = -\frac{GMm}{r^2}$$

$$\frac{1}{2}mv_e^2 + \frac{-GMm}{r} = 0 + 0$$

$$v_e = \sqrt{\frac{2GM}{r}}$$

Inter-atomic interaction between atoms or molecules

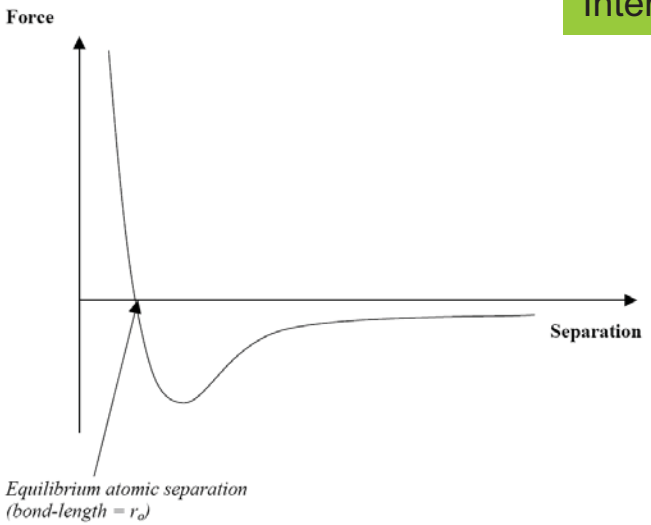

Ionic bond, Covalent bond, Metallic bond, Van-der-Waals bond.

$$F_i = -\sum_{\substack{i \neq j \\ i=1}}^{N} \nabla_i \Phi(\boldsymbol{r}_{ij})$$

$\Phi(\boldsymbol{r}_{ij})$: interatomic potential

Within an atom or a molecule

The **ionization potential**, **ionization energy** or **EI** of an atom or molecule is the energy required to remove an electron from the isolated atom or ion.

$$X \rightarrow X^{+} + e$$

The **electron affinity**, *E*ea, of an atom or molecule is the energy required to detach an electron from a singly charged negative ion

$$X^{-} \rightarrow X + e$$

Schrödinger's Equation:

$$j\hbar \frac{\partial \Psi}{\partial t} = - \frac{\hbar^2}{2m} \frac{\partial^2 \Psi}{\partial x^2} + U \Psi .$$

$$\langle G(x) \rangle = \int_{-\infty}^{\infty} \Psi^{*} G(x) \Psi \, dx .$$

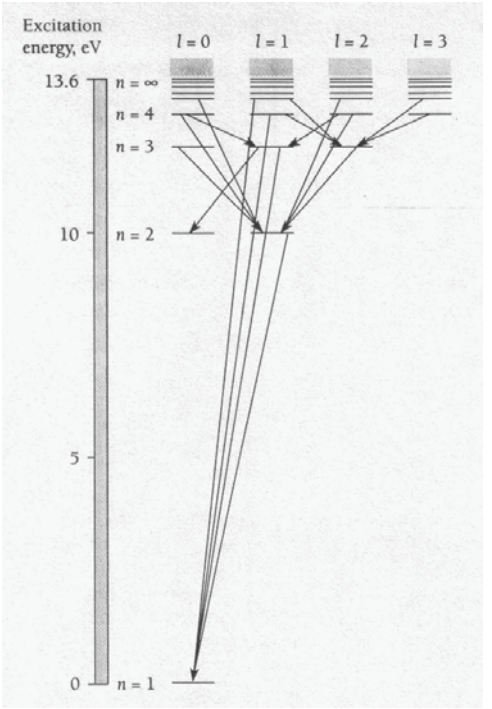

Table 6.1 Normalized Wave Functions of the Hydrogen Atom for $n = 1$, 2, and 3*

n	l	m_l	$\Phi(\phi)$	$\Theta(\theta)$	$R(r)$	$\psi(r, \theta, \phi)$
1	0	0	$\frac{1}{\sqrt{2\pi}}$	$\frac{1}{\sqrt{2}}$	$\frac{2}{a_0^{3/2}} e^{-r/a_0}$	$\frac{1}{\sqrt{\pi}\, a_0^{3/2}} e^{-r/a_0}$
2	0	0	$\frac{1}{\sqrt{2\pi}}$	$\frac{1}{\sqrt{2}}$	$\frac{1}{2\sqrt{2}\, a_0^{3/2}} \left(2 - \frac{r}{a_0}\right) e^{-r/2a_0}$	$\frac{1}{4\sqrt{2\pi}\, a_0^{3/2}} \left(2 - \frac{r}{a_0}\right) e^{-r/2a_0}$
2	1	0	$\frac{1}{\sqrt{2\pi}}$	$\frac{\sqrt{6}}{2} \cos\theta$	$\frac{1}{2\sqrt{6}\, a_0^{3/2}} \frac{r}{a_0} e^{-r/2a_0}$	$\frac{1}{4\sqrt{2\pi}\, a_0^{3/2}} \frac{r}{a_0} e^{-r/2a_0} \cos\theta$
2	1	± 1	$\frac{1}{\sqrt{2\pi}} e^{\pm i\phi}$	$\frac{\sqrt{3}}{2} \sin\theta$	$\frac{1}{2\sqrt{6}\, a_0^{3/2}} \frac{r}{a_0} e^{-r/2a_0}$	$\frac{1}{8\sqrt{\pi}\, a_0^{3/2}} \frac{r}{a_0} e^{-r/2a_0} \sin\theta\, e^{\pm i\phi}$
3	0	0	$\frac{1}{\sqrt{2\pi}}$	$\frac{1}{\sqrt{2}}$	$\frac{2}{81\sqrt{3}\, a_0^{3/2}} \left(27 - 18\frac{r}{a_0} + 2\frac{r^2}{a_0^2}\right) e^{-r/3a_0}$	$\frac{1}{81\sqrt{3\pi}\, a_0^{3/2}} \left(27 - 18\frac{r}{a_0} + 2\frac{r^2}{a_0^2}\right) e^{-r/3a_0}$
3	1	0	$\frac{1}{\sqrt{2\pi}}$	$\frac{\sqrt{6}}{2} \cos\theta$	$\frac{4}{81\sqrt{6}\, a_0^{3/2}} \left(6 - \frac{r}{a_0}\right) \frac{r}{a_0} e^{-r/3a_0}$	$\frac{\sqrt{2}}{81\sqrt{\pi}\, a_0^{3/2}} \left(6 - \frac{r}{a_0}\right) \frac{r}{a_0} e^{-r/3a_0} \cos\theta$
3	1	± 1	$\frac{1}{\sqrt{2\pi}} e^{\pm i\phi}$	$\frac{\sqrt{3}}{2} \sin\theta$	$\frac{4}{81\sqrt{6}\, a_0^{3/2}} \left(6 - \frac{r}{a_0}\right) \frac{r}{a_0} e^{-r/3a_0}$	$\frac{1}{81\sqrt{\pi}\, a_0^{3/2}} \left(6 - \frac{r}{a_0}\right) \frac{r}{a_0} e^{-r/3a_0} \sin\theta\, e^{\pm i\phi}$
3	2	0	$\frac{1}{\sqrt{2\pi}}$	$\frac{\sqrt{10}}{4} (3\cos^2\theta - 1)$	$\frac{4}{81\sqrt{30}\, a_0^{3/2}} \frac{r^2}{a_0^2} e^{-r/3a_0}$	$\frac{1}{81\sqrt{6\pi}\, a_0^{3/2}} \frac{r^2}{a_0^2} e^{-r/3a_0} (3\cos^2\theta - 1)$
3	2	± 1	$\frac{1}{\sqrt{2\pi}} e^{\pm i\phi}$	$\frac{\sqrt{15}}{2} \sin\theta \cos\theta$	$\frac{4}{81\sqrt{30}\, a_0^{3/2}} \frac{r^2}{a_0^2} e^{-r/3a_0}$	$\frac{1}{81\sqrt{\pi}\, a_0^{3/2}} \frac{r^2}{a_0^2} e^{-r/3a_0} \sin\theta \cos\theta\, e^{\pm i\phi}$
3	2	± 2	$\frac{1}{\sqrt{2\pi}} e^{\pm 2i\phi}$	$\frac{\sqrt{15}}{4} \sin^2\theta$	$\frac{4}{81\sqrt{30}\, a_0^{3/2}} \frac{r^2}{a_0^2} e^{-r/3a_0}$	$\frac{1}{162\sqrt{\pi}\, a_0^{3/2}} \frac{r^2}{a_0^2} e^{-r/3a_0} \sin^2\theta\, e^{\pm 2i\phi}$

Iso-surface of electron distribution (the square of wave function)

Atomic Orbital (AO)

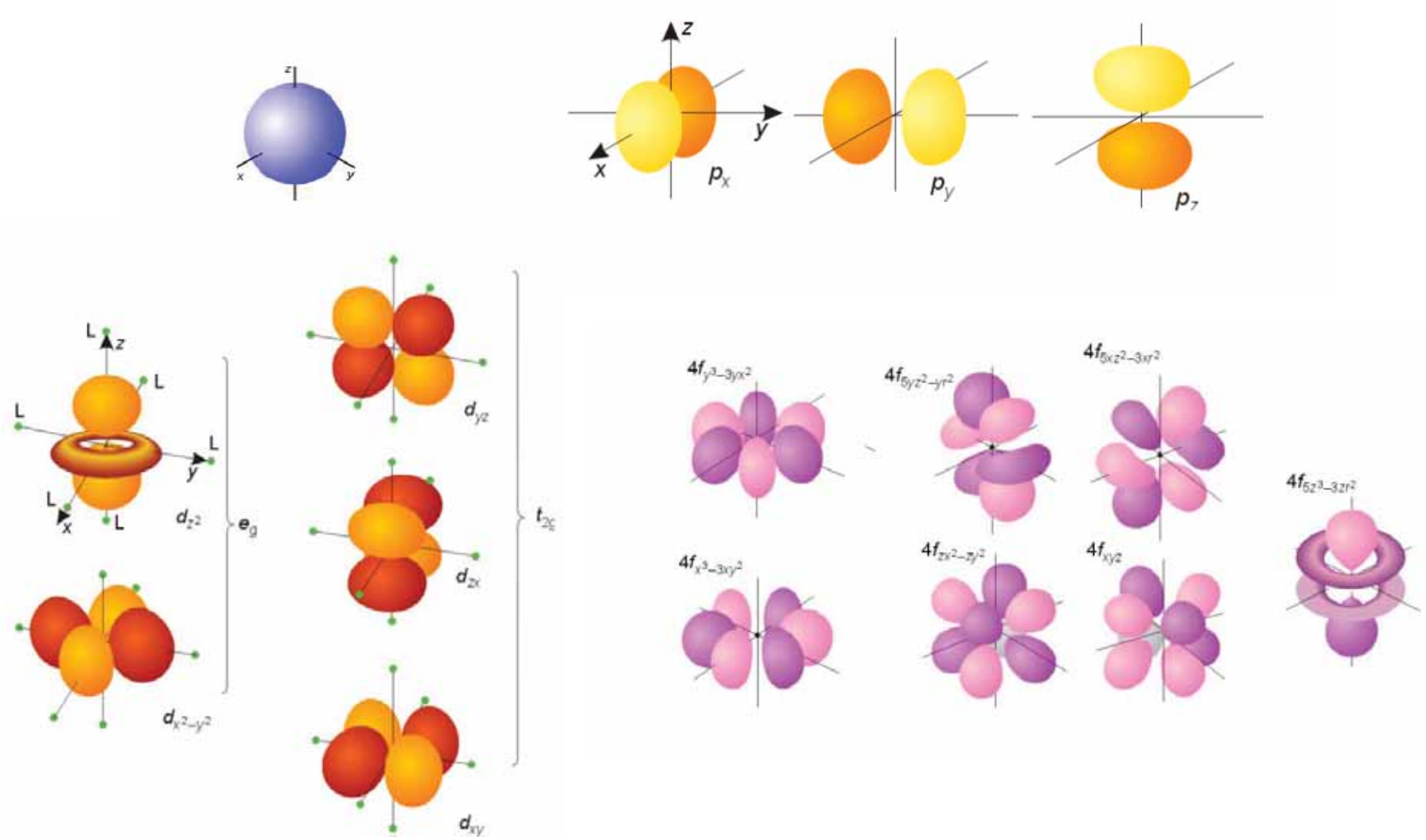

Molecular Orbital (MO) of a H_2 molecule

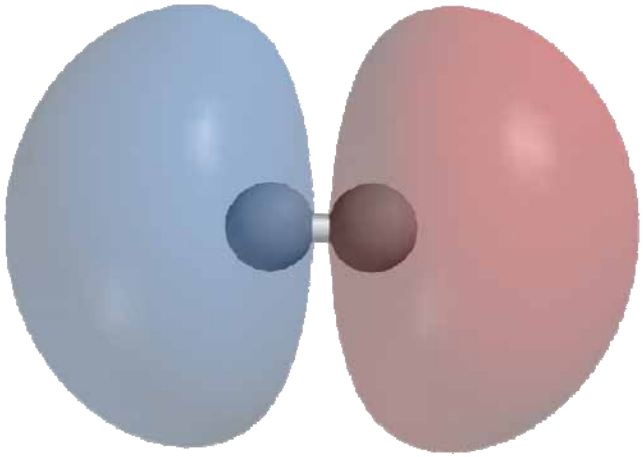

Hellmann–Feynman theorem

$$\frac{\partial E}{\partial \lambda} = \frac{\partial}{\partial \lambda}\langle\psi|\hat{H}|\psi\rangle$$

$$= \langle\frac{\partial \psi}{\partial \lambda}|\hat{H}|\psi\rangle + \langle\psi|\frac{\partial \hat{H}}{\partial \lambda}|\psi\rangle + \langle\psi|\hat{H}|\frac{\partial \psi}{\partial \lambda}\rangle$$

$$= E\langle\frac{\partial \psi}{\partial \lambda}|\psi\rangle + \langle\psi|\frac{\partial \hat{H}}{\partial \lambda}|\psi\rangle + E\langle\psi|\frac{\partial \psi}{\partial \lambda}\rangle$$

$$= E\frac{\partial}{\partial \lambda}\langle\psi|\psi\rangle + \langle\psi|\frac{\partial \hat{H}}{\partial \lambda}|\psi\rangle$$

$$= \langle\psi|\frac{\partial \hat{H}}{\partial \lambda}|\psi\rangle.$$

λ = R (Inter-atomic distance)

Hellmann–Feynman Force

Length and Time Scales in Numerical Modeling

(Dynamics simulation)

1. Force and velocity are required to get time evolution of the system
2. A stable integrator the integrate the equation of motion.

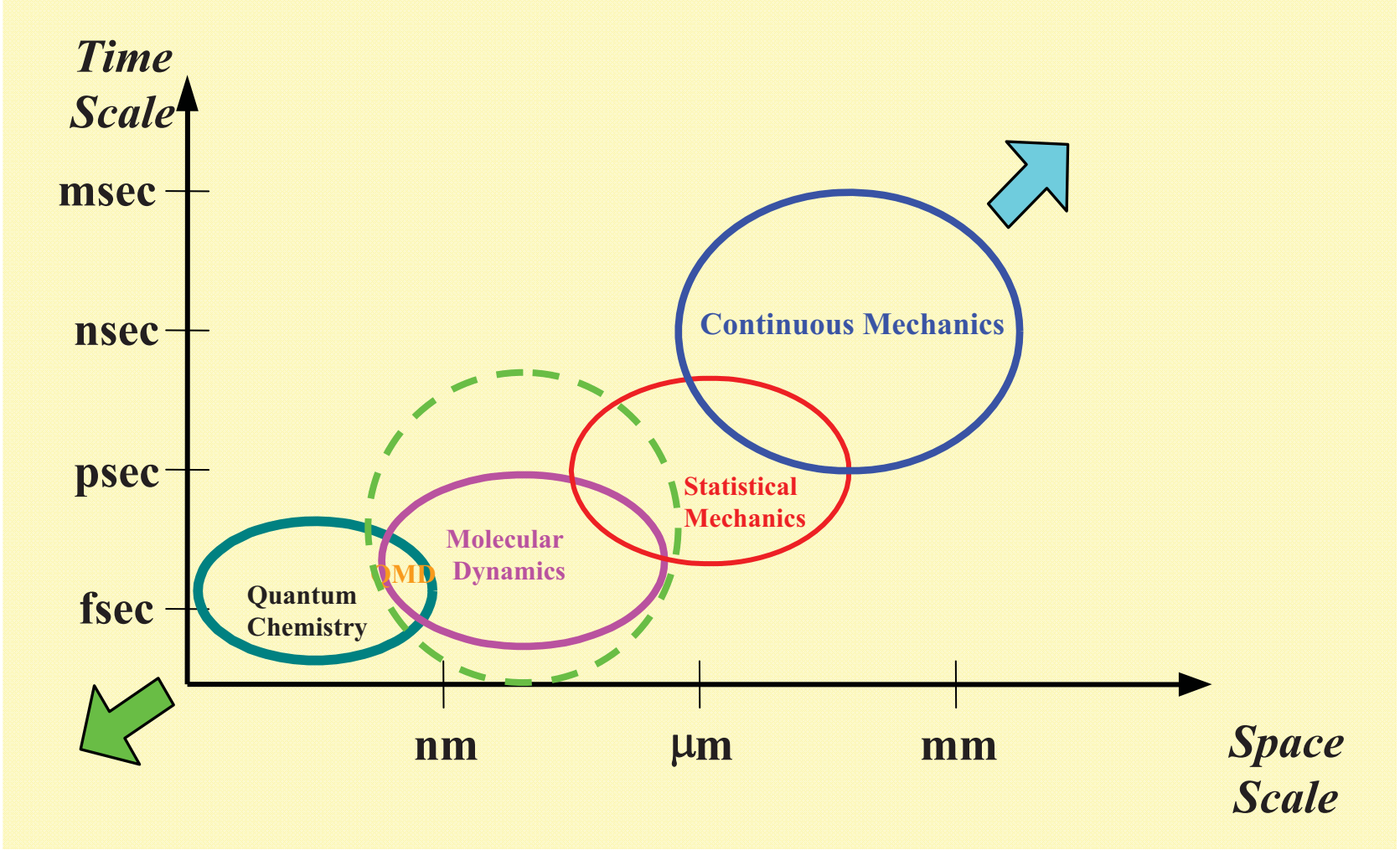

Interatomic potential

Pairwise Potential

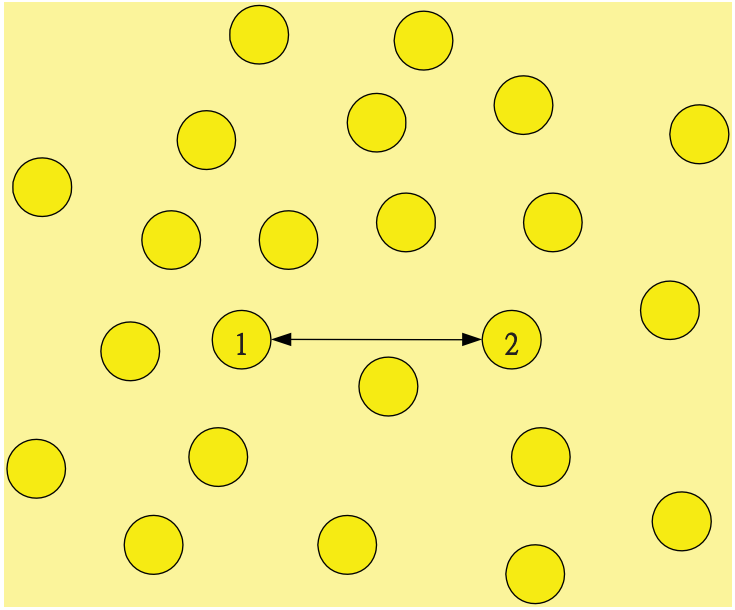

Many body potential

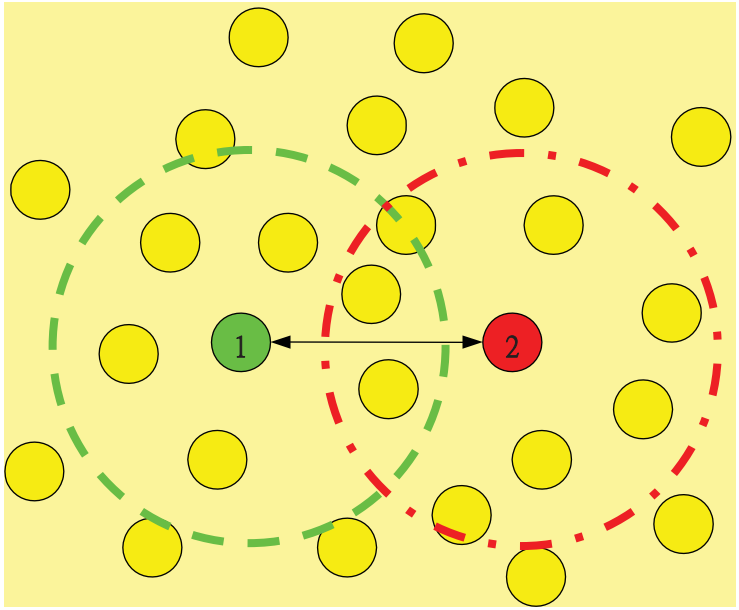

•Lennard-Jones potential

$$U\left(r_{ij}\right) = 4\varepsilon\left[\left(\frac{\sigma}{r_{ij}}\right)^{12} - \left(\frac{\sigma}{r_{ij}}\right)^{6}\right]$$

Usually used for describing Van der Waals interaction in force-matching method

•Morse potential

$$\phi\left(r_{ij}\right) = D\left\{\exp\left\{-2\alpha(r_{ij} - r_o\right\} - 2 * \exp\left\{-\alpha(r_{ij} - r_o\right\}\right\}$$

Usually used for describing a chemical bond in force-matching method

Potential models for ionic oxides

(J. Phys. C: Solid State Phys.. **18** (1985) 1149-1161.)

$$V_{ij}(r_{ij}) = A_{ij}\exp(-r_{ij}/\rho) - C_{ij}r_{ij}^{-6}.$$

Table 1. Potential parameters derived using method (*a*).†

Cation	Charge	A(eV)	ρ(Å)
Ca	2	1227.7	0.3372
Sc	2	838.6	0.3372
Ti	2	633.3	0.3372
V	2	557.8	0.3372
Cr	2	619.8	0.3372
Mn	2	832.7	0.3372
Fe	2	725.7	0.3372
Co	2	684.9	0.3372
Ni	2	641.2	0.3372
Zn	2	700.3	0.3372
Zr	4	1453.8	0.3500
Cd	2	868.3	0.3500
Hf	4	1454.6	0.3500
Ce	4	1017.4	0.3949
Eu	2	665.2	0.3949
Tb	4	905.3	0.3949
Th	4	1144.6	0.3949
U	4	1055.0	0.3949

Empirical force field for macromolecules

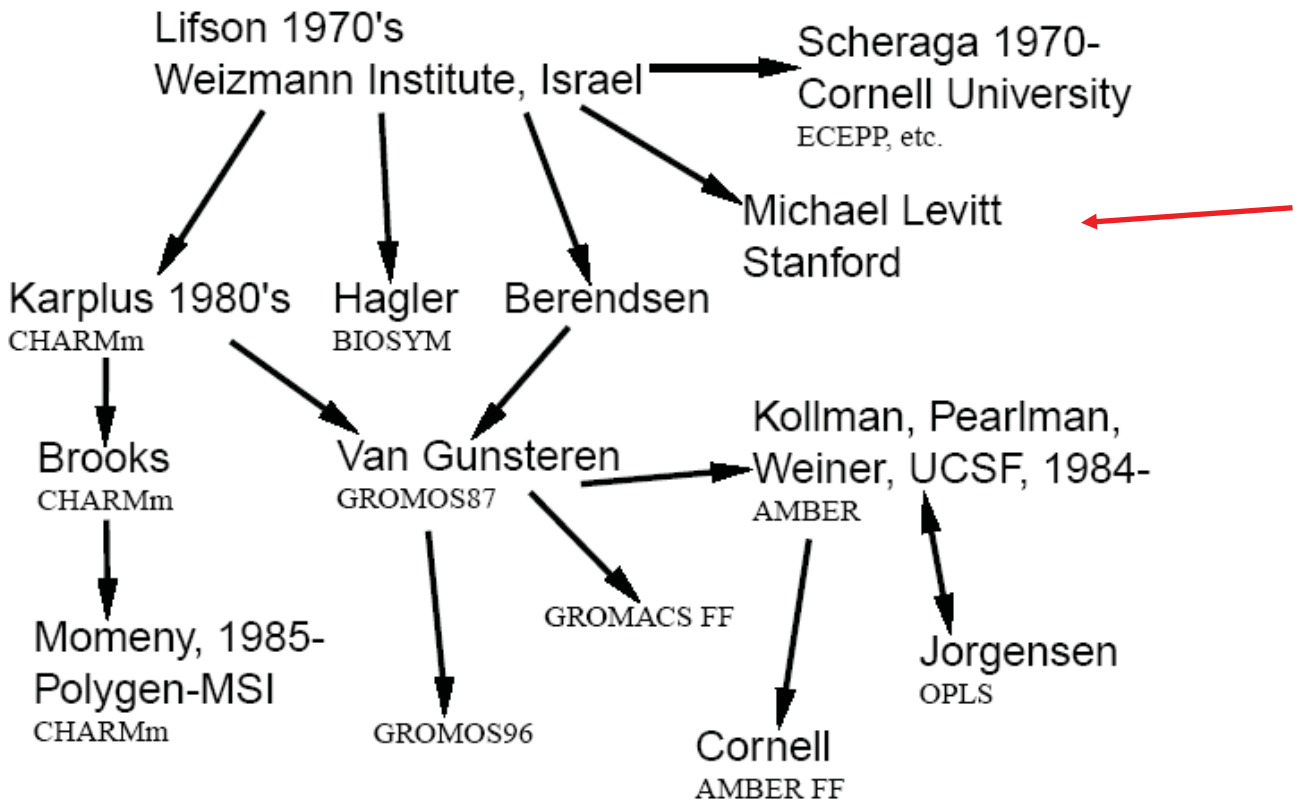

Free software Tinker uses this force field

Potentials used in the MD simulation for marcomolecules

(Energy Calculation and Dynamics, ENCAD)

$$U_{total} = U_{bond} + U_{bending} + U_{dihedral} + U_{vdw} + U_{coul}$$

(a) bond strength

$$V_{\text{bond length}} = \sum_{N=1}^{N_b} 1/2\ k_b^i\ (b_i - b_0^i)^2$$

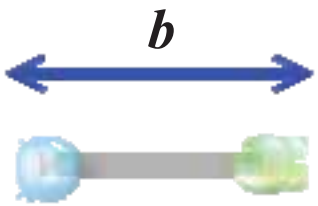

(b) bond bending

$$V_{bending} = \sum_{N=1}^{N_\theta} k_\theta^i\ (\theta_i - \theta_0^i)^2$$

(c) bond torsion

$$V_{dihedral} = \sum_{n=1}^{N_\varphi} K_\varphi^i \{1-\cos[n^i(\varphi_i - \varphi_0^i)]\}$$

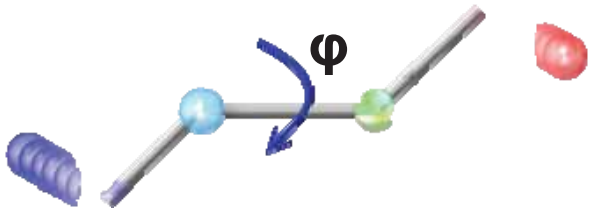

(d) Van der Wail

$$V_{vdw} = [A_{SC}\varepsilon^{ij}(r_0^{ij}/r_{ij})^{12} - 2\varepsilon^{ij}(r_0^{ij}/r_{ij})^{6} - S_{vdw}^{A}(r_{ij})]$$

$$S_{vdw}^{A}(r_{ij}) = [A_{SC}\varepsilon^{ij}(r_0^{ij}/r_{ij})^{12} - 2\varepsilon^{ij}(r_0^{ij}/r_{ij})^{6}] - 12(r - r_c)[A_{SC}\varepsilon^{ij}(r_0^{ij}/r_{ij})^{12} - 2\varepsilon^{ij}(r_0^{ij}/r_{ij})^{6}]/r_c$$

(e) Coulomb force

$$V_{coul.} = 332 \sum_{partial\ charges} [q^i q^j / r_{ij} - S_{els}^{A}(r_{ij})]$$

$$S_{els}^{A}(r_{ij}) = \frac{q^i q^j}{r_c} - (r_{ij} - r_c)\frac{q^i q^j}{r_c^{\,2}}$$

- Many body potential
  - **Tight-binding potential** (Co, Cu, Ti, …)

$$E = -\left\{\sum_j \xi^2 \exp\left[-2q\left(\frac{r_{ij}}{r_0}-1\right)\right]\right\}^{1/2} + \sum_j A \exp\left[-p\left(\frac{r_{ij}}{r_0}-1\right)\right]$$

Many-body term-long range force, attractive force

Born-Mayer type pairwise term-short range, repulsive force

  - Where ξ is an effective hopping integral
  - r_{ij} is the distance between atom *i* and *j*

    r_o is the first-neighbor distance

The Embedded-Atom method (EAM) :

(Materials Science Reports 9 (1993) 251-310)

$$E_{\mathrm{coh}} = G[\rho] + \frac{1}{2}\sum_{i,j}{}' \frac{Z_i Z_j}{R_{ij}} - \sum_i \int \frac{Z_i \rho(\boldsymbol{r})}{|\boldsymbol{r} - \boldsymbol{R}_i|}\, \mathrm{d}\boldsymbol{r} + \frac{1}{2}\int\int \frac{\rho(\boldsymbol{r}_1)\rho(\boldsymbol{r}_2)}{r_{12}}\, \mathrm{d}\boldsymbol{r}_1\, \mathrm{d}\boldsymbol{r}_2 - E_{\mathrm{atoms}}, \quad (3)$$

DFT calculation

Simplified into EAM potential

$$E_{\mathrm{coh}} = \sum_i G_i\left(\sum_{j\neq i} \rho_j^{\mathrm{a}}(R_{ij})\right) + \tfrac{1}{2}\sum_{i,j(j\neq i)} U_{ij}(R_{ij}),$$

Embedding Function

$$\bar{\rho} = \sum_n \rho^{\mathrm{a}}(\boldsymbol{R}_n) \qquad \rho^a(R) = n_s\rho_s(R) + n_d\rho_d(R)\ ,$$

Electron gas density

TABLE I. Parameters defining the effective charges for the pair interactions [Eq. (7)] and atomic electron density [Eq. (6)]. The last row specifies the atomic configuration used to calculate ρ_s and ρ_d.

	Cu	Ag	Au	Ni	Pd	Pt
Z_0	11.0	11.0	11.0	10.0	10.0	10.0
α	1.7227	2.1395	1.4475	1.8633	1.2950	1.2663
β	0.1609	1.3529	0.1269	0.8957	0.0595	0.1305
ν	2	2	2	1	1	1
n_s	1.000	1.6760	1.0809	1.5166	0.8478	1.0571
Atomic configuration	$3d^{10}4s^1$	$4d^95s^2$	$5d^{10}6s^1$	$3d^84s^2$	$4d^95s^1$	$5d^96s^1$

Clementi and Roetti from HF calculation

$$\rho_s(r)=\left|\sum_i C_i R_i(r)\right|^2 \Big/ 4\pi$$

$$R_i(r)=\frac{(2\zeta_i)^{(n_i+1/2)}}{[(2n_i)!]^{1/2}} r_i^{n_i-1}\exp(-\zeta_i r)$$

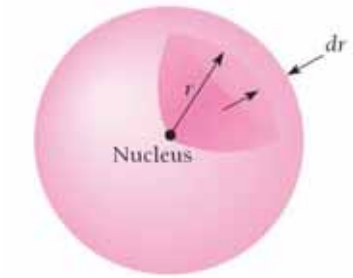

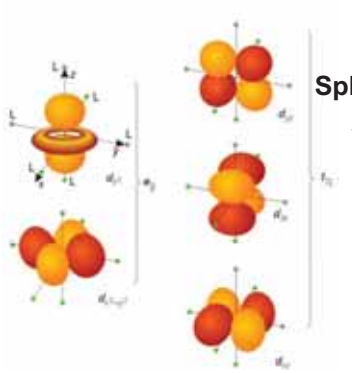

Spherical symmetry wave function

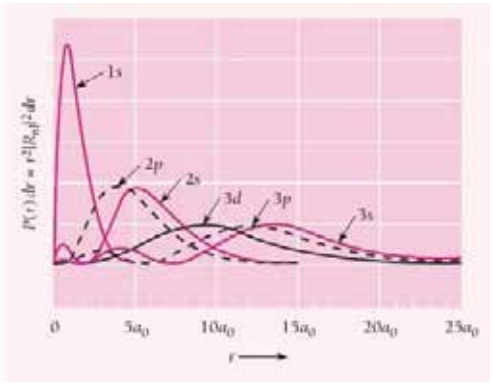

表 3.2 Ni 和 Pd 的 n_i、ζ_i 和 C_i（ζ_i 的单位为 nm^{-1}）

	n_i	ζ_i	C_i
		Ni	
1s			
1	1	548.888 5	−0.003 89
2	1	384.843 1	−0.029 91
3	2	274.270 3	−0.031 89
4	2	208.820 4	0.152 89
5	3	109.570 7	−0.200 48
6	3	73.195 8	−0.054 23
7	4	39.265 0	0.492 92
8	4	21.528 9	0.618 75
3d			
1	3	126.758 2	0.421 20
2	3	54.325 3	0.706 58
		Pd	
5s			
1	1	892.192 8	−0.000 71
2	1	619.098 3	0.024 24
3	2	401.274 1	0.168 08
4	2	384.270 3	−0.242 34
5	3	269.274 1	−0.016 86
6	3	183.979 8	0.191 78
7	4	106.834 6	−0.277 59
8	4	72.411 2	−0.022 57
9	5	42.022 9	0.552 09
10	5	23.398 9	0.570 52
4d			
1	3	298.656 0	−0.087 21
2	3	168.019 5	−0.238 76
3	4	90.203 8	0.570 74
4	4	46.714 7	0.582 01

Embedding Function

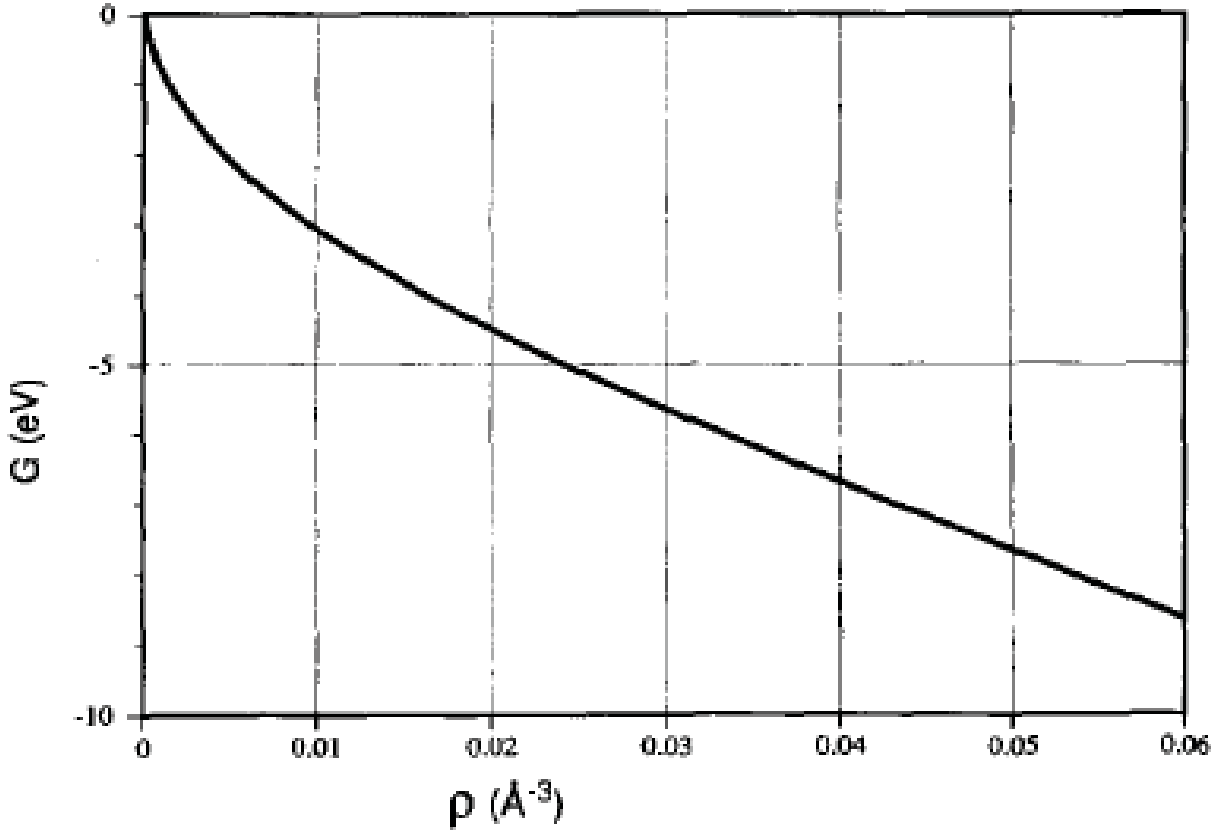

Fig. 1. Embedding energy for Ni as a function of the background electron density.

(http://www.ide.titech.ac.jp/~takahak/EAMers/)

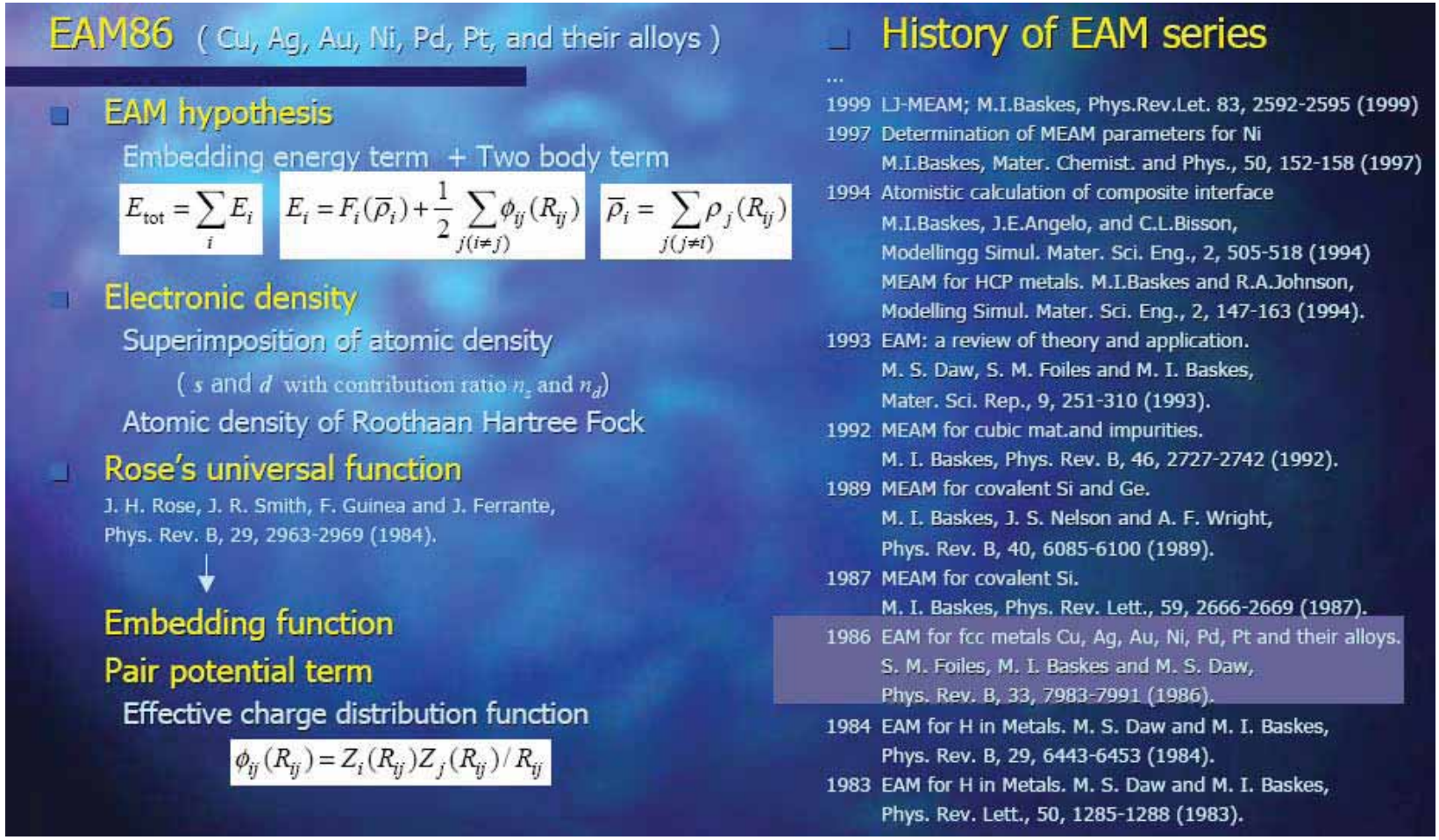

- **EAM hypothesis**

  Embedding energy term + Two body term

$$E_{tot} = \sum_i E_i \qquad E_i = F_i(\bar{\rho}_i) + \frac{1}{2}\sum_{j(i\neq j)} \phi_{ij}(R_{ij})$$

- **Embedding function**

  Fixed

$$F_i(\bar{\rho}_i) = A_i E_0 \frac{\bar{\rho}_i}{\bar{\rho}_i^{\,0}} \ln\left(\frac{\bar{\rho}_i}{\bar{\rho}_i^{\,0}}\right)$$

- **Electronic density**

  Superimposition of atomic density

  s, p, d, f symmetry

  Parameterized atomic density

$$(\bar{\rho}_i)^2 = \sum_{l=0}^{3} t_i^{(l)} \left(\rho_i^{(l)}\right)^2$$

- **Pair potential term**

  Reference structure

$$\rho_i^{a(l)} = \exp\left\{-\beta_i^{(l)}\left(\frac{R_{ij}}{R_i^0} - 1\right)\right\}$$

- **Rose's universal function**

  J. H. Rose, J. R. Smith, F. Guinea and J. Ferrante,
  Phys. Rev. B, 29, 2963-2969 (1984).

- **Screening function**

  to neglect farther atoms ?

1999 LJ-MEAM; M.I.Baskes, Phys.Rev.Let. 83, 2592-2595 (1999)

1997 Determination of MEAM parameters for Ni
M.I.Baskes, Mater. Chemist. and Phys., 50, 152-158 (1997)

1994 Atomistic calculation of composite interface
M.I.Baskes, J.E.Angelo, and C.L.Bisson,
Modellingg Simul. Mater. Sci. Eng., 2, 505-518 (1994)
MEAM for HCP metals. M.I.Baskes and R.A.Johnson,
Modelling Simul. Mater. Sci. Eng., 2, 147-163 (1994).

1993 EAM: a review of theory and application.
M. S. Daw, S. M. Foiles and M. I. Baskes,
Mater. Sci. Rep., 9, 251-310 (1993).

1992 MEAM for cubic mat.and impurities.
M. I. Baskes, Phys. Rev. B, 46, 2727-2742 (1992).

1989 MEAM for covalent Si and Ge.
M. I. Baskes, J. S. Nelson and A. F. Wright,
Phys. Rev. B, 40, 6085-6100 (1989).

1987 MEAM for covalent Si.
M. I. Baskes, Phys. Rev. Lett., 59, 2666-2669 (1987).

1986 EAM for fcc metals Cu, Ag, Au, Ni, Pd, Pt and their alloys.
S. M. Foiles, M. I. Baskes and M. S. Daw,
Phys. Rev. B, 33, 7983-7991 (1986).

1984 EAM for H in Metals. M. S. Daw and M. I. Baskes,
Phys. Rev. B, 29, 6443-6453 (1984).

1983 EAM for H in Metals. M. S. Daw and M. I. Baskes,
Phys. Rev. Lett., 50, 1285-1288 (1983).

Electronic density in MEAM92

- Superimposition of atomic density
- *s, p, d, f* symmetry

$$E_{tot} = \sum_i E_i$$

$$E_i = F_i(\bar{\rho}_i) + \frac{1}{2}\sum_{j(i\neq j)} \phi_{ij}(R_{ij})$$

$$(\bar{\rho}_i)^2 = \sum_{l=0}^{3} t_i^{(l)} \left(\rho_i^{(l)}\right)^2$$

$$\bar{\rho}_i = \rho_i^{(0)} \left\{ 1 + \frac{1}{2}\sum_{l=0}^{3} t_i^{(l)} \left(\rho_i^{(l)} / \rho_i^{(0)}\right)^2 + \ldots \right\}$$

s (*l*=0) $\rho_i^{(0)} = \sum_{j(\neq i)} \rho_j^{a(0)}(R_{ij})$

p (*l*=1) $\left(\rho_i^{(1)}\right)^2 = \sum_{\alpha} \left\{ \sum_{j(\neq i)} x_{ij}^{\alpha} \rho_j^{a(1)}(R_{ij}) \right\}^2$

$x_{ij}^{\alpha} = R_{ij}^{\ \alpha} / R_{ij}$

d (*l*=2) $\left(\rho_i^{(2)}\right)^2 = \sum_{\alpha,\beta} \left\{ \sum_{j(\neq i)} x_{ij}^{\alpha} x_{ij}^{\beta} \rho_j^{a(2)}(R_{ij}) \right\}^2 - \frac{1}{3} \left\{ \sum_{j(\neq i)} \rho_j^{a(2)}(R_{ij}) \right\}^2$

f (*l*=3) $\left(\rho_i^{(3)}\right)^2 = \sum_{\alpha,\beta,\gamma} \left\{ \sum_{j(\neq i)} x_{ij}^{\alpha} x_{ij}^{\beta} x_{ij}^{\gamma} \rho_j^{a(3)}(R_{ij}) \right\}^2$

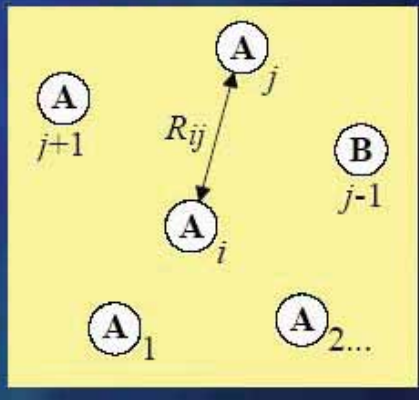

Force-matching Method implemented in GULP

Target Function

In order to get the adaptive parameter of potential function(Z), the target is used for the purpose.

$$Z = Z_F + Z_C$$

$$Z_F = \sum_{j=1}^{N_A} \sum_{\alpha=x,y,z} W_j \frac{(f_{i\alpha} - f_{0,j\alpha})^2}{f_{0,j}^{\,2} + \varepsilon_j} \qquad Z_C = \sum_{k=1}^{N_C} W_k \frac{(A_k - A_{0,k})^2}{A_{0,k}^{\,2} + \varepsilon_k}$$

Force: total force per atom **Global: stresses, energies**

$A_{0,k}$ $f_{0,j\alpha}$ **Reference data: from the *Ab Initio* simulation or experiments.**

A_k $f_{i\alpha}$ **: obtained from the potential function which we pick.**

W : weight function, N: data number, ε **: small and positive data**

NANO
LETTERS

2009
Vol. 9, No. 2
576-582

Numerical Investigations into the Tensile Behavior of TiO_2 Nanowires: Structural Deformation, Mechanical Properties, and Size Effects

Table 1. Parameter Values for Simplified Matsui and Akaogi's Potential[11]

q_{Ti} (e)	q_O (e)	A (eV)	B (Å)	C (eV-Å^6)
2.196	−1.098	16286	0.194	1215

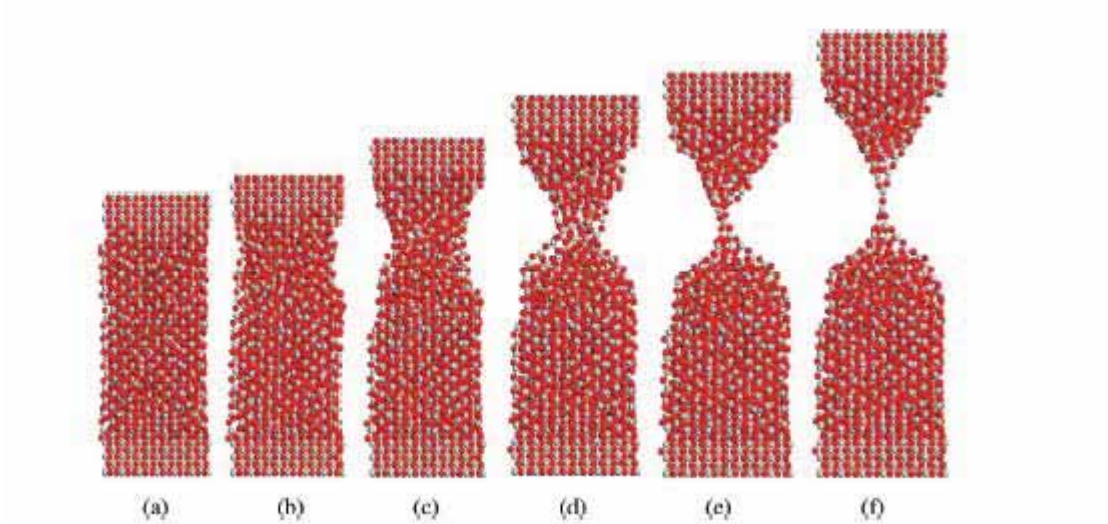

igure 3. Tensile loading of TiO_2 nanowire at strain levels of (a) 1.6%, (b) 8.4%, (c) 20%, (d) 35.2%, (e) 43.6%, and (f) 53.7%.

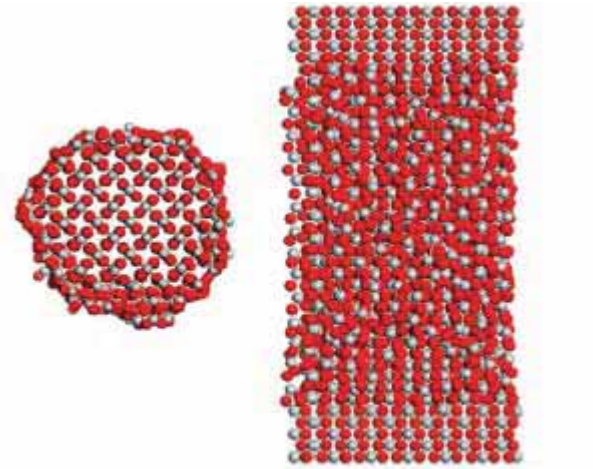

Figure 2. Cross sectional (left) and longitudinal (right) views of equilibrated cylindrical TiO_2 nanowire model. The relaxed surface at

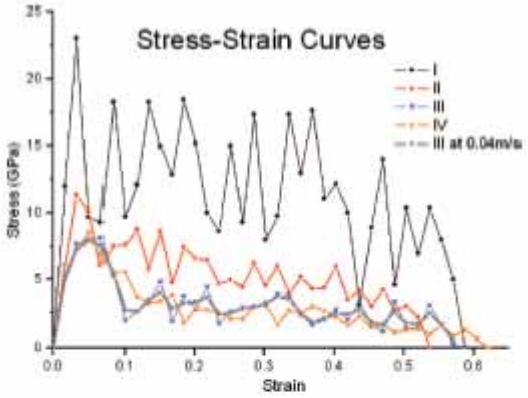

Figure 7. Tensile stress−strain curves for the four nanowires with different cross-sectional diameters.

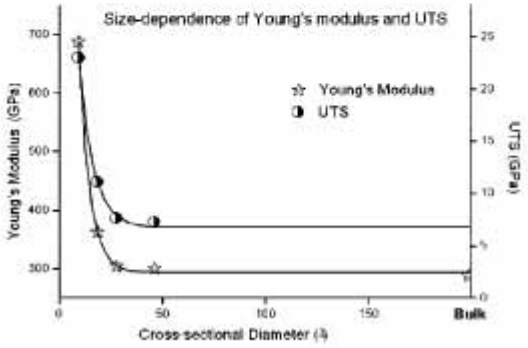

Figure 8. Plots of Young's modulus and UTS as functions of nanowire cross-sectional diameters.

Molecular Dynamics

- A computer simulation technique that allows one to predict the time evolution of a system of interacting particles (atoms, molecules,.. etc.)

- **Solving a set of classical equations of motion**

$$m\ddot{r}_i = F_i$$

$$F_i = -\sum_{\substack{i=1 \\ i \neq j}}^{N} \nabla_i \Phi(r_{ij})$$

$\Phi(r_{ij})$: interatomic potential

Integration Algorithms

1. **Verlet Algorithm**
2. **Leapfrog Algorithm**
3. **Velocity Verlet Algorithm**
4. **Gear Predictor-Corrector Algorithm**

Au nanowire with diameter smaller than 2 nm

Jenn-Sen Lin, **Shin-Pon Ju**, and Wen-Jay Lee, **Physical Review B** 72, 85448 (2005) .

Wen-Jay Lee, **Shin-Pon Ju**, Shih-Jye Sun, Meng-Hsiung Weng , Nanotechnology 17 (2006) 3253–3258

Shin-Pon Ju et al., Nanotechnology **18** (2007) 205706

(7-1)

0.577nm

(11-4)

0.887nm

(13-6)

1.043nm

(14-7-1)

1.122nm

(15-8-1)

1.201nm

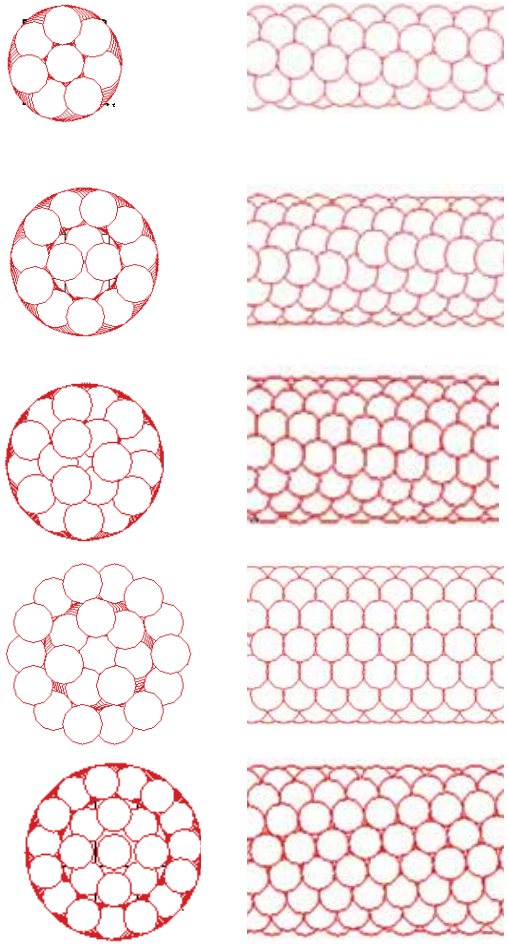

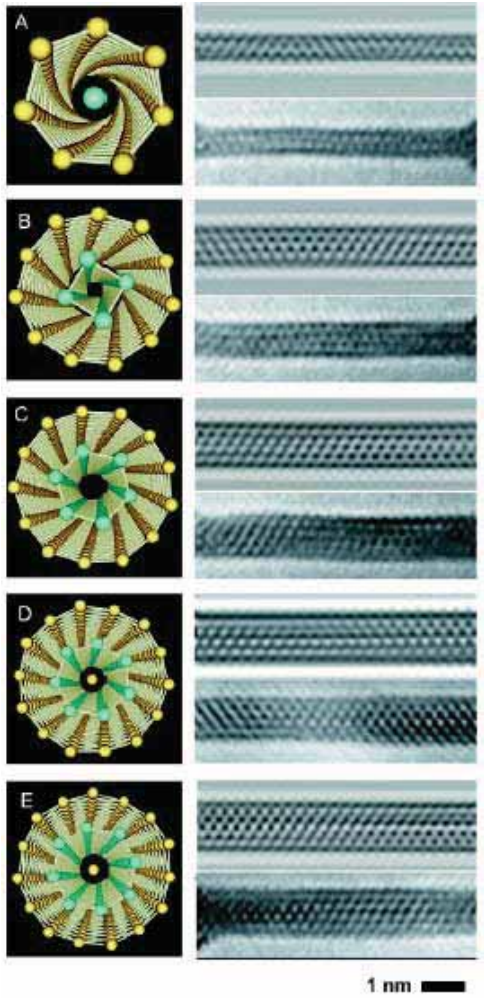

Ref：Y. Kondo and K. Takayanagi SCIENCE VOL289 ,606 (2000July)

Ref：V. Rodrigues and D. Ugarte Physical Review B Volume 64, 073405 (2001 January)

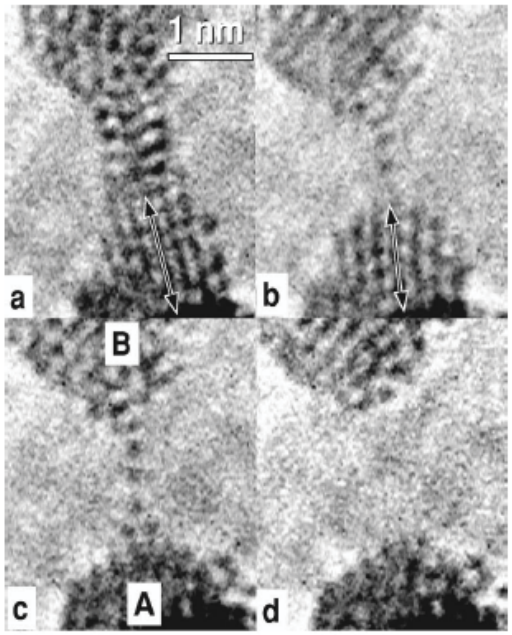

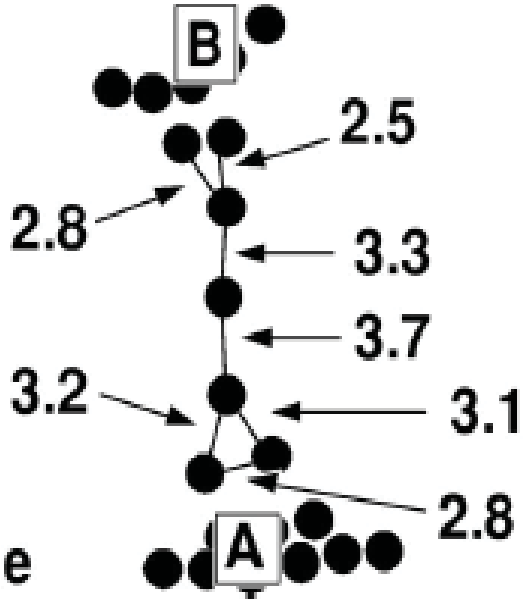

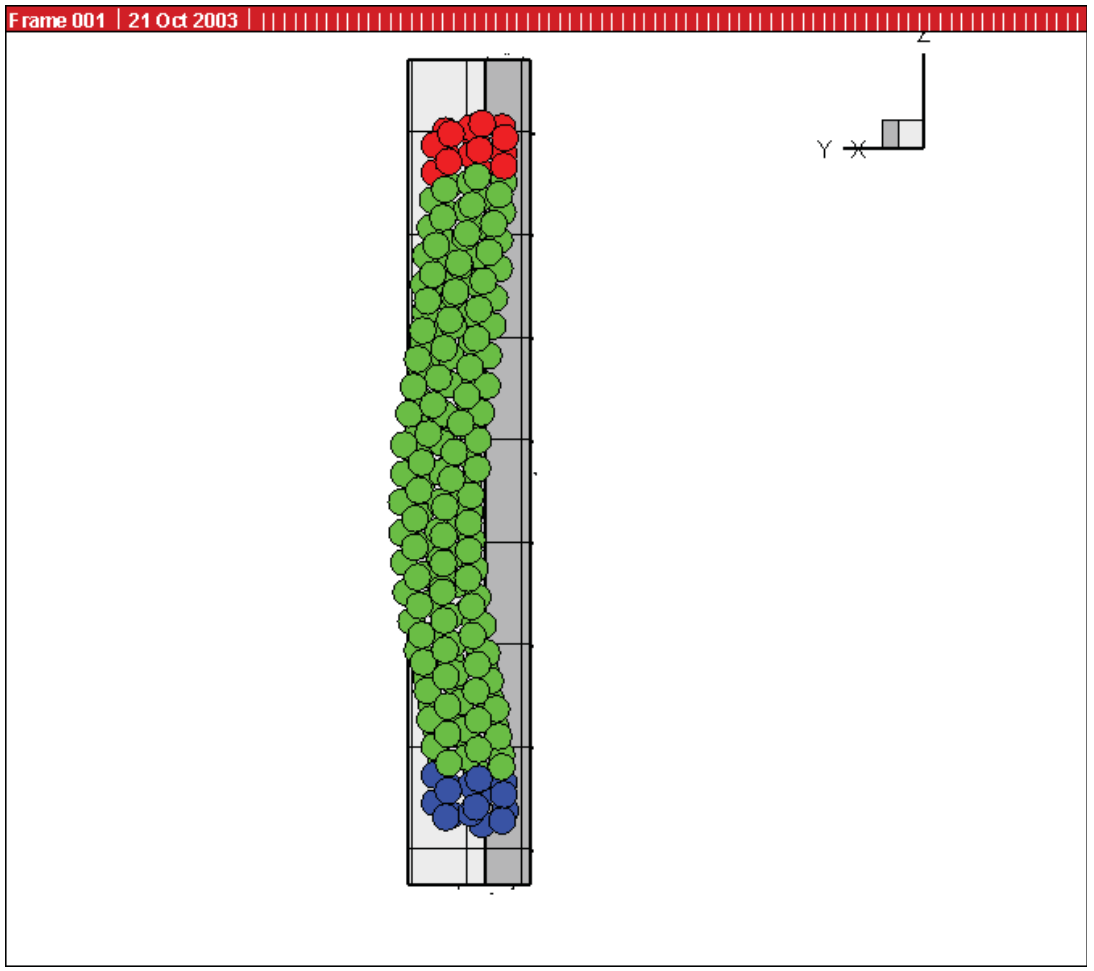

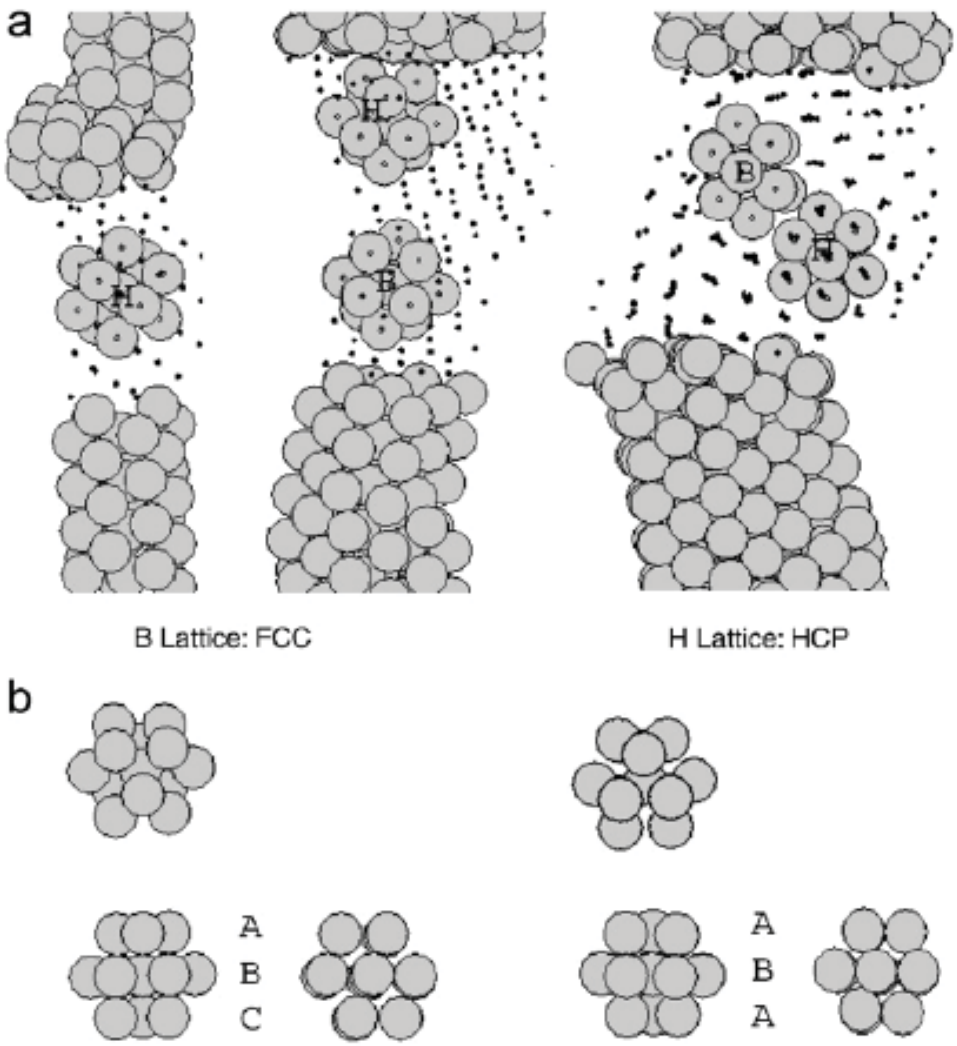

Fig. 5. (a) Snapshots of deformed nanowires showing B and H lattices at a strain of 0.3. (b) Illustration of B and H lattices, i.e. FCC and HCP structures, respectively.

Atomic configurations of gold nanowire at selected elongation stage for 7-1 structure at room temperature

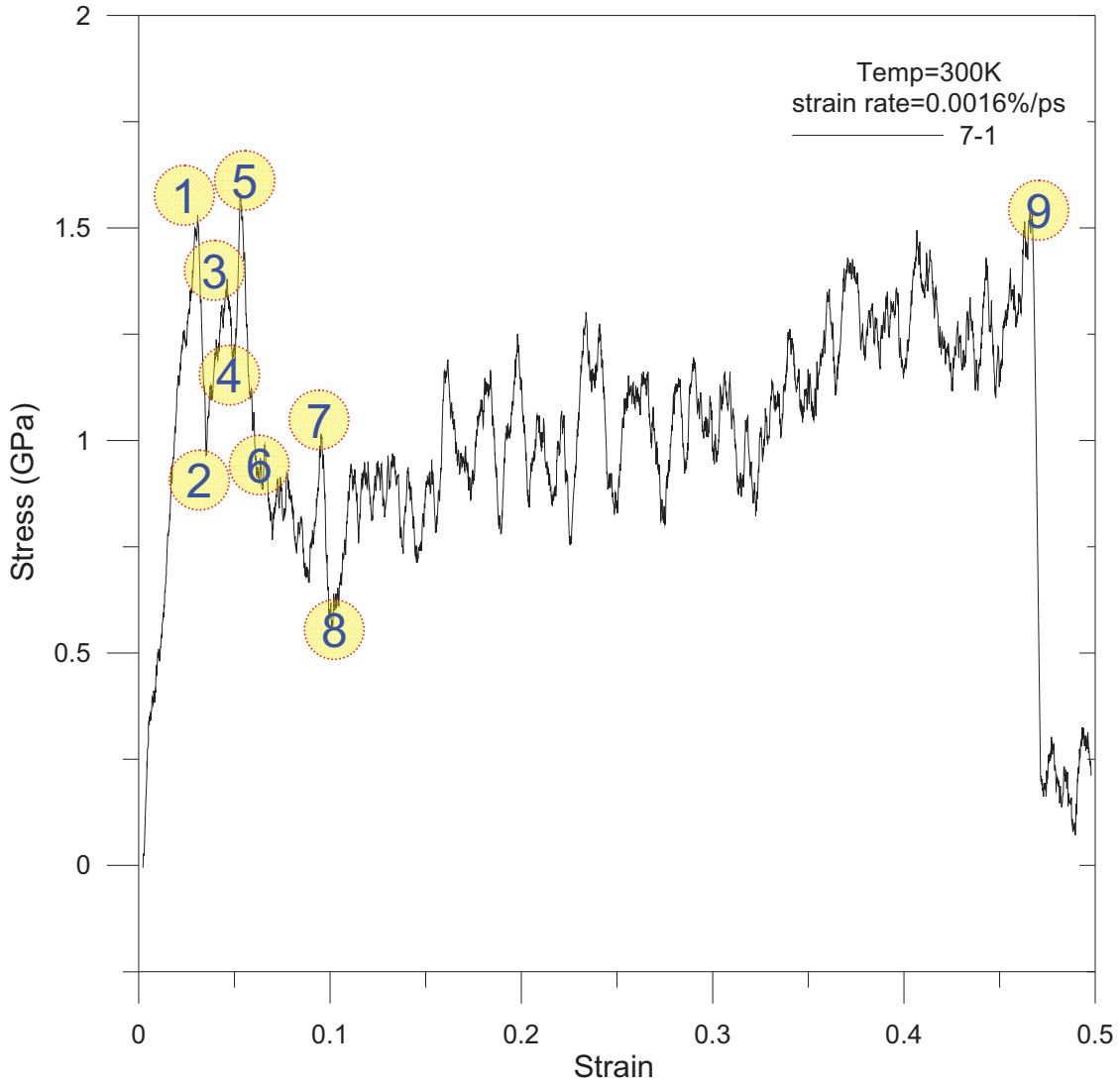

Mechanical properties under elongation test with different length/diameter ratio.

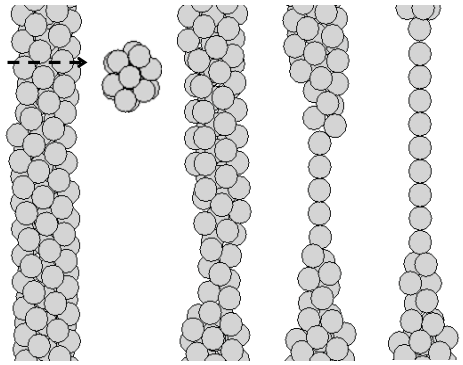

	L/D	Cohesive Energy(eV)	Young's Modulus(GPa)	Yield Stress(GPa)	Yield strain	breaking Force(nN)	Maximum strain	Elongate Length
7-1	7	3.432	165.978	6.588	0.066	1.393	0.931	35.843
	11	3.456	143.504	6.984	0.069	1.526	0.981	59.350
11-4	7	3.530	115.683	4.036	0.046	1.272	0.408	23.448
	11	3.541	112.784	3.904	0.043	1.302	0.408	36.846
14-7-1	7	3.578	105.287	4.441	0.063	1.322	0.264	19.255
	11	3.585	91.897	4.306	0.059	1.465	0.194	22.042
FCC	6nm[100]	3.714	42.704	5.182	0.097	—	0.892	53.52
	6nm[111]	3.718	101.737	4.578	0.047	1.305	1.728	103.68
	Nanowrie	—	40-100[16]	2-8[16]	—	—	—	—
	Bulk	3.77[27]	79[15]	0.2[15]	—	—	—	—

Mechanical properties under compression test with different length/diameter ratio.

	L/D	Young's Modulus (GPa)	Yielding Stress (GPa)	Yielding strain	Buckle Stress (GPa)	Buckle strain
7-1	7	192.404	10.358	0.046	—	—
	11	191.752	—	—	3.162	0.032
11-4	7	151.118	5.064	0.031	—	—
	11	144.664	—	—	1.771	0.025
14-7-1	7	139.750	9.766	0.0631	—	—
	11	140.610	—	—	2.327	0.031
FCC	6nm[100]	59.628	2.082	0.056	—	—
	6nm[111]	101.078	8.098	0.059	—	—

The collective motion of carbon atoms in a (10,10) single wall carbon nanotube under axial tensile strain

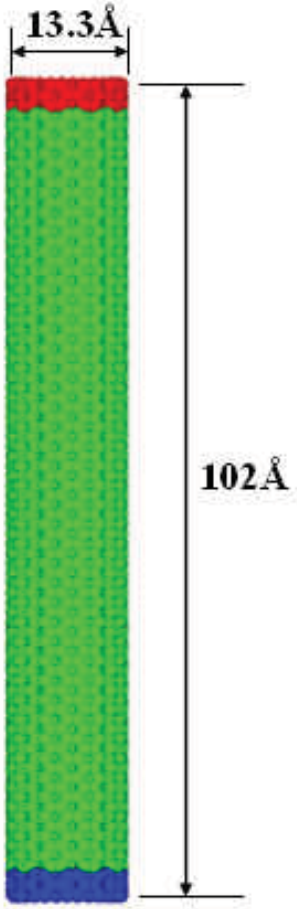

Slip vector

$$S^{\alpha} = \frac{1}{n_s} \sum_{\beta \neq \alpha}^{n} \left(\vec{r}^{\,\alpha\beta} - \vec{r}_0^{\,\alpha\beta} \right)$$

JAP, 2009 (in press)

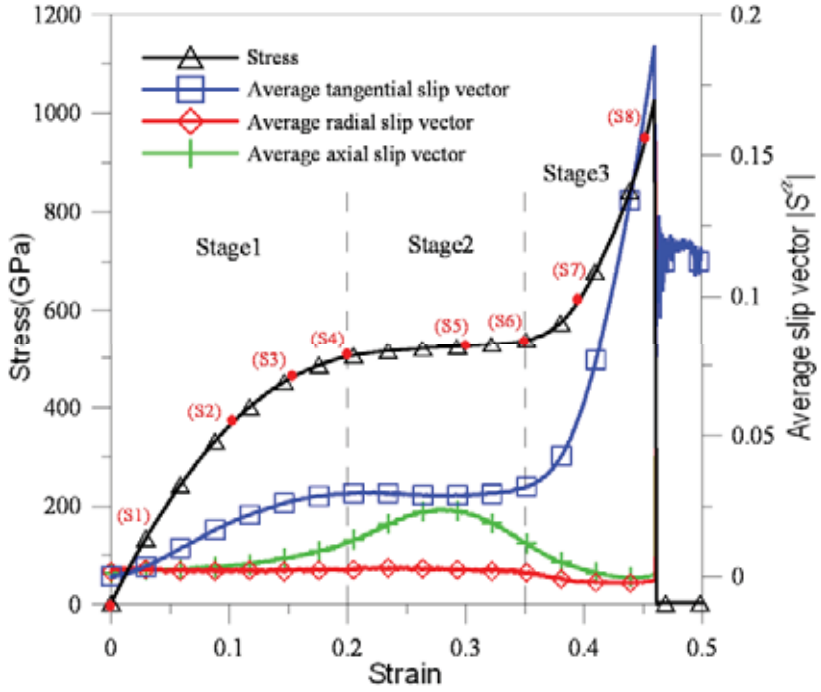
Stress
Average tangential slip vector
Average radial slip vector
Average axial slip vector
Stage1
Stage2
Stage3
(S1)
(S2)
(S3)
(S4)
(S5)
(S6)
(S7)
(S8)
Stress(GPa)
Average slip vector |S''|
Strain

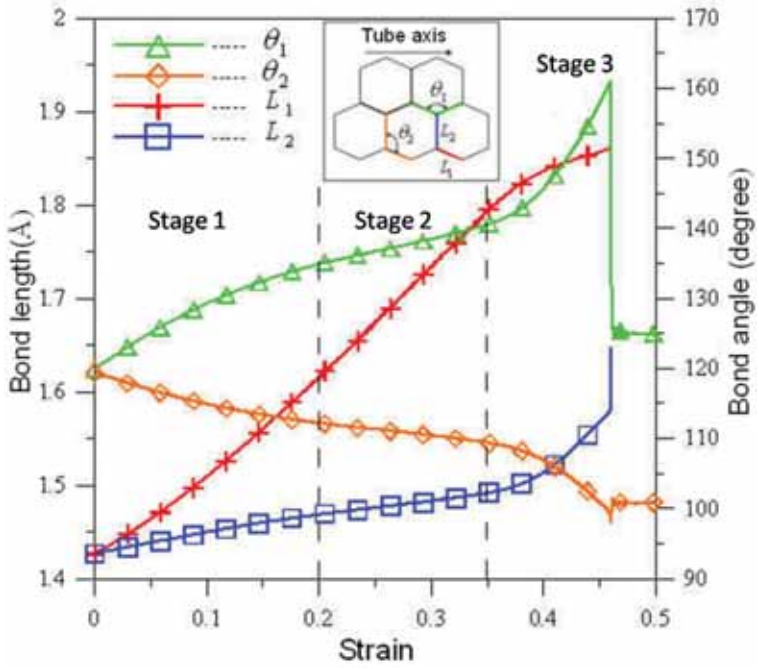
Tube axis
Stage 1
Stage 2
Stage 3
Bond length(Å)
Bond angle (degree)
Strain

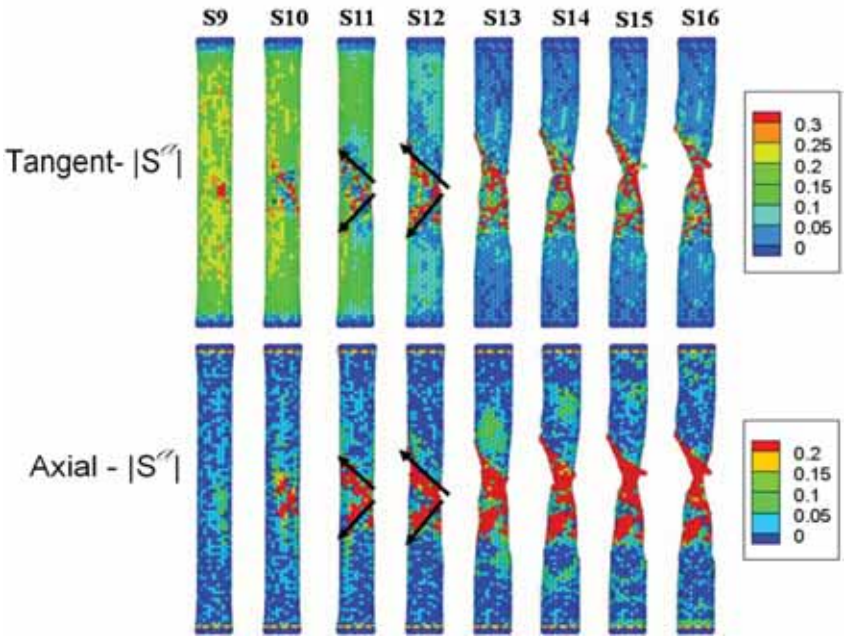
S9
S10
S11
S12
S13
S14
S15
S16
Tangent- |S''|
Axial - |S''|

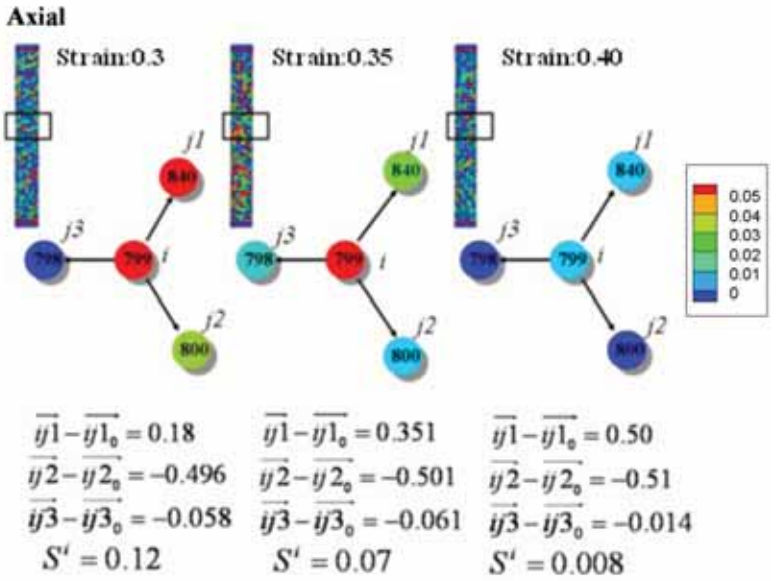
Axial
Strain:0.3
Strain:0.35
Strain:0.40
$\overrightarrow{ij1}-\overrightarrow{ij1_0}=0.18$
$\overrightarrow{ij2}-\overrightarrow{ij2_0}=-0.496$
$\overrightarrow{ij3}-\overrightarrow{ij3_0}=-0.058$
$S'=0.12$
$\overrightarrow{ij1}-\overrightarrow{ij1_0}=0.351$
$\overrightarrow{ij2}-\overrightarrow{ij2_0}=-0.501$
$\overrightarrow{ij3}-\overrightarrow{ij3_0}=-0.061$
$S'=0.07$
$\overrightarrow{ij1}-\overrightarrow{ij1_0}=0.50$
$\overrightarrow{ij2}-\overrightarrow{ij2_0}=-0.51$
$\overrightarrow{ij3}-\overrightarrow{ij3_0}=-0.014$
$S'=0.008$

APPLIED PHYSICS LETTERS **94**, 261106 (2009)

Photocurrent properties of freely suspended carbon nanotubes under uniaxial strain

S. M. Kaniber,[1] L. Song,[2] J. P. Kotthaus,[2] and A. W. Holleitner[1,2,a)]
[1]*Department of Physik and Walter Schottky Institut, Technische Universität München, Am Coulombwall 3, D-85748 Garching, Germany*
[2]*Fakultät für Physik and Center for NanoScience, Ludwig-Maximilians-Universität, Geschwister-Scholl-Platz 1, D-80539 München, Germany*

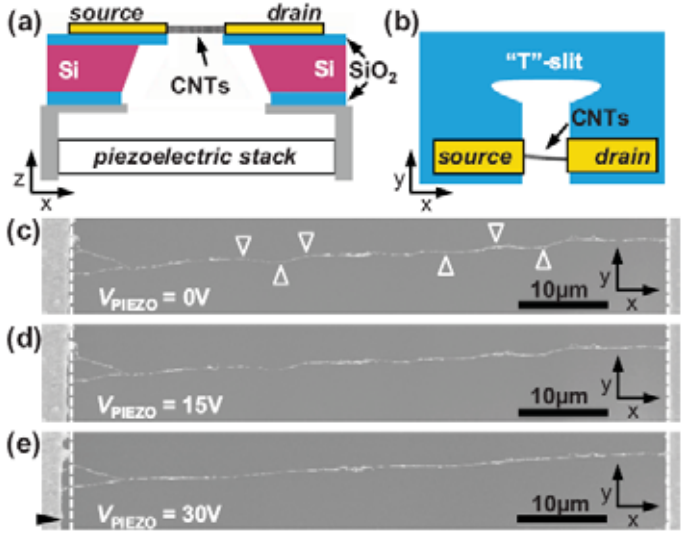

FIG. 1. (Color online) Schematic side (a) and top (b) view of a Si/SiO_2 sample with a "T"-slit and freely suspended single-walled CNTs mounted on a piezoelectric stack. Applying a voltage V_{PIEZO} to the piezoelectric stack allows applying uniaxial strain to the CNTs. [(c)–(e)] SEM images of CNTs at V_{PIEZO}=0, 15, and 30 V at RT.

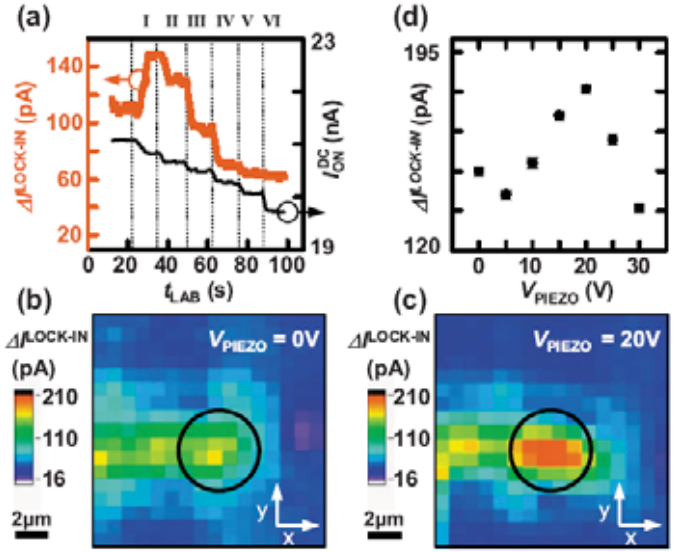

FIG. 3. (Color online) (a) I_{ON}^{DC} and $\Delta I^{LOCK\text{-}IN}$, simultaneously measured, across CNTs as a function of laboratory time, when V_{PIEZO} is increased from 0 to 30 V in six steps of 5 V (λ_{LASER}=714 nm, V_{SD}=+50 mV, f_{CHOP} =912 Hz, RT). [(b) and (c)] Photocurrent image of $\Delta I^{LOCK\text{-}IN}$ of a bundle of CNTs close to a metal contact (λ_{LASER}=714 nm, V_{SD}=+50 mV, f_{CHOP} =912 Hz, RT). (d) Maximum values of $\Delta I^{LOCK\text{-}IN}$ taken from encircled area in (b) and (c) and further photocurrent scans as a function of V_{PIEZO}.

ARTICLES

First-Principles Calculations on the Emission Properties of Pristine and N-Doped Carbon Nanotubes

Chun Wang,† Liang Qiao,†,‡ Chaoqun Qu,† Weitao Zheng,*,† and Qing Jiang†

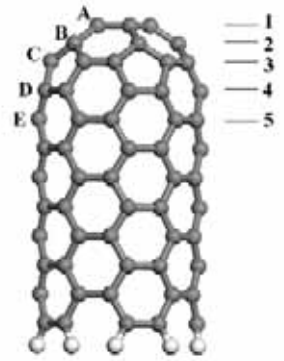

Figure 1. Geometrical structure of the CNT used in our calculation. The letters denote the different doping positions of the substitutional nitrogen atom in each atomic layer, which is indexed by the number.

IOP PUBLISHING NANOTECHNOLOGY
Nanotechnology 20 (2009) 085704 (6pp) doi:10.1088/0957-4484/20/8/085704

The effects of O_2 and H_2O adsorbates on field-emission properties of an (8, 0) boron nitride nanotube: a density functional theory study

Jing-xiang Zhao[1,2] and Yi-hong Ding[1]

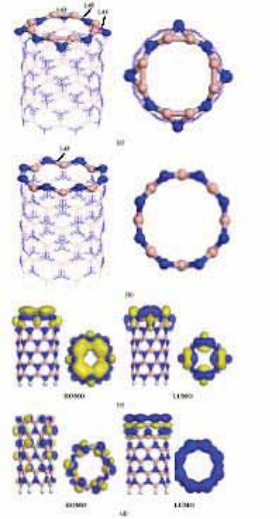

Figure 1. Optimized geometrical structures of open BNNTs: (a) B-rich-ended (8, 0), (b) N-rich-ended (8, 0) BNNTs. Side and top views of HOMO and LUMO of (c) B-rich-ended (8, 0) BNNT and (d) N-rich-ended (8, 0) BNNT. The bond lengths are in units of Å.

Mechanical, Electrical, and Magnetic Properties of Ni Nanocontacts

M. R. Calvo, M. J. Caturla, D. Jacob, C. Untiedt, and J. J. Palacios

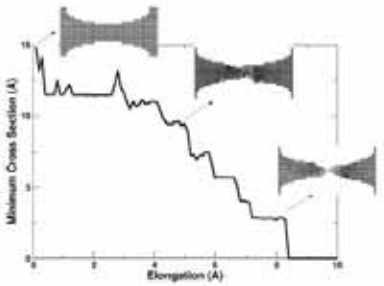

Fig. 3. Minimum cross section as a function of elongation along the [1 0 0] direction for a case with 2645 atoms. Insets shows configurations at different stages of the deformation.

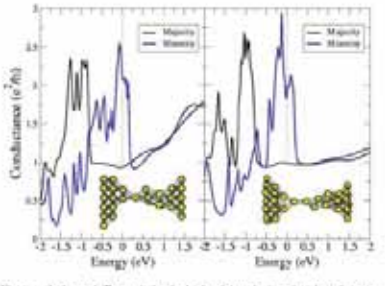

Fig. 6. (Left panel) Transmission for both spin species as a function of energy for the monomer configuration (shown in the inset) before failure. (Right panel) The same, but for a dimer configuration before failure.

J. Phys. Chem. C 2008, 112, 9045–9049 9045

Structures and Quantum Conduction of Copper Nanowires under Electric Fields Using First Principles

C. He, P. Zhang, Y. F. Zhu, and Q. Jiang*

Key Laboratory of Automobile Materials (Jilin University), Ministry of Education, and Department of Materials Science and Engineering, Jilin University, Changchun 130022, China

Received: January 29, 2008; Revised Manuscript Received: April 2, 2008

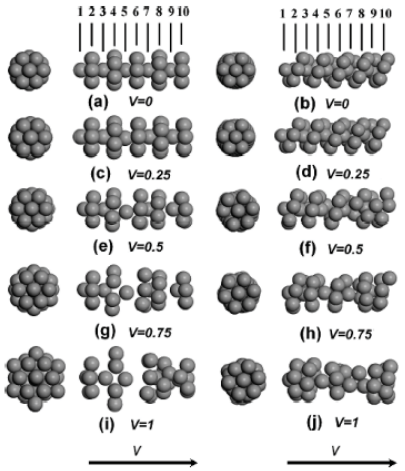

Figure 1. Morphologies of Cu NWs as a function of V: a, c, e, g, and i denote 6-1a, and b, d, f, h, and j show 6-1b under $V = 0$, $V = 0.25$, $V = 0.50$, $V = 0.75$, and $V = 1$ V/Å, respectively. The arrow shows the direction of V.

碳化矽奈米管(Silicon Carbide Nanotubes)是由碳原子及矽原子形成之石墨網狀結構所捲成的無縫、中空管體，依照所管壁層數的不同,可分為:

1.單壁碳化矽奈米管(Single-Wall Silicon Carbide Nanotubes)

2.多壁碳化矽奈米管(Muti-Wall Silicon Carbide Nanotubes)

J.A.C.S., **124**, 14464 (2002)

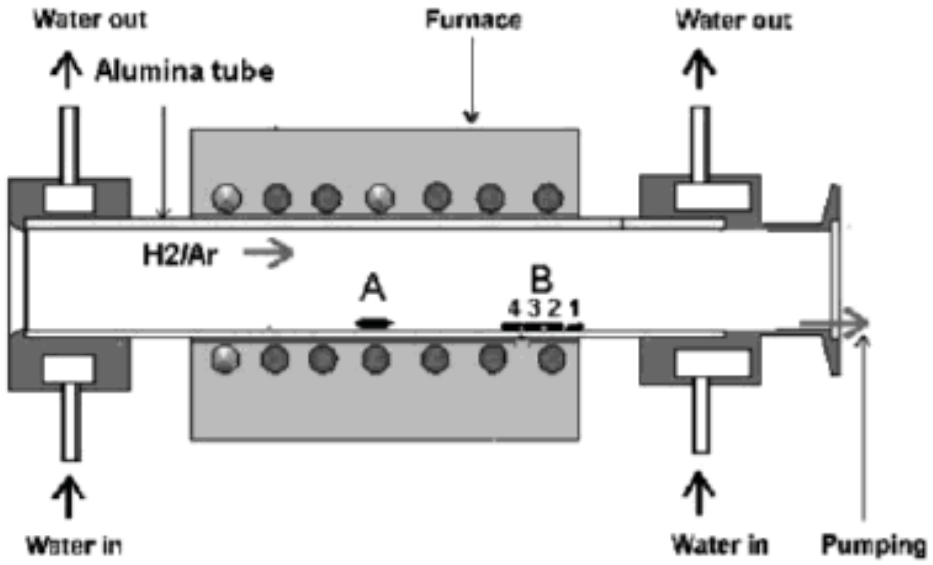

Figure 1. The schematic diagram of the synthesis apparatus.

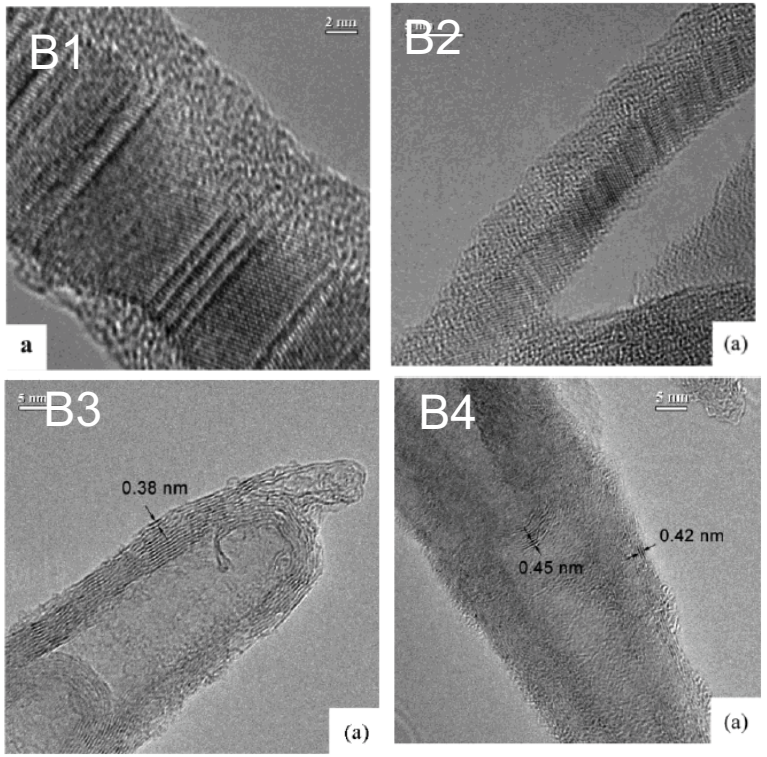

$SiO_2(99.95\%)+MWCNT \rightarrow SiCNT$

•Introduction & Motivation (Previous work)

Nano letters, **3**, 1481 (2003)

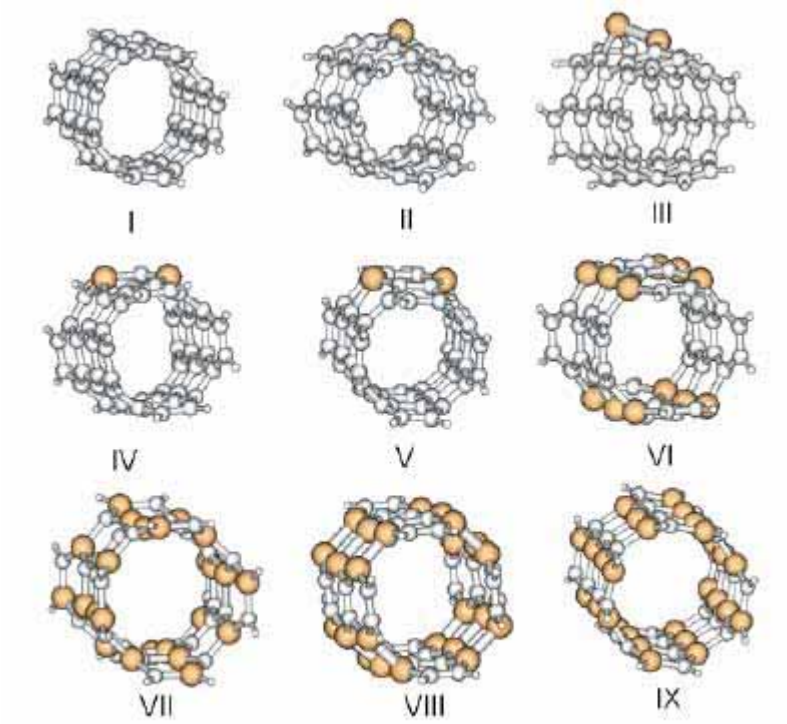

Figure 1. DFT optimized geometries of finite-sized, single-walled silicon−carbon nanotubes (SiCNT) with various Si/C ratios.

case	stoichiometry	energy	
		total (Hartree)	B. E./atom (eV)
I	C_{56}	−2142.066127	8.229
II	$C_{55}Si$	−2393.355348	8.126
III	$C_{54}Si_2$	−2644.667359	8.035
IV		−2644.660102	8.031
V		−2644.679661	8.040
VI	$C_{44}Si_{12}$	−5158.006401	7.226
VII	$C_{32}Si_{24}$	−8174.380359	6.466
VIII		−8173.839303	6.171
IX	$C_{28}Si_{28}$	−9179.983654	6.241

當Si:C=1:1時，結構最為穩定(DFT模擬)

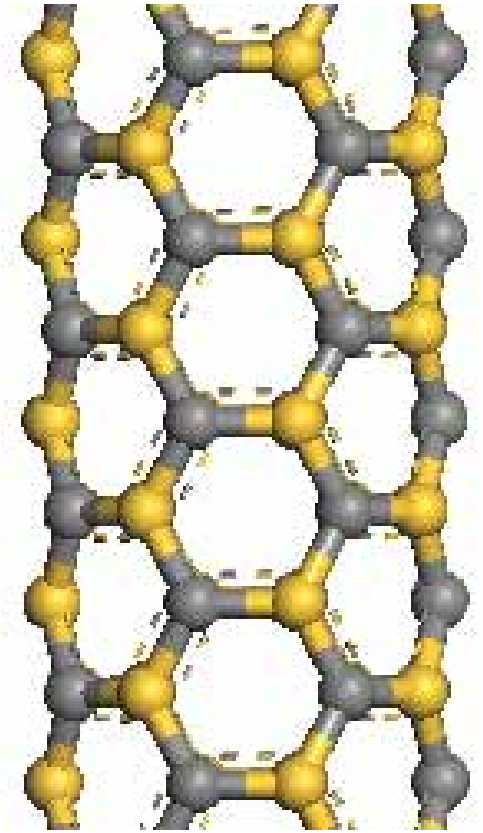

(4,4)armchair SiCNT

Advantage:
1.High thermal conductivity.
2.High radiation resistance
3.Good semiconductor

Difference with CNT:
1.In armchair configuration, it is always semiconductor.
2.For some gas molecules, it have good sensitivity, like CO_2[*] 、NO 、NO_2[**] 、HCN[***].

* *J. Chem. Theory Com.*, **5** ,1099 (2009)
** *J. Chem. Theory Com.*, **4** ,1690 (2008)
*** *J. Phys. Chem. C*, **112**, 15985 (2008)

•Simulation Modeling

Dangling bonding

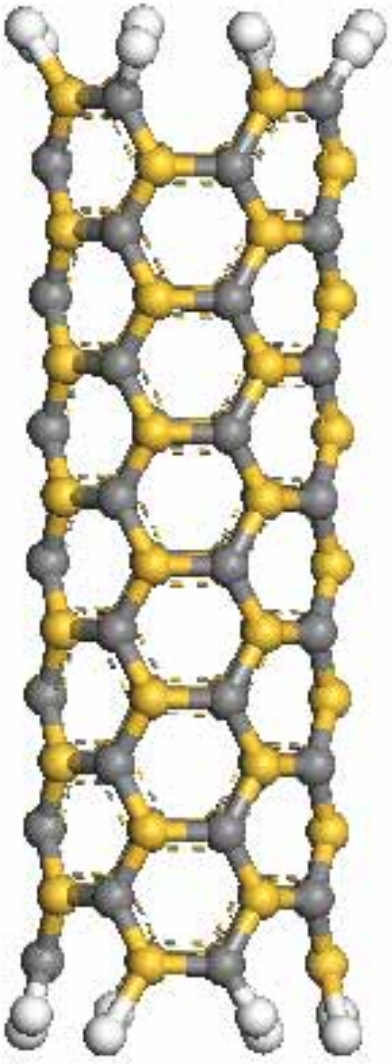

Dangling bonding

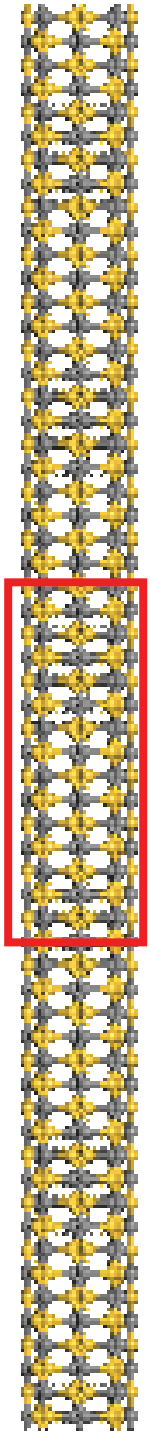

•Simulation Modeling

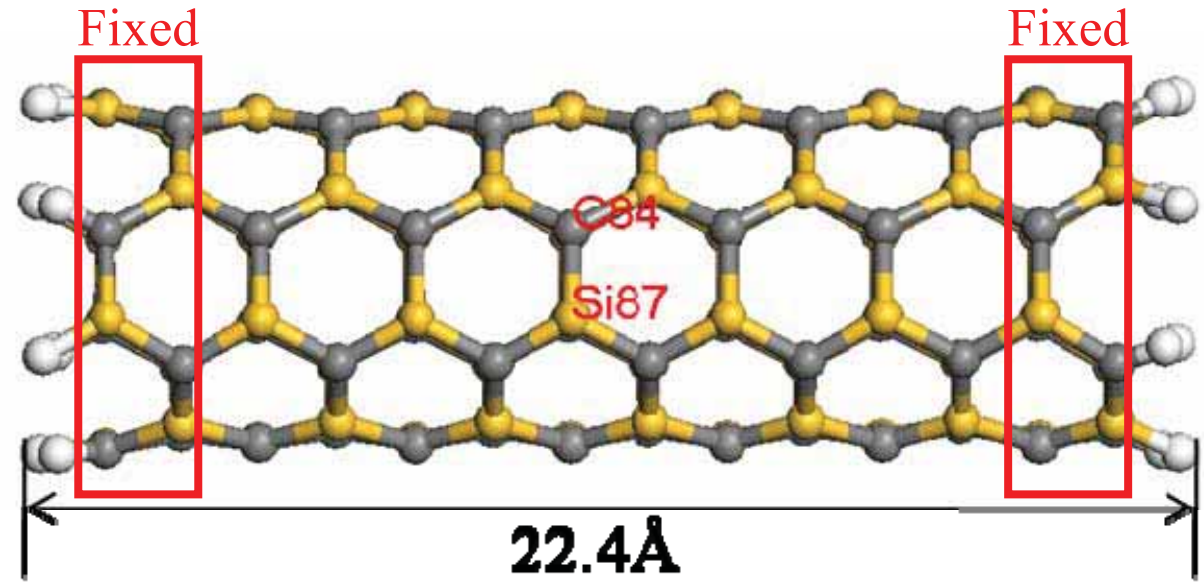

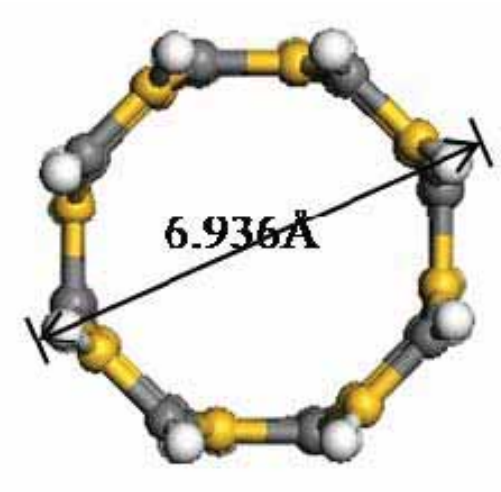

Atom numbers : 128

Stoichiometry : $C_{56}Si_{56}H_{16}$

•Result and Discussion (拉伸模擬的結構與電性分析)

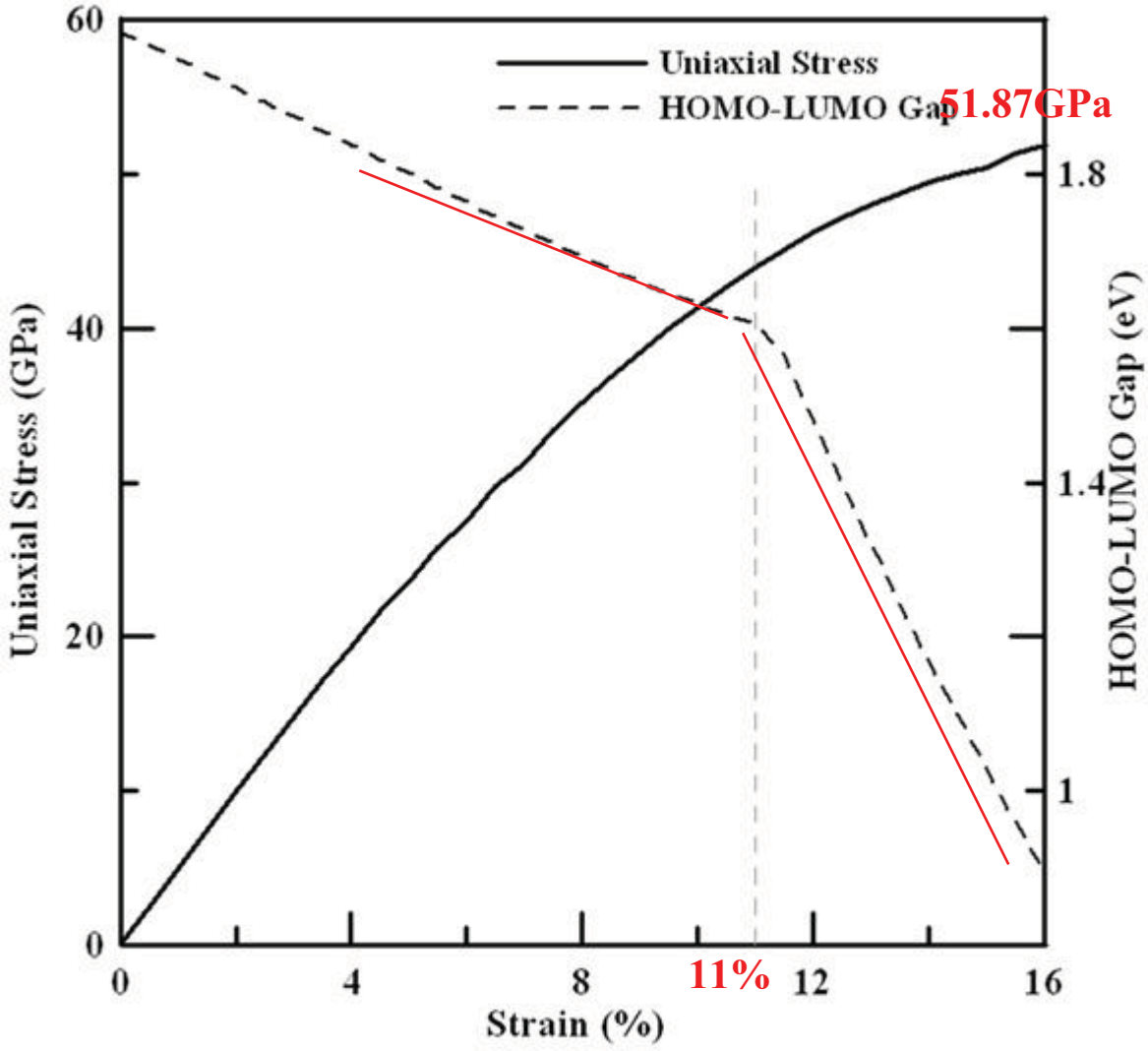

圖1、(4,4)扶手型碳化矽奈米管應力應變曲線與HOMO-LUMO Gap變化。實線為應力應變曲線；虛線為HOMO-LUMO gap-應變曲線。

•Result and Discussion (結構-Radial Buckling)

Radial Buckling β 此參數來說明結構產生了何種變化。定義如下式:

$$\beta = r_c - r_{Si}$$

其中 r_c 為碳原子的平均半徑，而 r_{Si} 為矽原子的平均半徑。

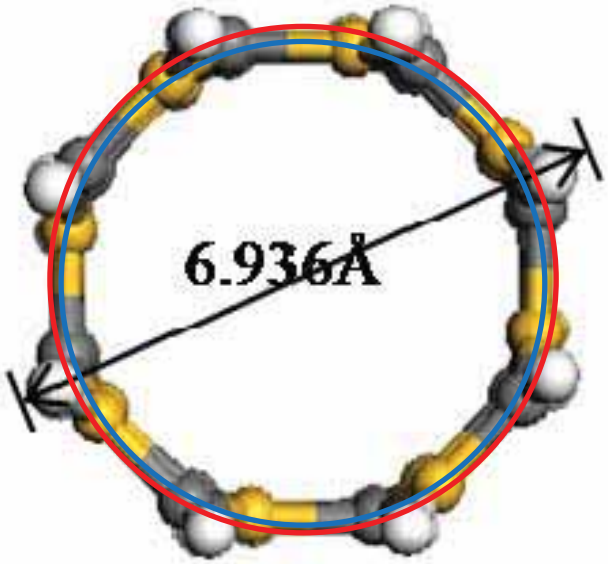

•Result and Discussion(結構-鍵長鍵角)

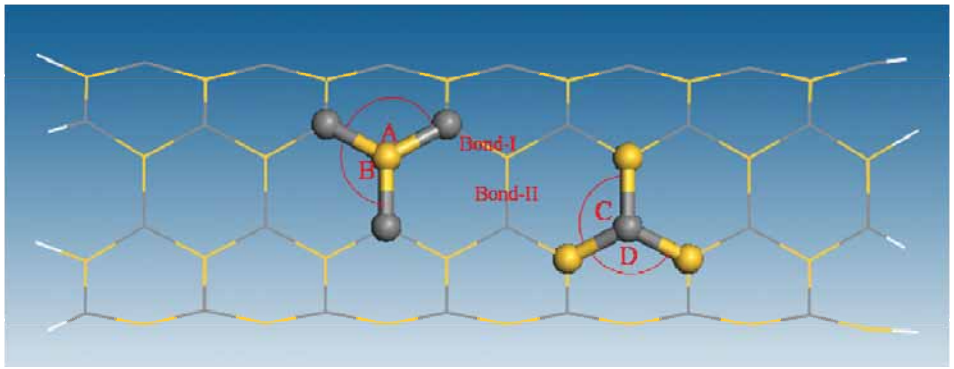

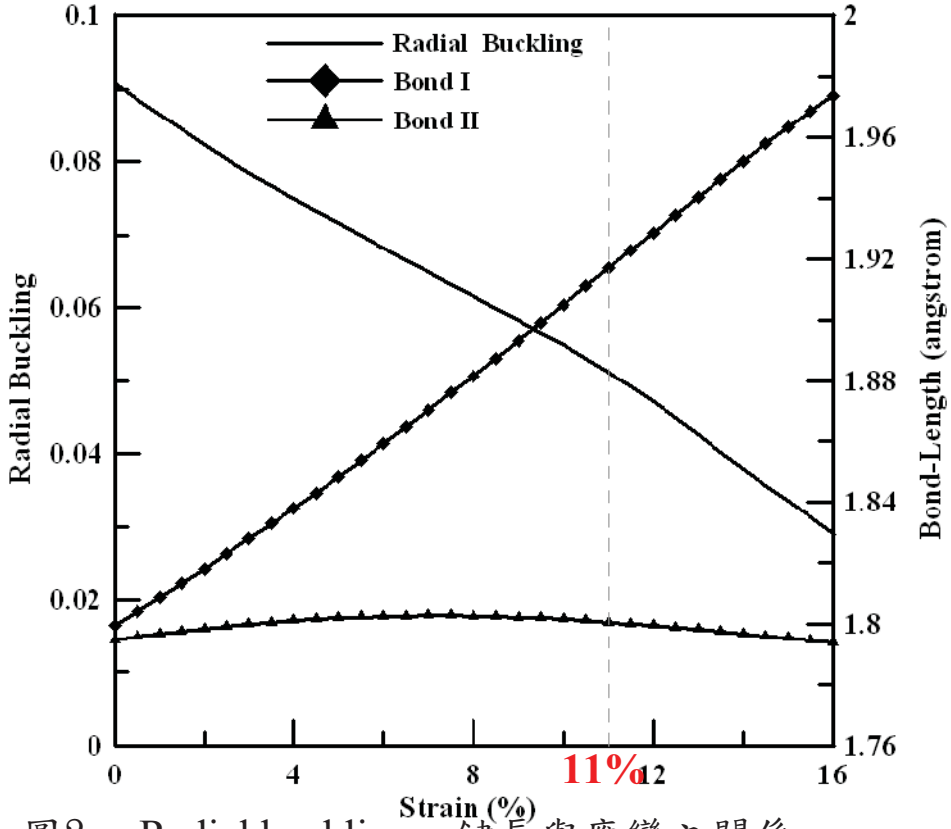

圖2 、Radial buckling、鍵長與應變之關係圖 。

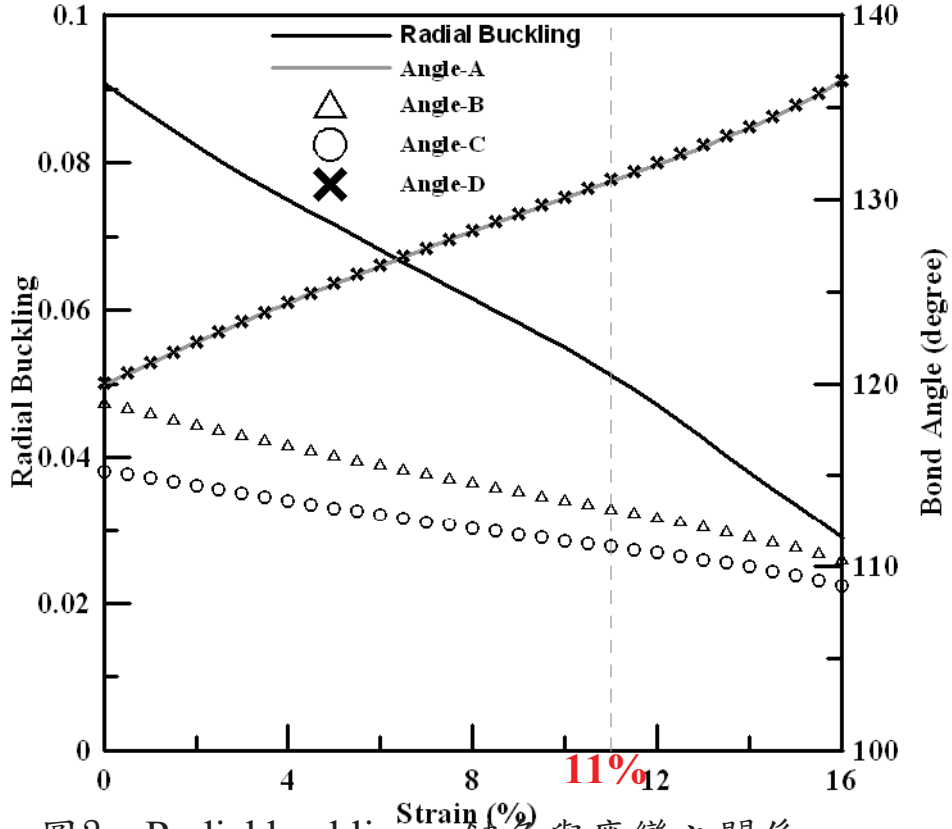

圖3、Radial buckling、鍵角與應變之關係圖 。

•Result and Discussion (結構-Radial Buckling)

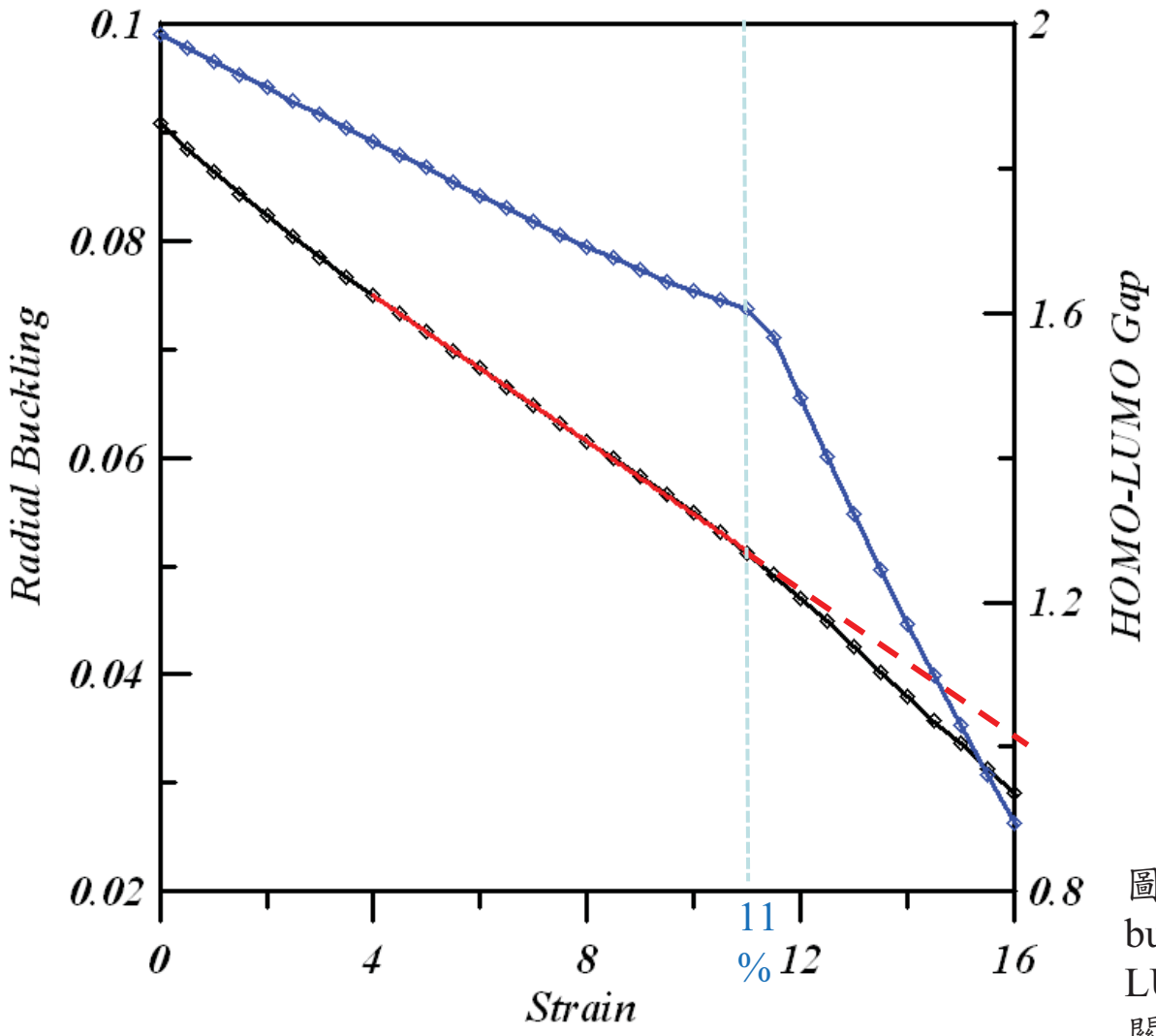

圖4、Radial buckling、HOMO-LUMO Gap與應變之關係圖。

•Result and Discussion (電性-deformation density)

Total Electron Density

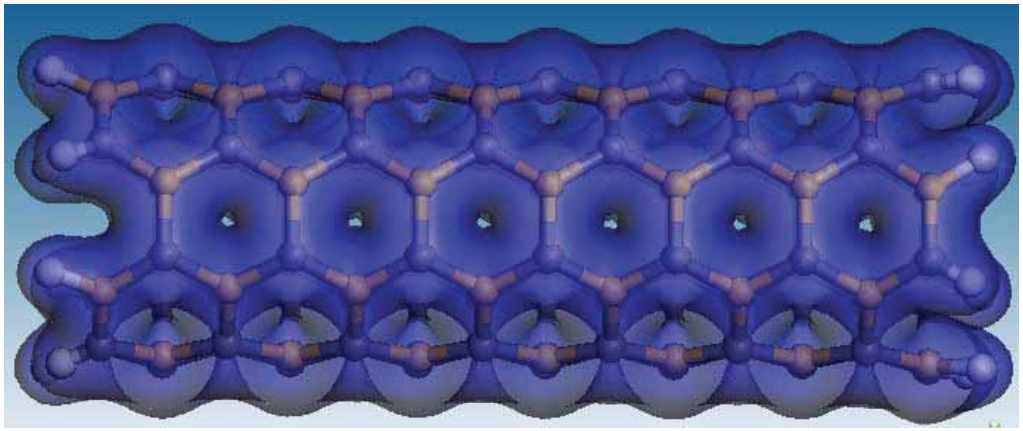

Single Electron Density

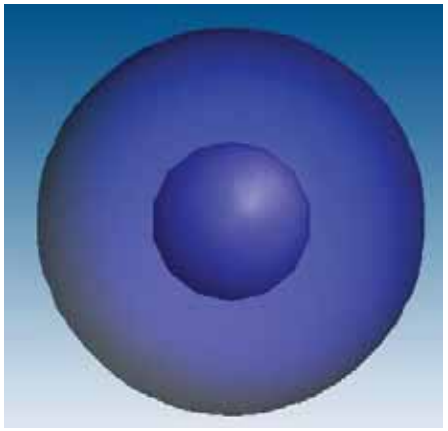

Deformation density

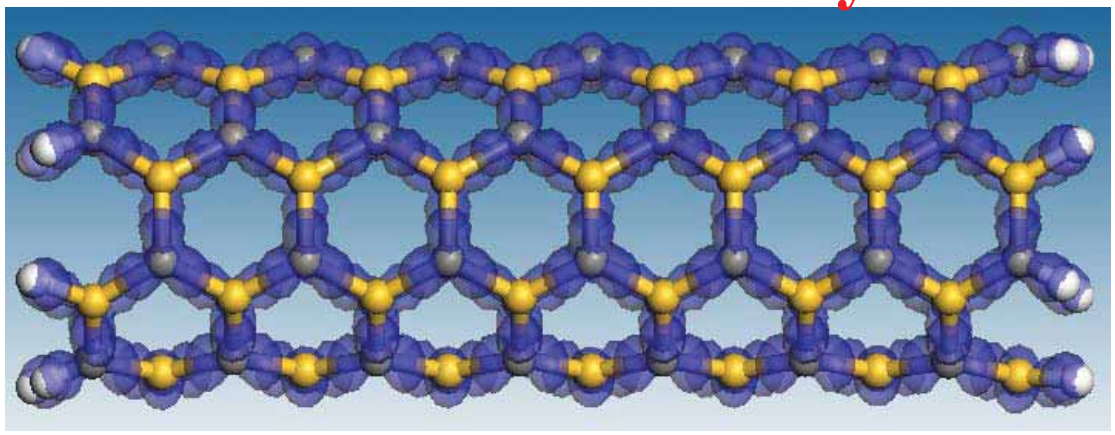

•Result and Discussion (電性-deformation density& BO)

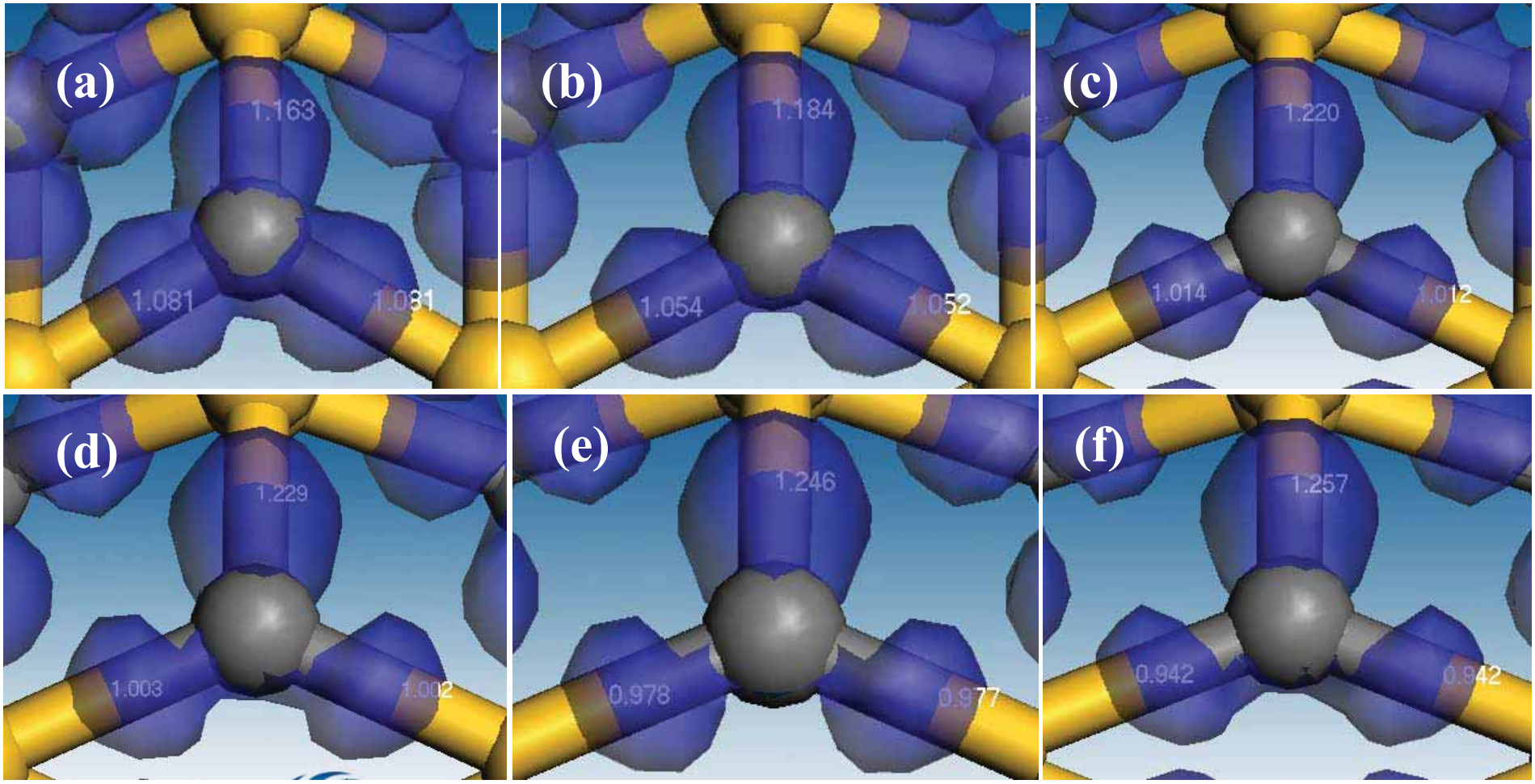

圖7、 不同應變率下的鍵級與電子態密度差。
(a)應變率=0%，(b)應變率=6%，(c)應變率=11%
(d)應變率=12%，(e)應變率=14%，(f)應變率=16%。

•Introduction & Motivation

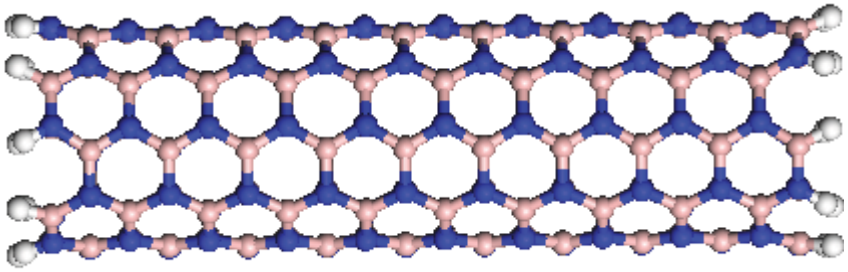

(4,4)armchair BNNT

Advantage:

1. High thermal stability.
2. High oxidation resistance
3. Good semiconductor
4. Good carrier for H_2 storage.*
5. Excellent candidates for field-emission device.**

Difference with CNT:

1.In armchair and zigzag configuration, it is always semiconductor.

Application:

1.Fule storage*

2.Semiconductor

* *Applied physic letters.*, **94** ,183110 (2009)

** *Nanotechnology.*, **20** ,085704 (2009)

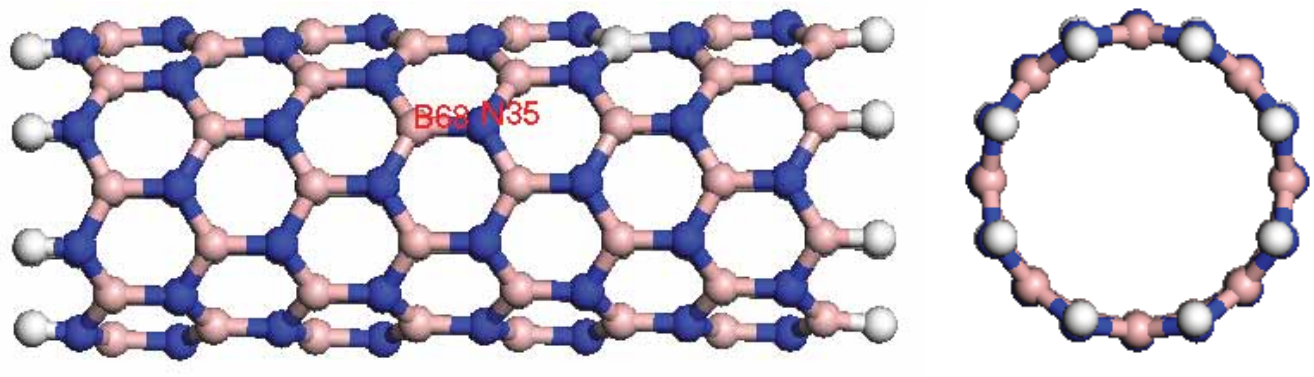

(a) single wall Zig-zag (8,0) BN Nanotube

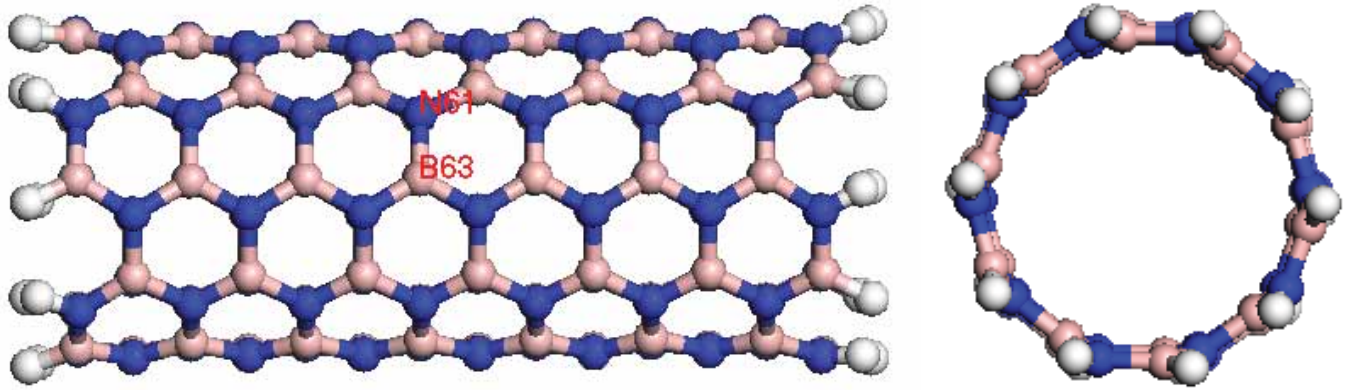

(b) single wall Armchair (5,5) BN Nanotube

The stress-strain profiles for (a)(8,0) Zigzag BN nanotube and (b)(5,5) Armchair BN nanotube.

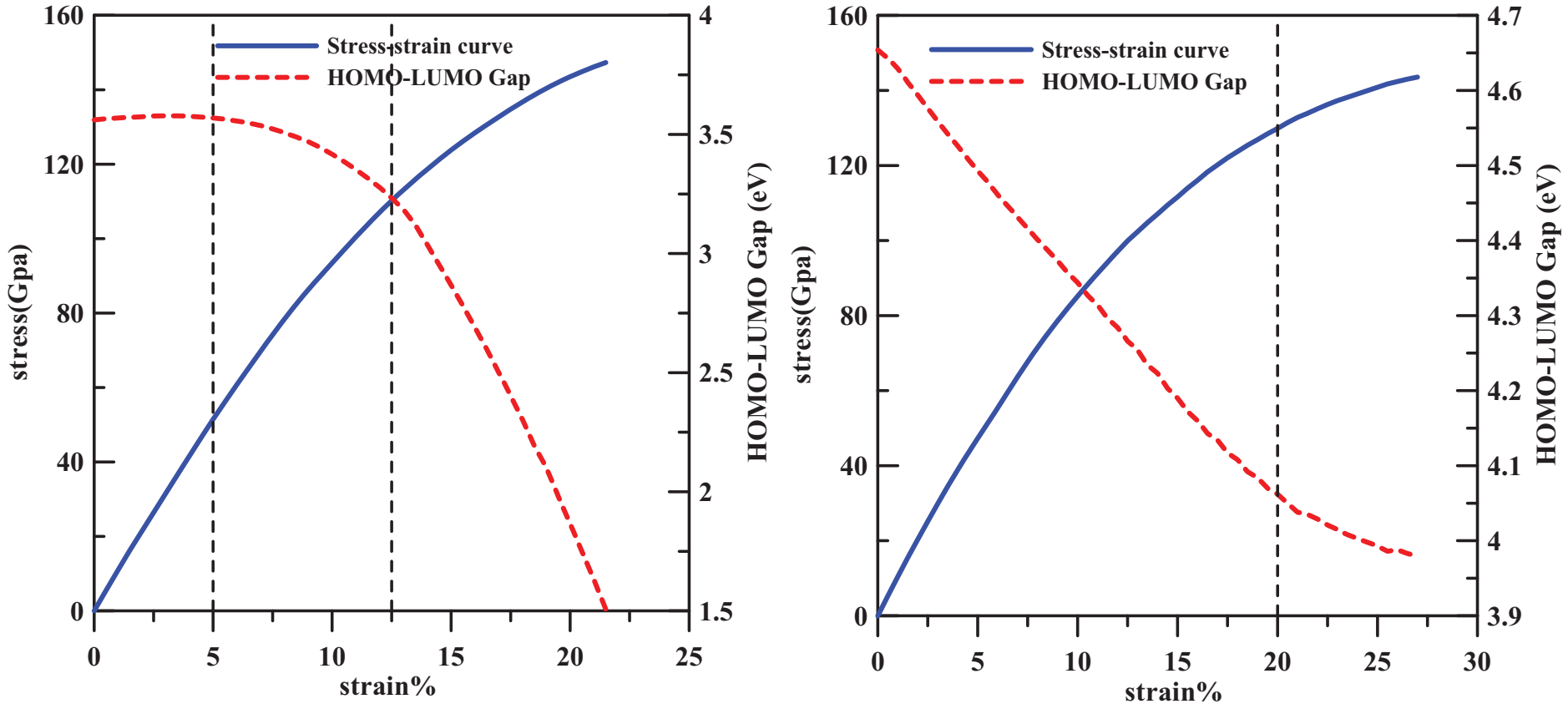

(a) (b)

*And the red line shows HOMO-LUMO gap variation with different strains.

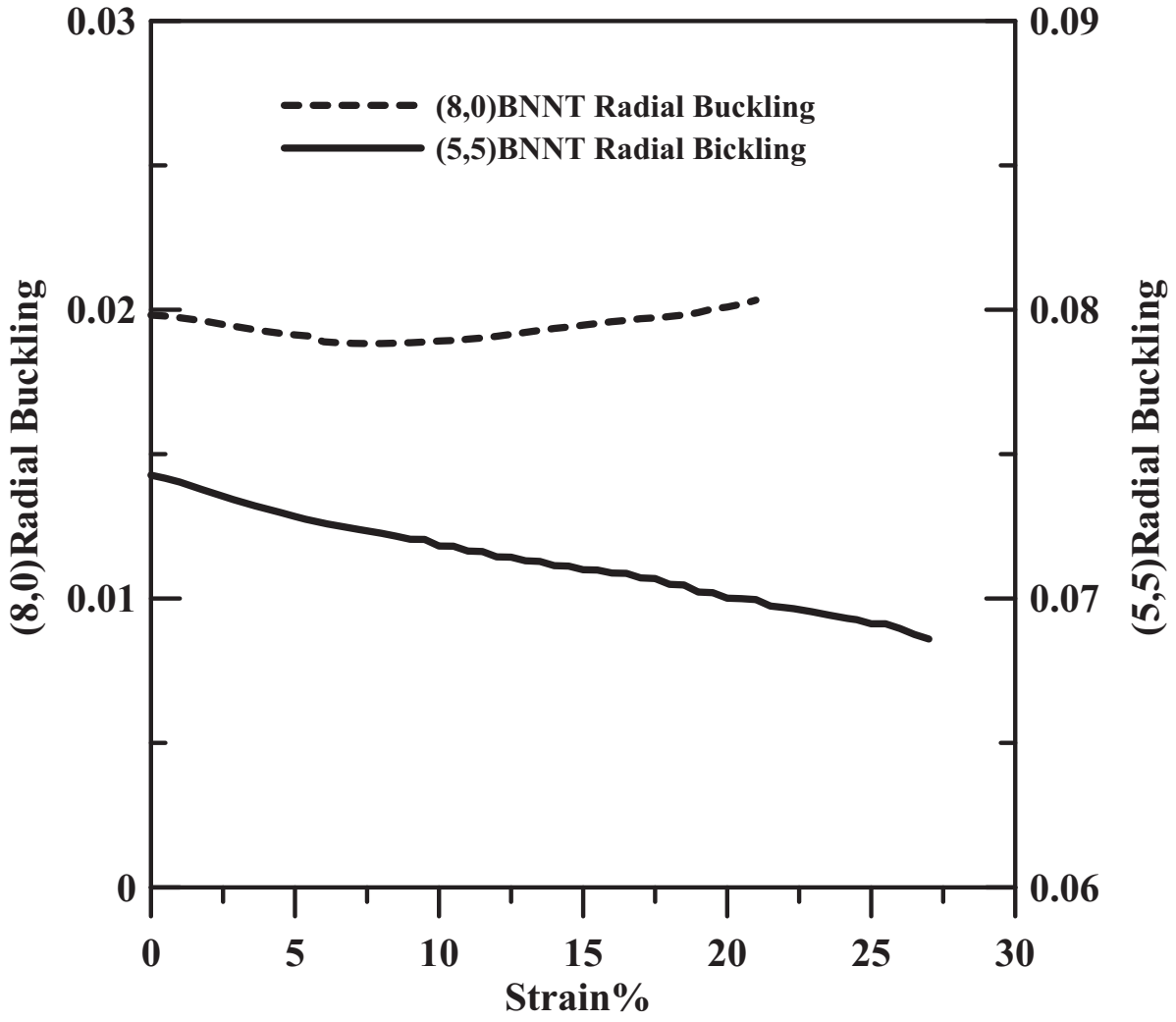

The Radial Buckling of (8,0) and (5,5) BN Nanotube.

•Introduction & Motivation

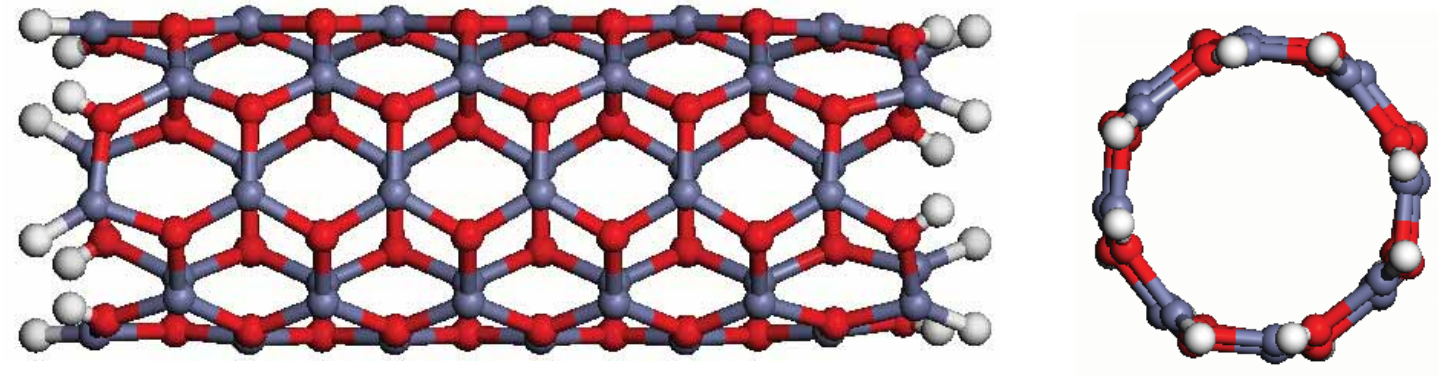

(4,4)armchair SiCNT

Advantage:

1. Wide direct band gap of 3.37 eV
2. Large exciton binding energy of 60 MeV
3. Good semiconductor

Application:

1. Gas Sensor[1]
2. Photo Catalysts[2]
3. Transparent Conductive Oxide [3]

1 *J Phys Chem C,* **111**, 1900 (2007)
2 *J Phys Chem B,* **104**, 319 (2000).
3 *J Phys D-Appl Phys,* **36**, 152 (2003)

•Result and Discussion (拉伸模擬的結構與電性分析)

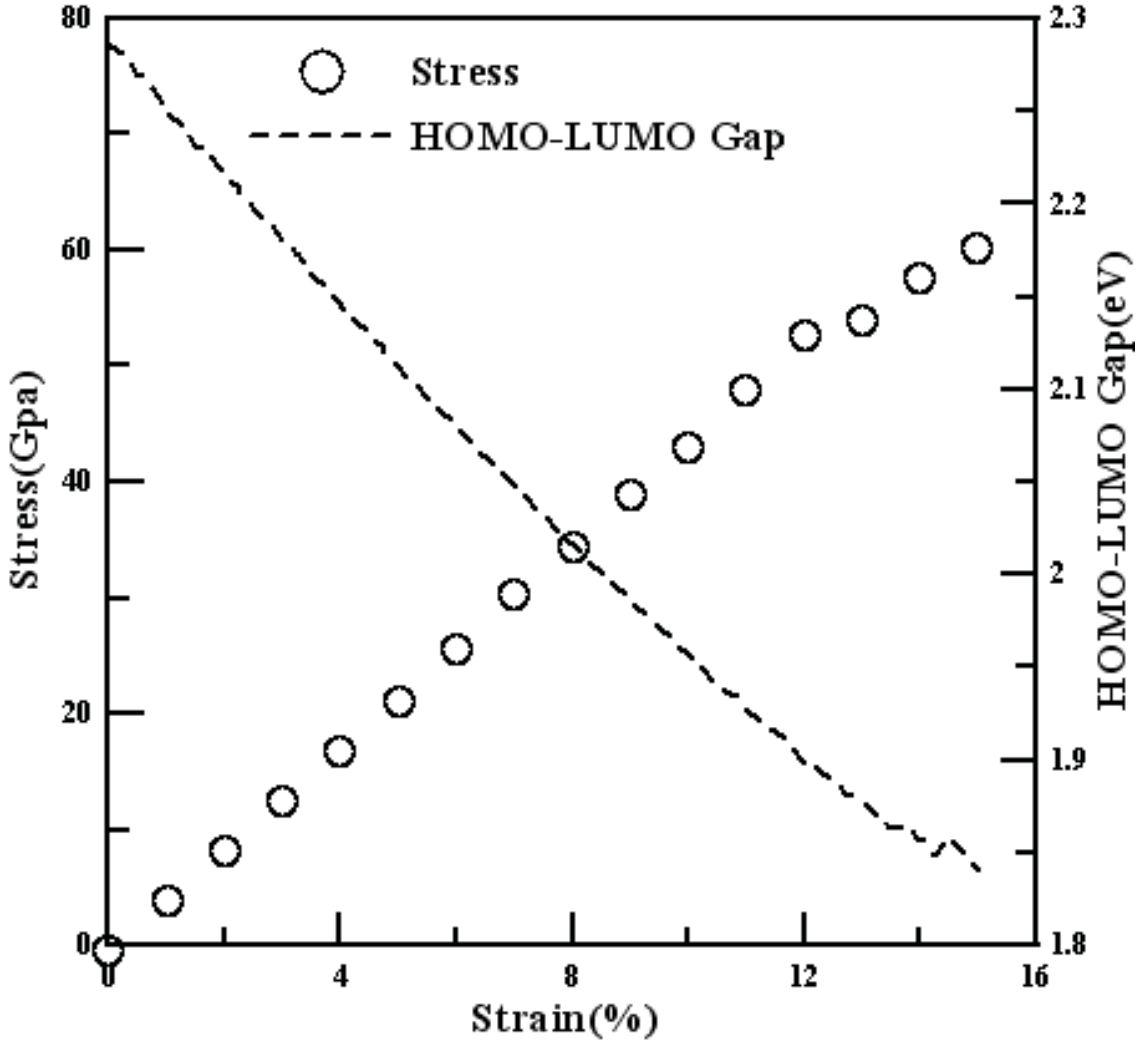

Solid line shows uni-axial stress-strain curve for (4,4) armchair ZNONT. Dashed line shows HOMO-LUMO gap variation with different strains.

•Result and Discussion(結構-鍵長鍵角)

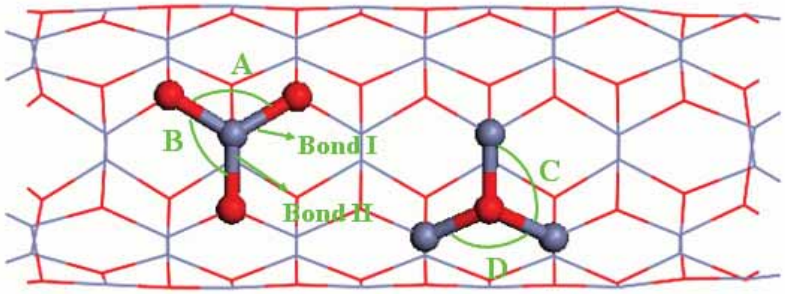

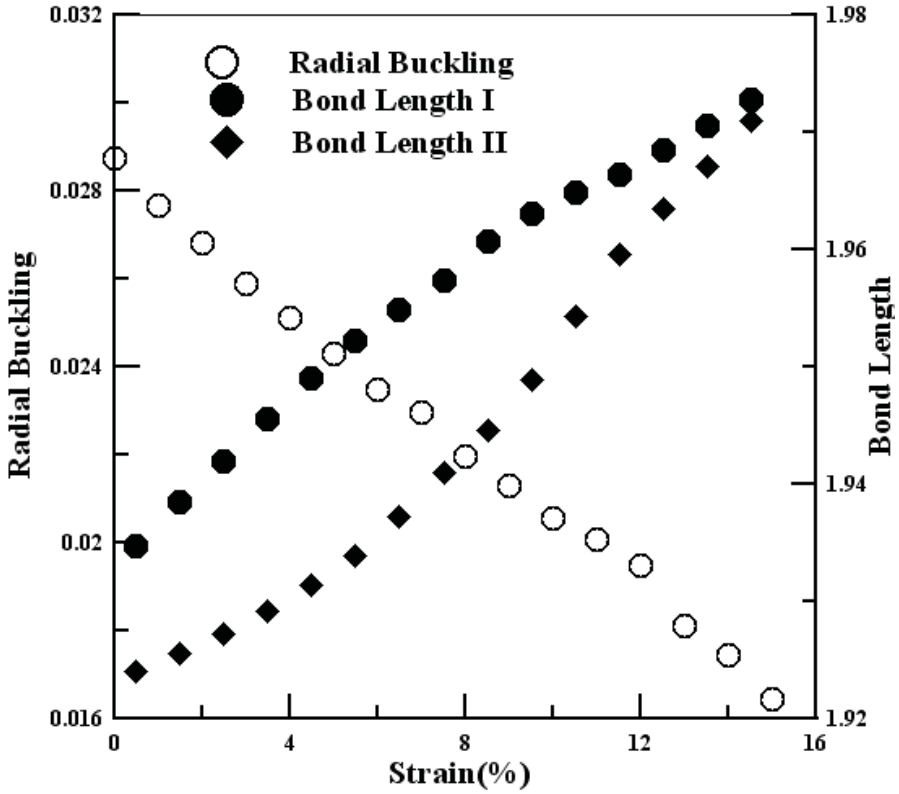

Variation of the radial buckling and bond lengths at different strains.

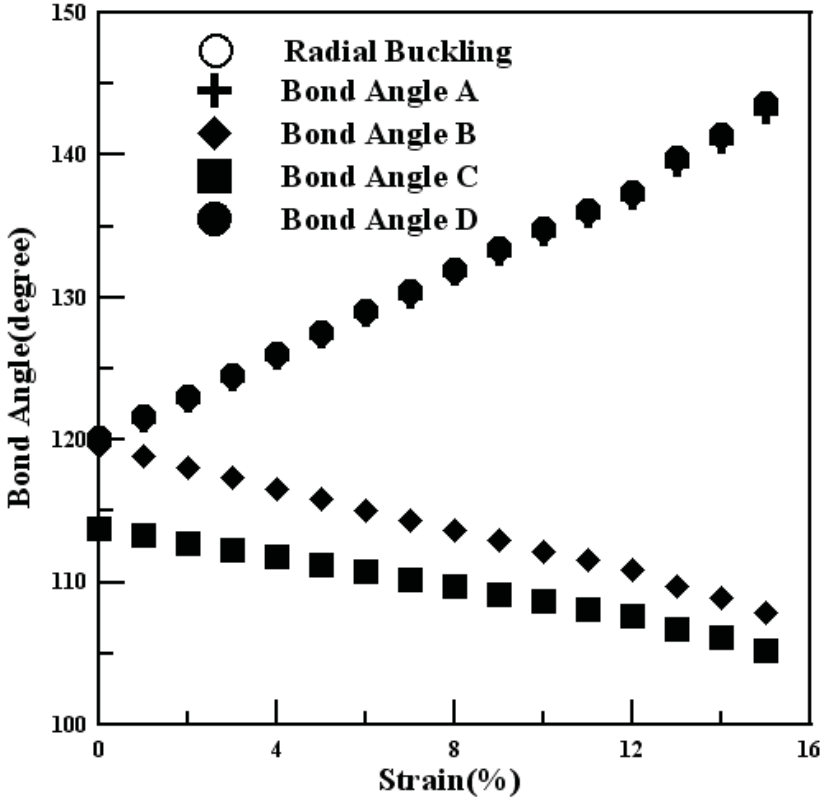

Variation of the bond angles are shown with the different strains.

•Result and Discussion (電性-charge transfer)

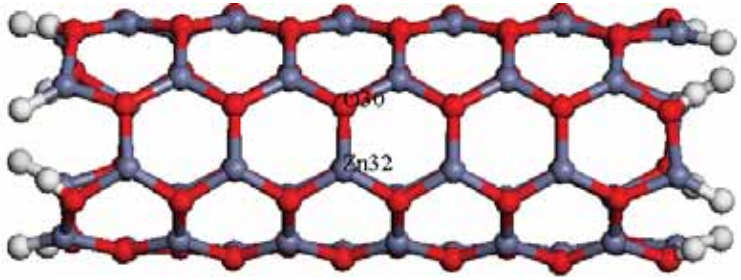

在應變率0%時，O30與Zn32的電荷量分別為0.705eV與-0.705eV，而當應變增加時，O30與Zn32的帶電量的變化並無較明顯的變化。

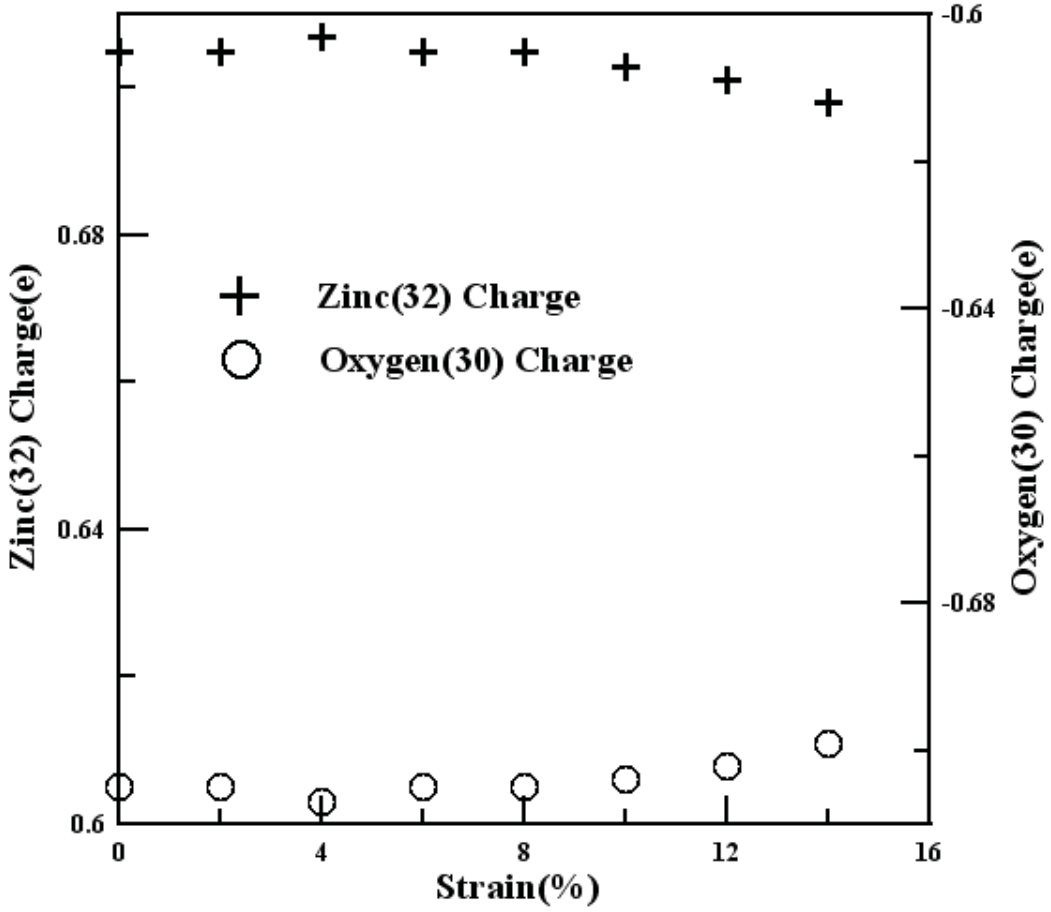

The solid line shows charge variation of O(30), and the dashed line shows Zn(32).

•Result and Discussion (電性-deformation density& BO)

(a) (b) (c)

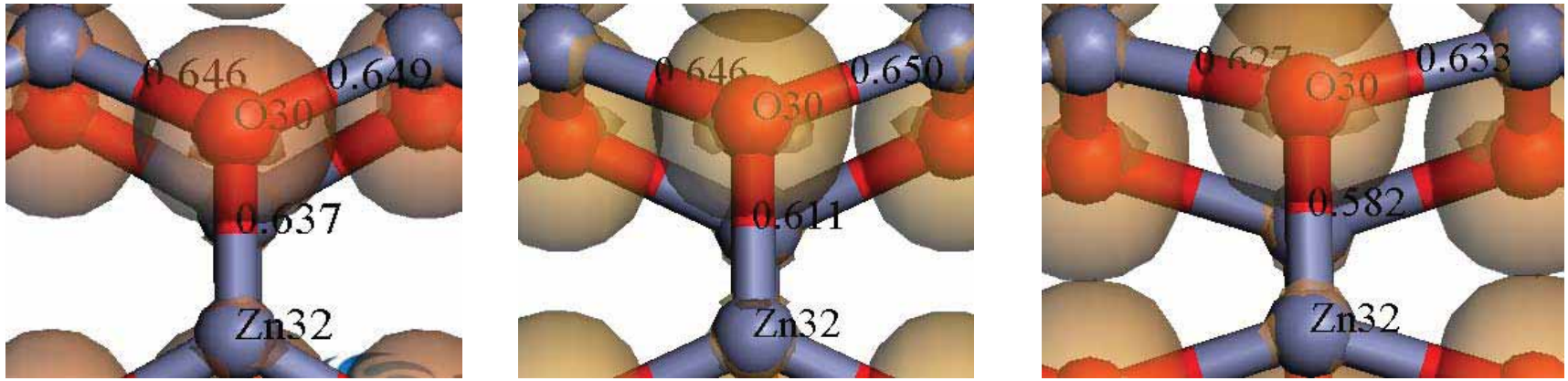

Deformation density and Mayer bond orders shown at different strains: (a)strain=0%, (b)strain=7.5%, (c)strain=15%

NATURE|Vol 454|21 August 2008

CHEMISTRY

Precious little catalyst

D. Wayne Goodman

In gold catalysis, less is more. Bulk gold is an inert metal, but tiny particles containing as few as 55 gold atoms are effective at catalysing the targeted oxidation of hydrocarbons.

doi:10.1038/nature07194

Selective oxidation with dioxygen by gold nanoparticle catalysts derived from 55-atom clusters

Mark Turner[1], Vladimir B. Golovko[1]†, Owain P. H. Vaughan[1], Pavel Abdulkin[1], Angel Berenguer-Murcia[1], Mintcho S. Tikhov[1], Brian F. G. Johnson[1] & Richard M. Lambert[1]

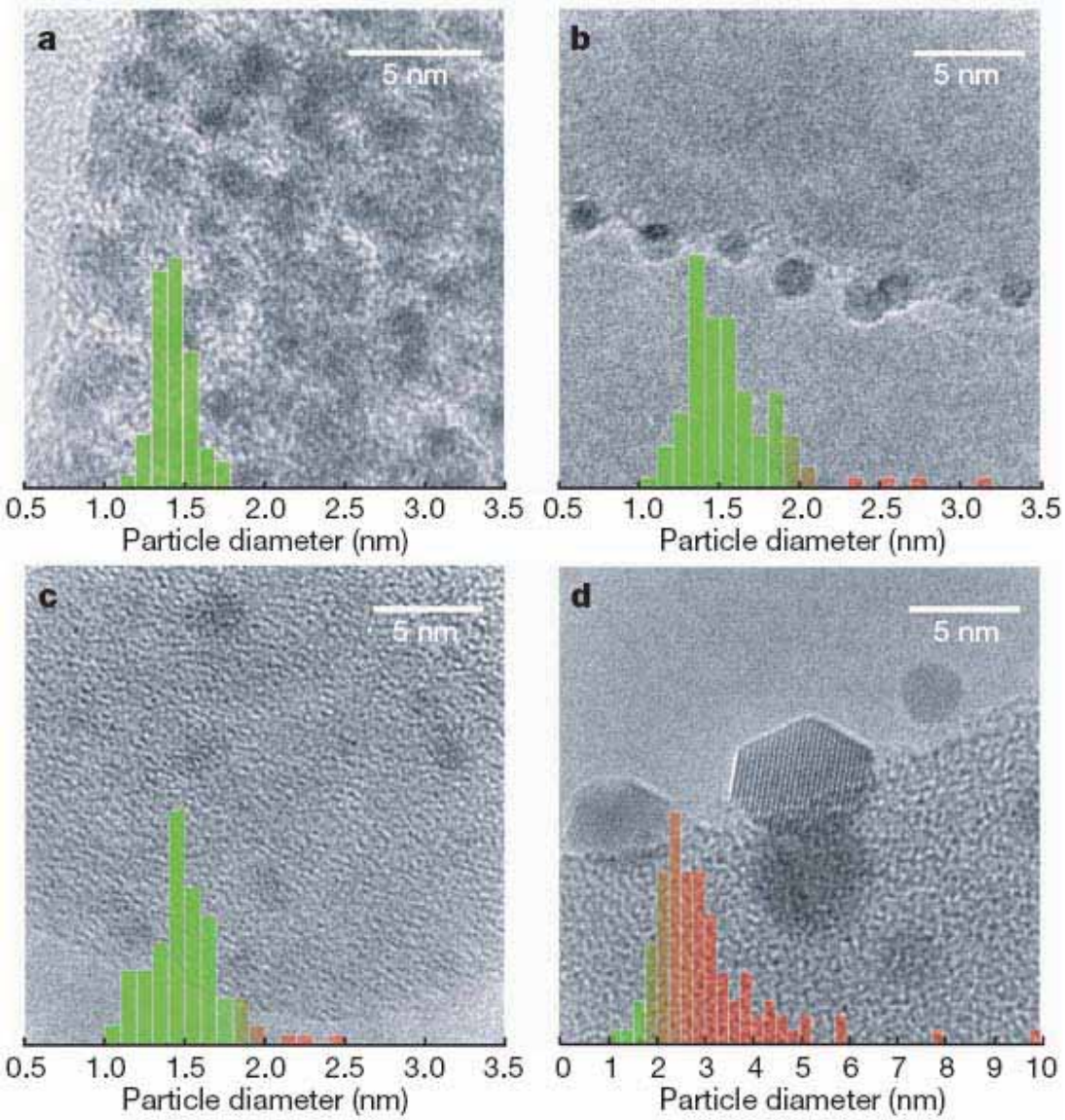

Figure 1 | High-resolution TEM images overlaid with corresponding particle size distributions for unsupported and supported Au_{55}. **a**, Freshly made, unsupported Au_{55}; **b**, 0.6-wt% Au_{55}/BN; **c**, 0.6-wt% Au_{55}/SiO_2; **d**, 6-wt% Au_{55}/SiO_2. Distributions are coloured to emphasize (green) the presence of particles of diameter <2 nm, which correlates with observed catalytic activity in the partial oxidation of styrene by O_2 alone.

Methods to find the lowest-energy nanoparticle structure

- Genetic algorithm (GA)
- Basin-Hopping (BH) method
- Big Bang method (BB)
- Generalized Simulated Annealing (by MC and MD)----- usually for very small nanoparticles (<10 atoms)

All are based on **Stochastic Method** and potential function is required to describe the interaction between atoms !!!!

Genetic Algorithm

J. Chem. Soc., *Dalton Trans.*, 2002, 4375–4388 (TB potential)

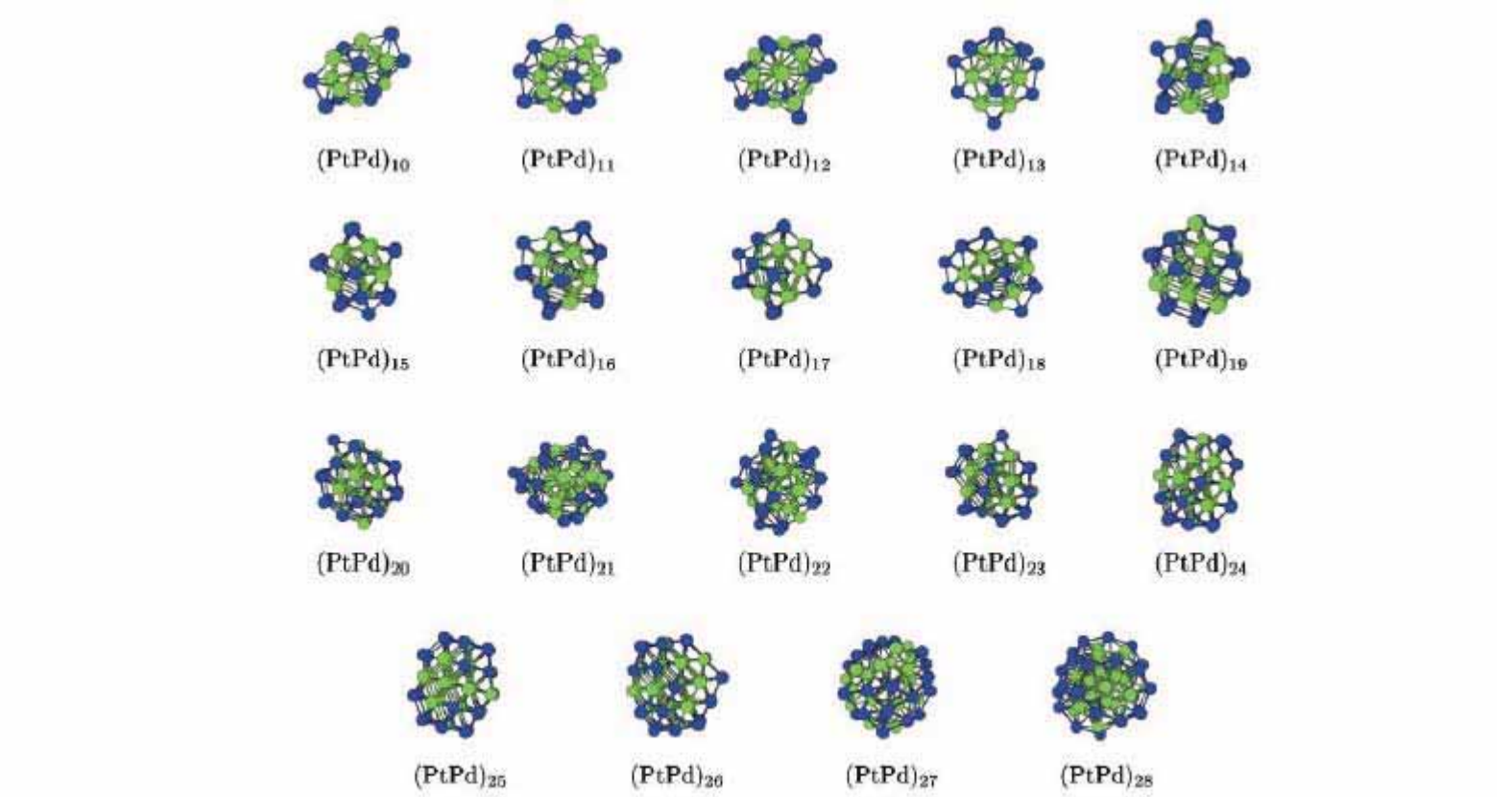

Fig. 5 GM for Pt–Pd nanoalloy clusters $(PtPd)_5$–$(PtPd)_{28}$, using Pt–Pd parameter set **I**. Colour scheme as in Figs. 1 and 3 (green = Pt; blue = P

GM Structures by tight-binding potential

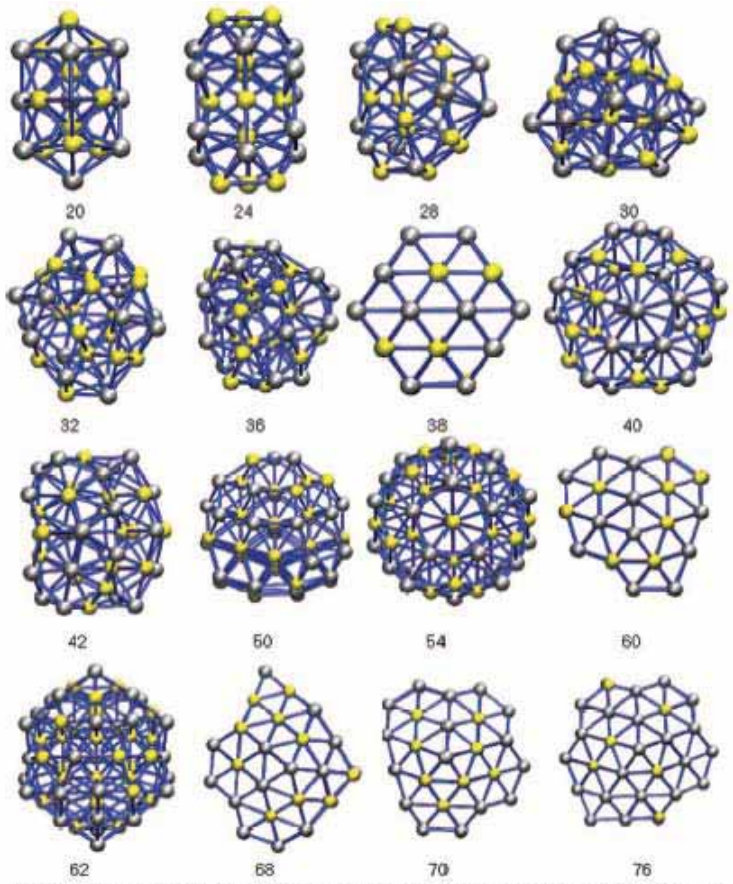

Figure 3. Typical geometries of $(AgAu)_n$ nanoalloys with 20–76 atoms. Gold atoms are shown in yellow.

GM structures by different potential functions

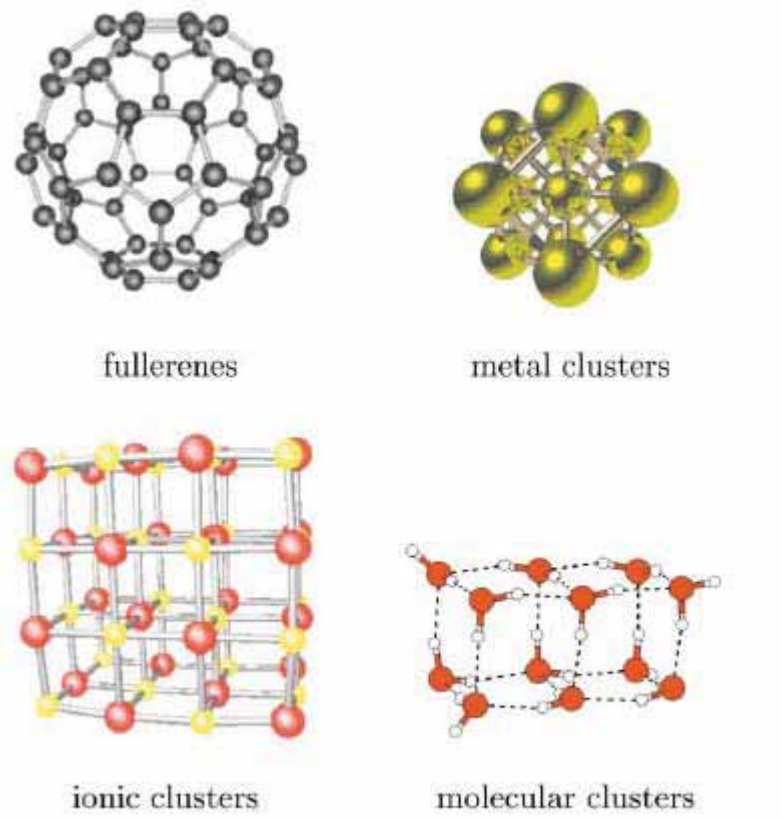

Fig. 1 Examples of some cluster types.

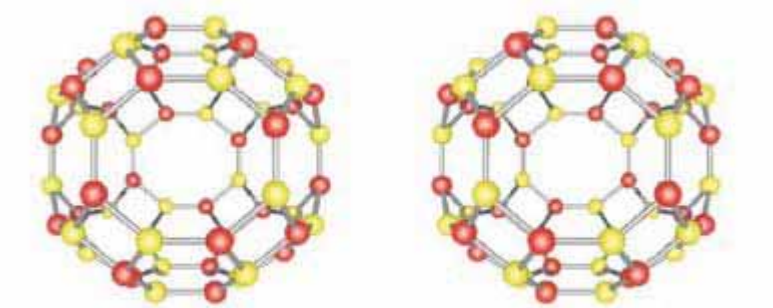

Fig. 13 Enantiomers of $(Mg^{2+}O^{2-})_{30}$.

Basin-Hopping method

(*J. Phys. Chem. A* **1997,** *101,* 5111-5116)

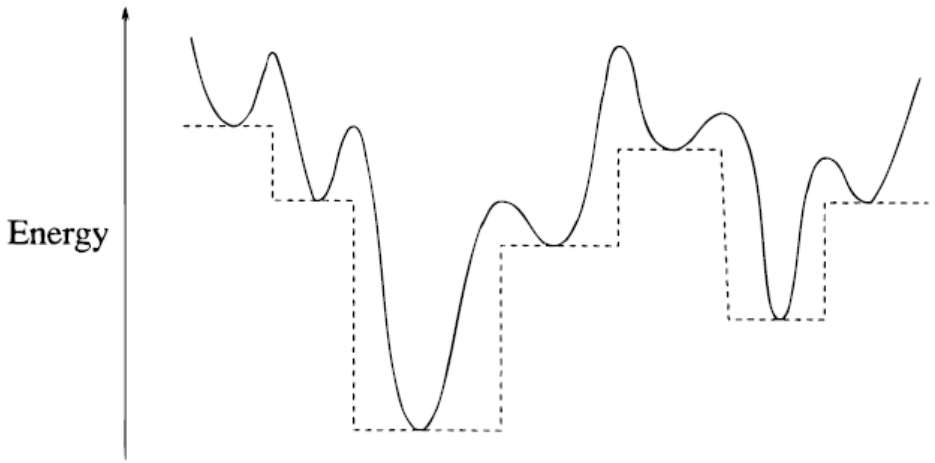

Figure 2. A schematic diagram illustrating the effects of our energy transformation for a one-dimensional example. The solid line is the energy of the original surface and the dashed line is the transformed energy $\tilde{E}$.

$$\tilde{E}(\mathbf{X}) = \min\{E(\mathbf{X})\}$$

MC+MS (CG)

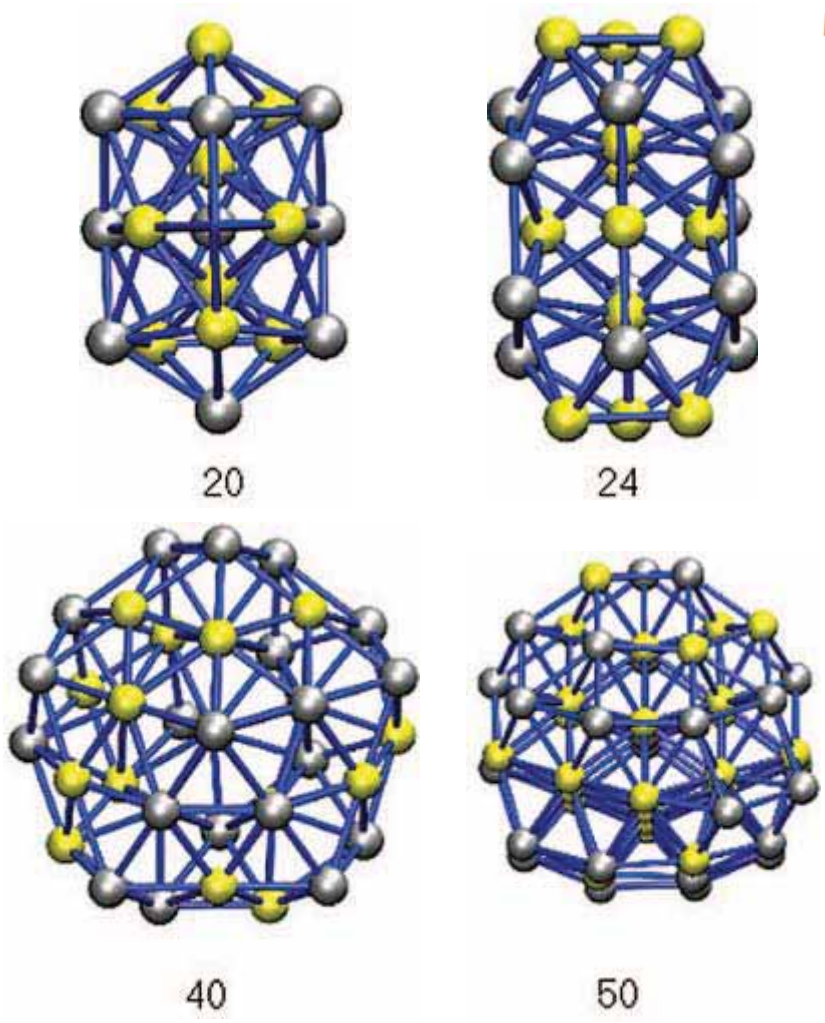

Fig.1 The $(AuAg)_n$ Geometries 20, 24, 40, and 50

TABLE 2. Energies and Structures of Putative Global Minima for Ag–Au Nanoalloys Using the Gupta Potential[a]

N	m	$V_{cluster}$ /eV	motif
20	0	−59.8055	twinned Ih_{13}
22	0	−66.0641	twinned Ih_{13}
24*	0	−72.4511	twinned Ih_{13}
26	0	−78.7359	twinned Ih_{13}
28	0	−85.1242	twinned Ih_{13}
30	0	−91.4427	twinned Ih_{13}
32	0	−97.8645	twinned Ih_{13}
34	0	−104.2488	twinned Ih_{13}
36	0	−110.6621	twinned Ih_{13}
38*	0	−117.3134	TO
40	0	−123.5324	Ih_{55}
42	1	−129.9734	twinned Ih_{13}
44	1	−136.2704	Ih_{55}
46	0	−142.8379	Ih_{55}
48	1	−149.3340	Ih_{55}
50	1	−155.7478	twinned Dh

Comparing to the our simulation result

N	m	$V_{cluster}$ /eV	motif
20	0	−59.8055	twinned Ih_{13}
24*	0	−72.4511	twinned Ih_{13}
40	0	−123.5324	Ih_{55}
50	1	−155.7478	twinned Dh

-59.80546

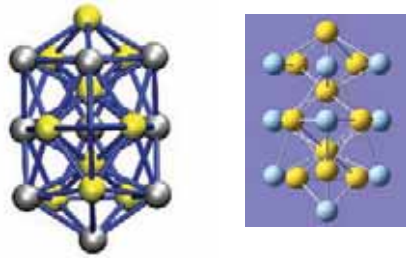

-72.45108

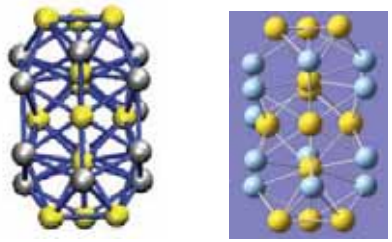

-123.5599

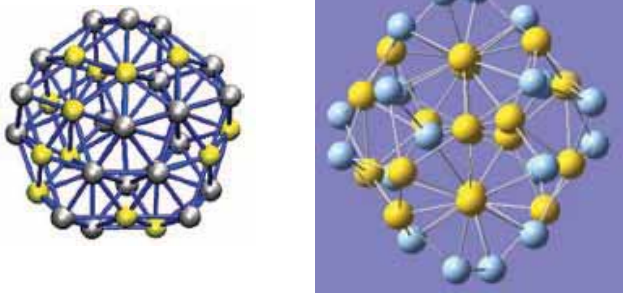

-155.9399

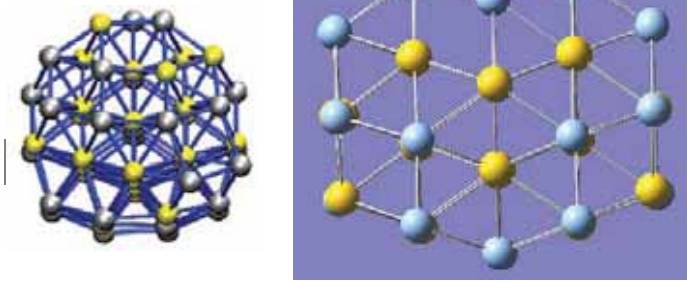

Statistical evaluation of the big bang search algorithm

(1. PRL (2004). 2.Computational Materials Science (2006))

1. Put atoms in a very small space.
2. Using molecular statics (LBFGS) to find local minimal structure.
3. Independent initial compressed structure and good for parallel calculation.

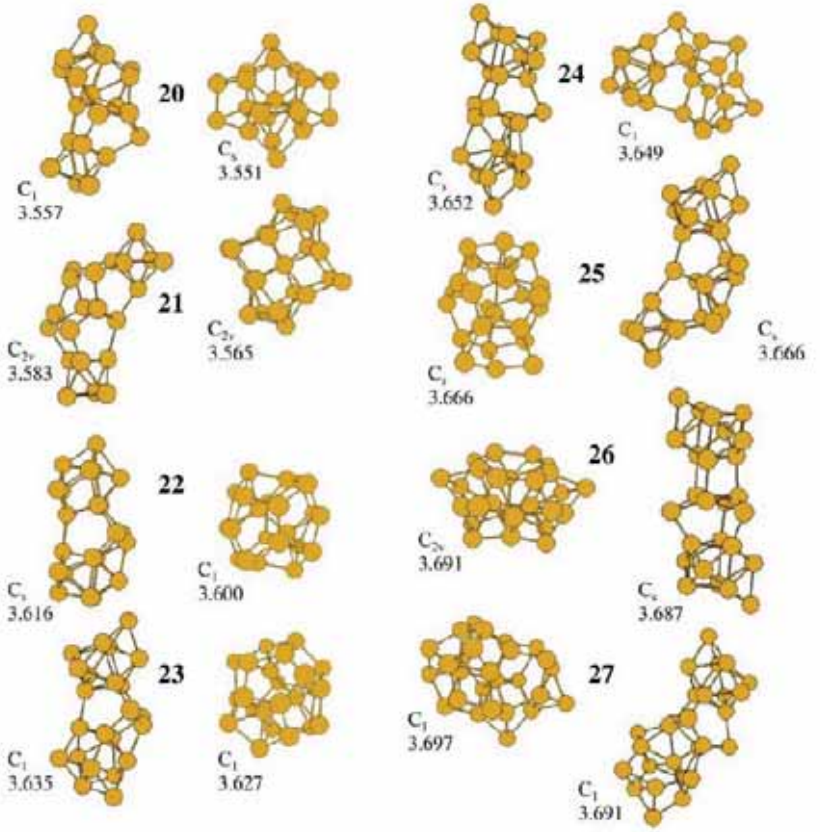

Fig. 5. Lowest energy prolate and compact structures for Si_n^+ for $n = 20$–27. The symmetry of the structures is given, along with the cohesive energy per atom in eV.

Our Study- Find the chemical reaction sites of a $(AuAg)_n$ nanoparticle

(Big Bang + Basin-Hopping methods)

$(AuAg)_{10}$ Fukui Function (+) Fukui Function (-)

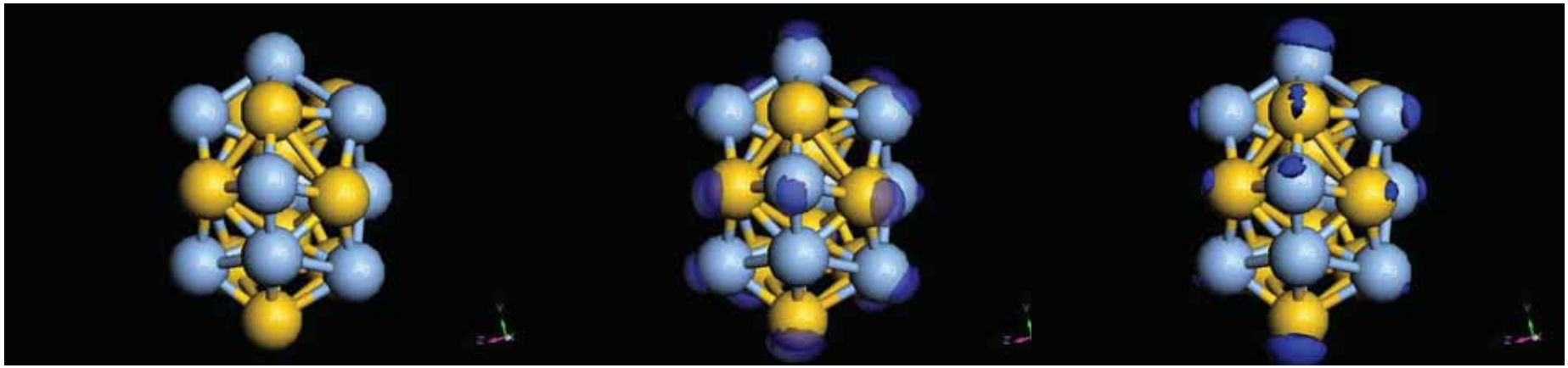

$(AuAg)_{19}$ Fukui Function (+) Fukui Function (-)

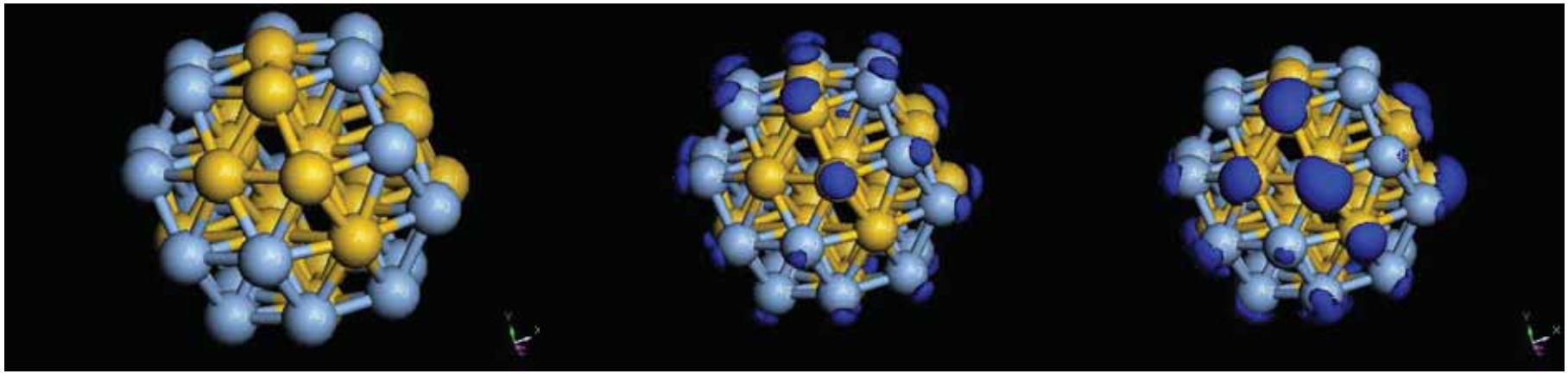

Atomic structure evolution of Zr-Ni Bulk Metallic Material (BMG) during severe deformation by HA pair analysis

1. *P. J. Hsieh, Yu-Chieh Lo, Chung-Ting Wang, J. C. Huang , and Shin-Pon Ju, intermetallic (2007)*
2. *Yu-Chieh Lo, J. C. Huang, Shin-Pon Ju, and X. H. Du Physical Review B* (2007)

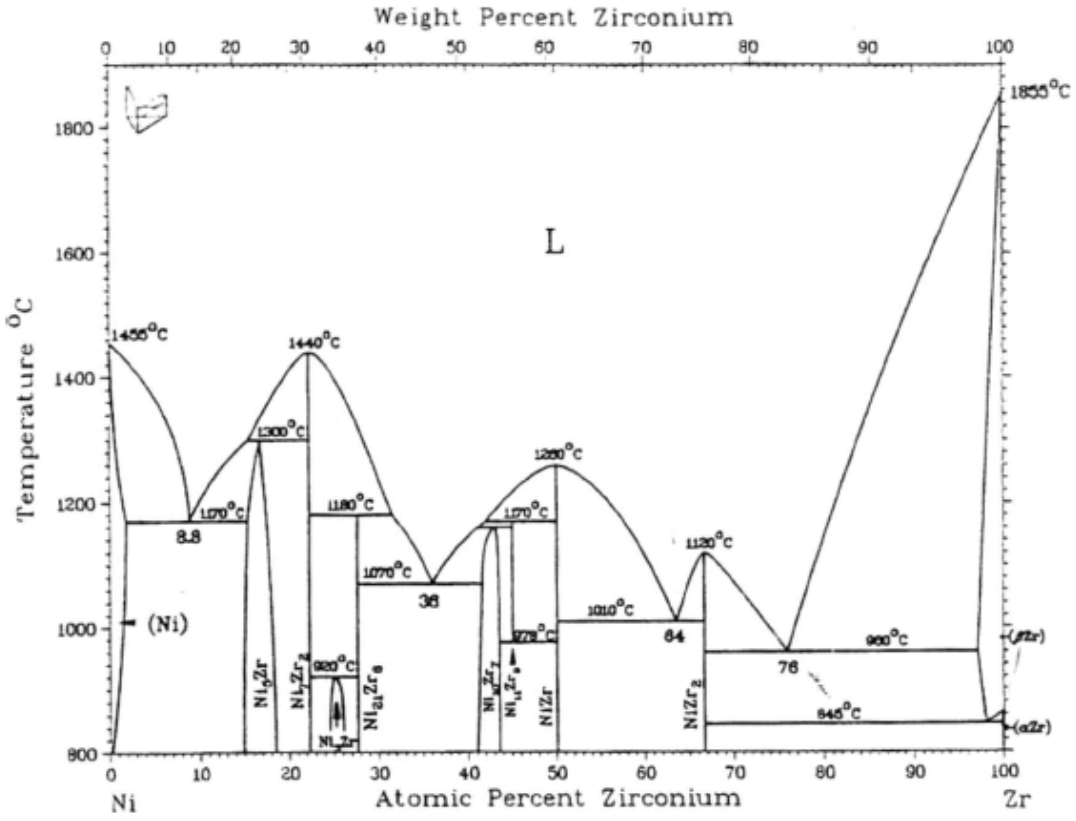

FIG. 2. Equilibrium phase diagrams for Zr-Ni (Ref. 37).

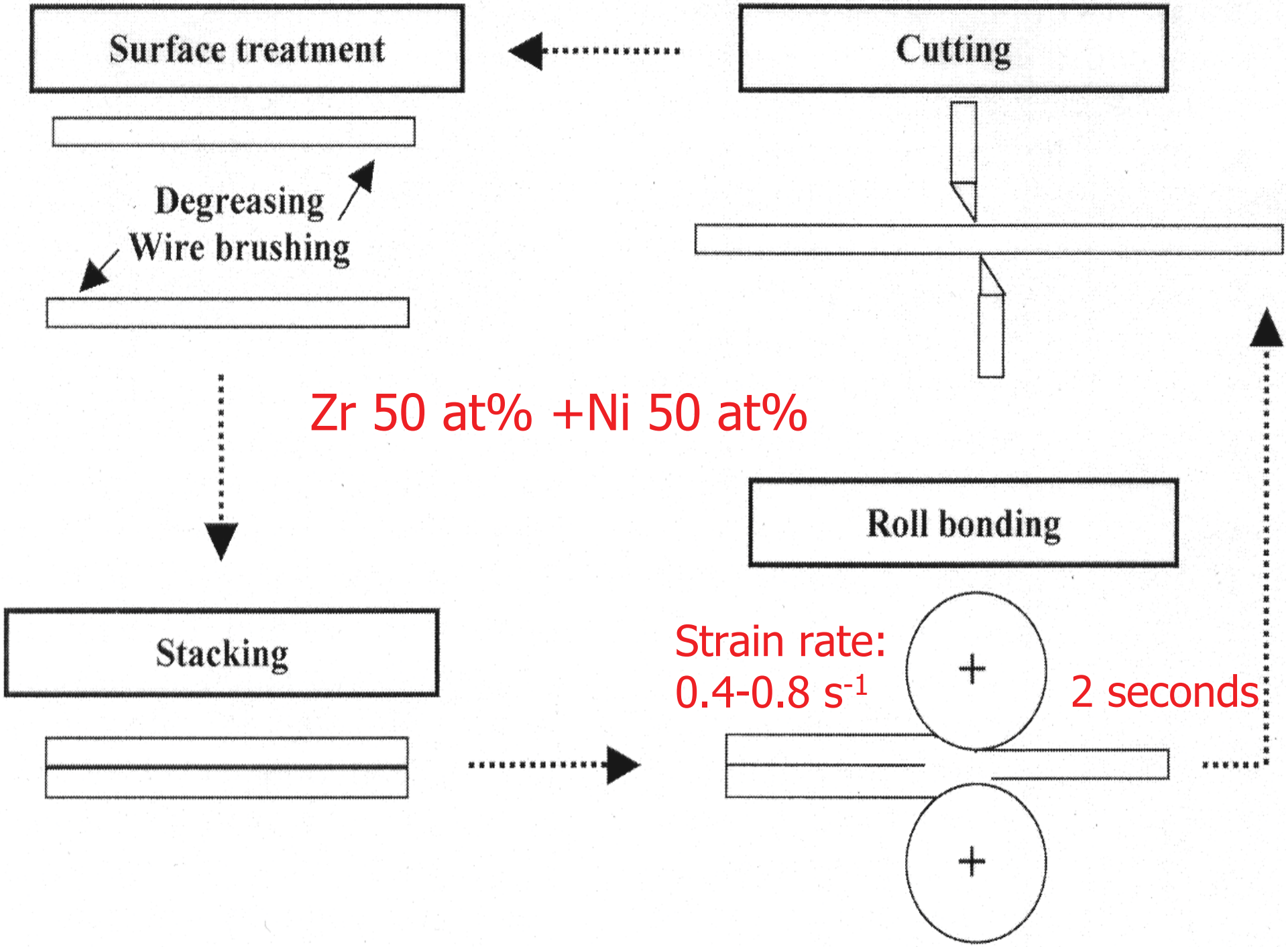
Surface treatment
Cutting
Degreasing
Wire brushing
Zr 50 at% +Ni 50 at%
Roll bonding
Stacking
Strain rate:
0.4-0.8 s-1
2 seconds

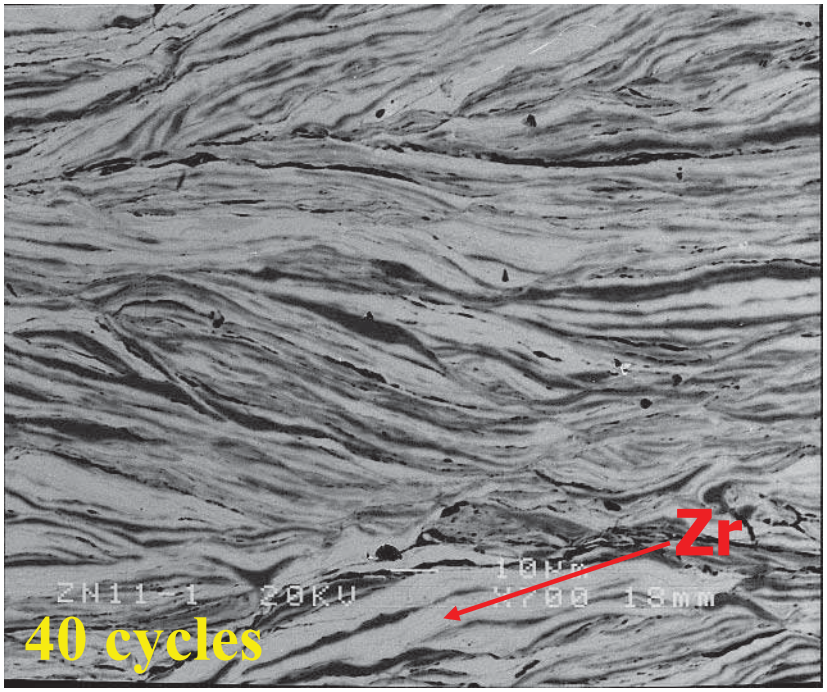
Zr
40 cycles


60 cycles

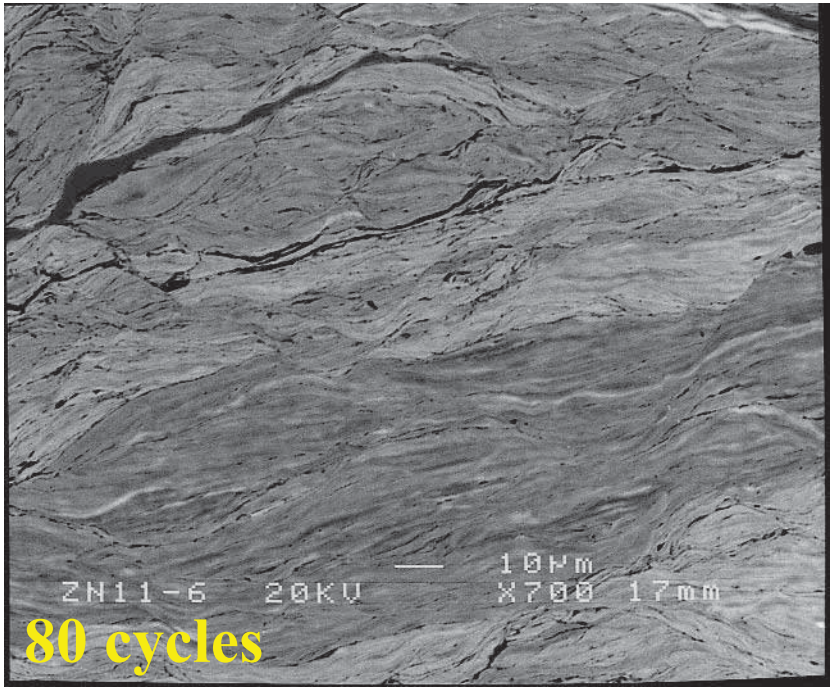
ZN11-6 20KV
10μm
X700 17mm
80 cycles

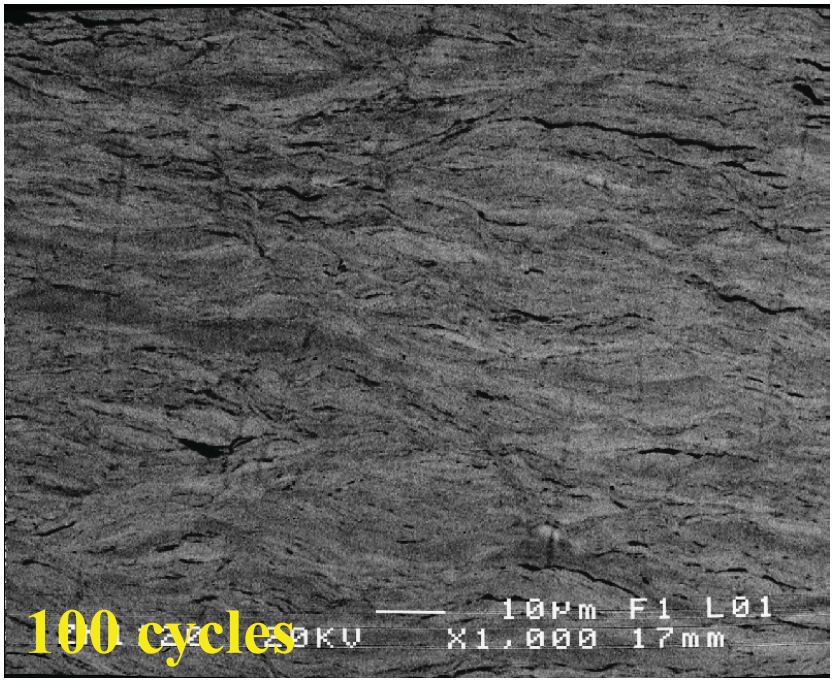
10μm F1 L01
X1,000 17mm
100 cycles

MD simulations

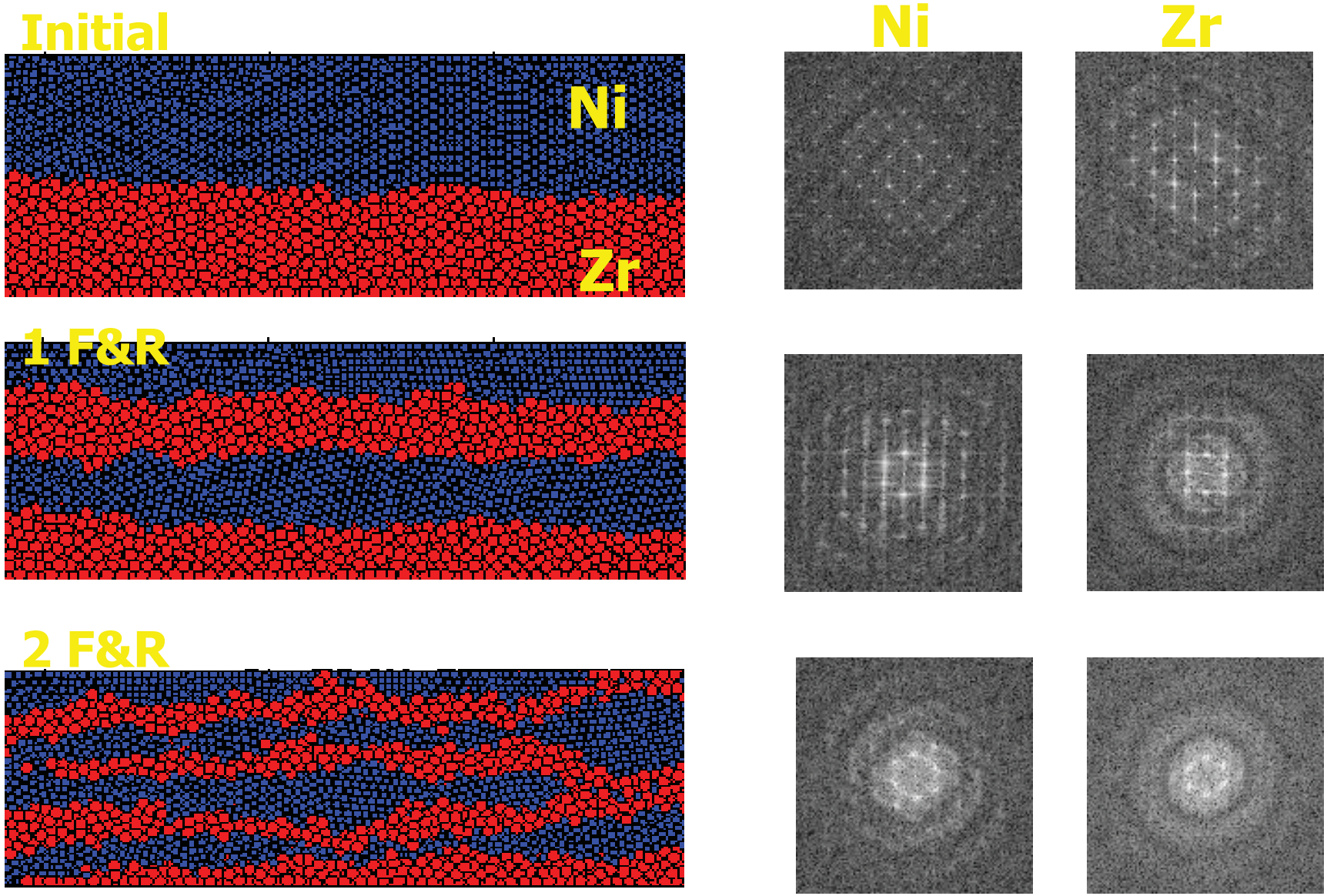

3 F&R

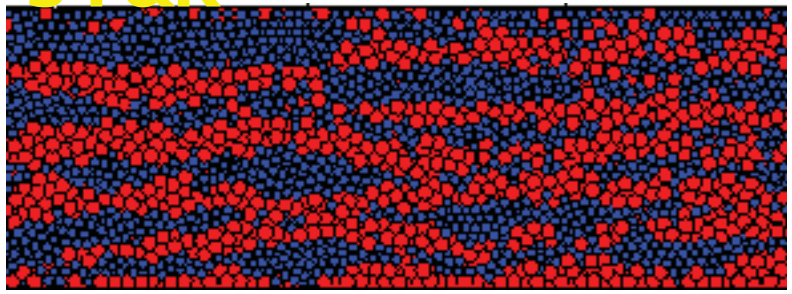

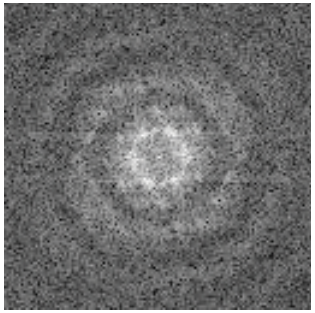

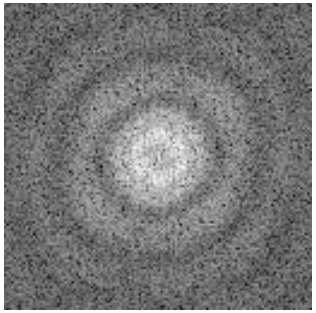

4 F&R

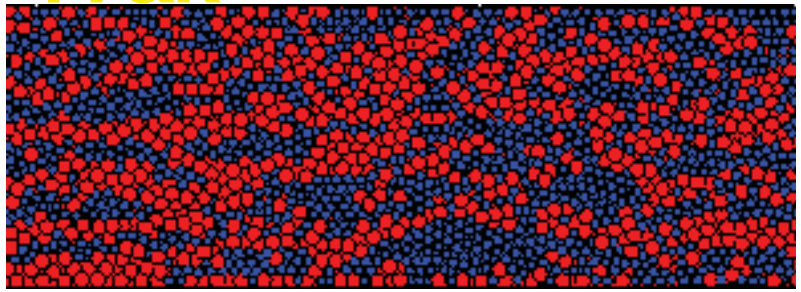

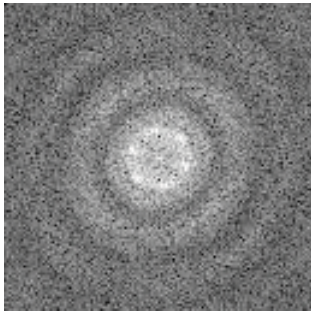

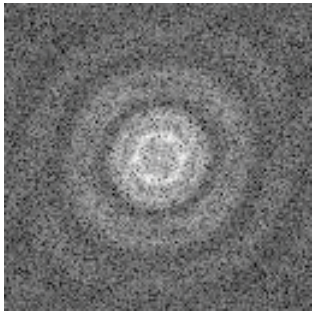

5 F&R

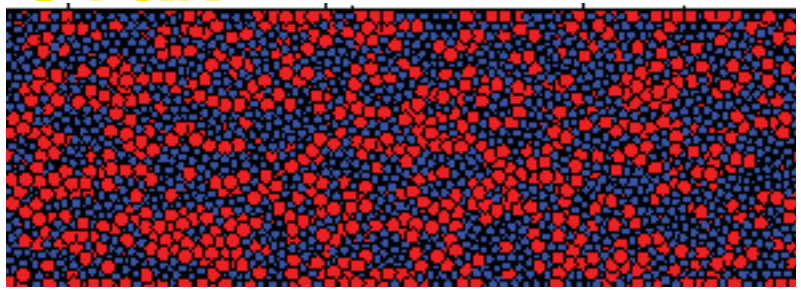

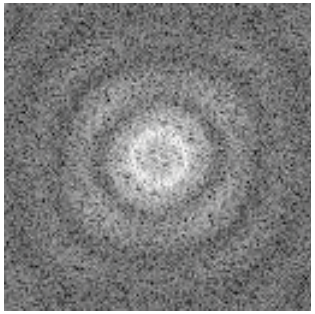

6 F&R

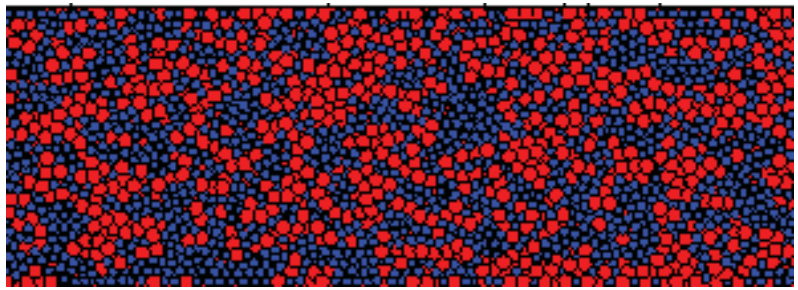

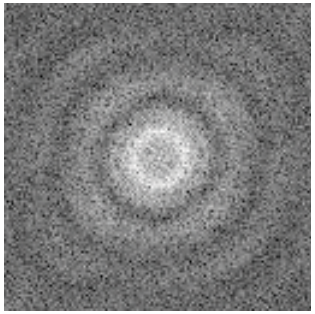

Potential Energy via various F&R cycles

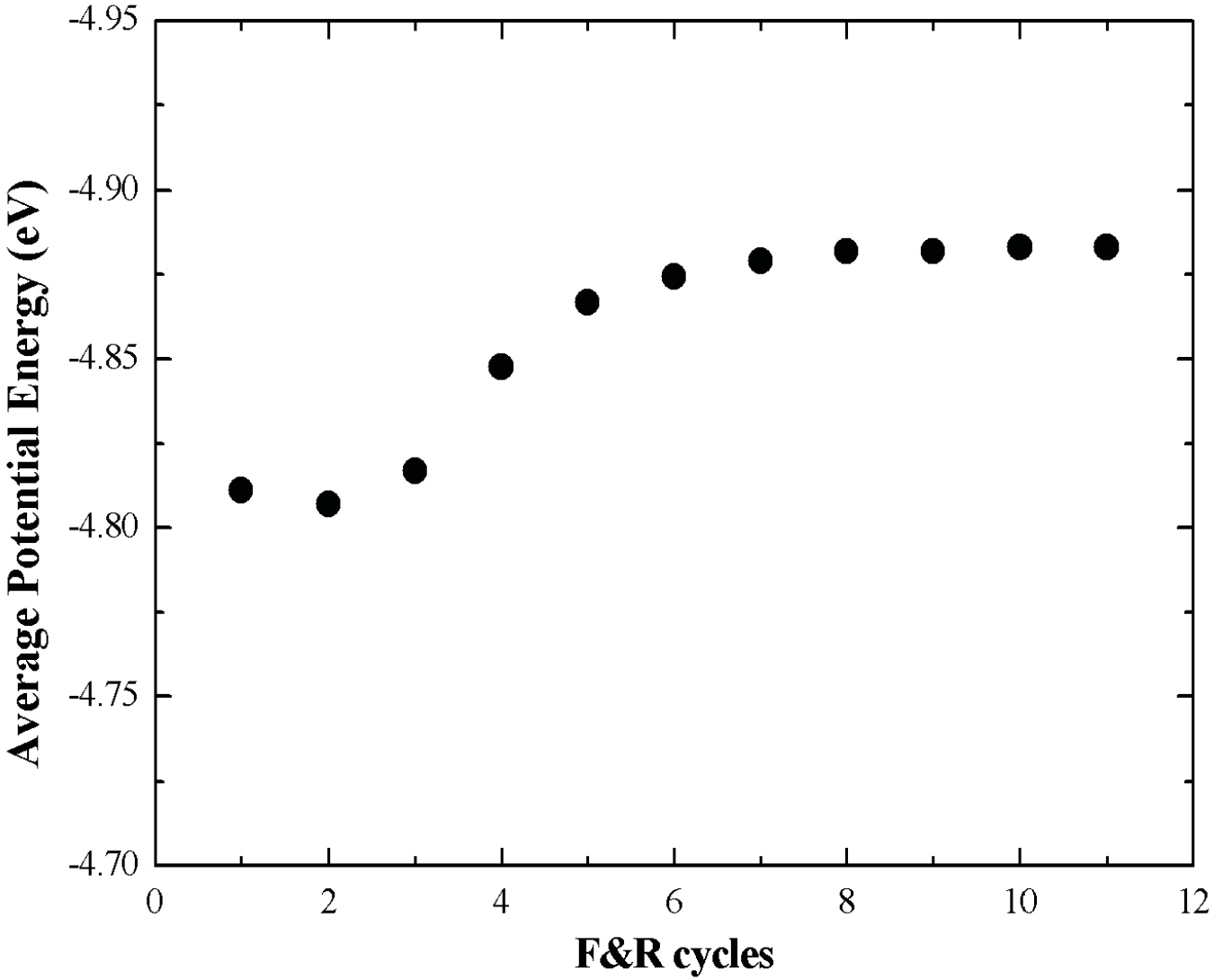

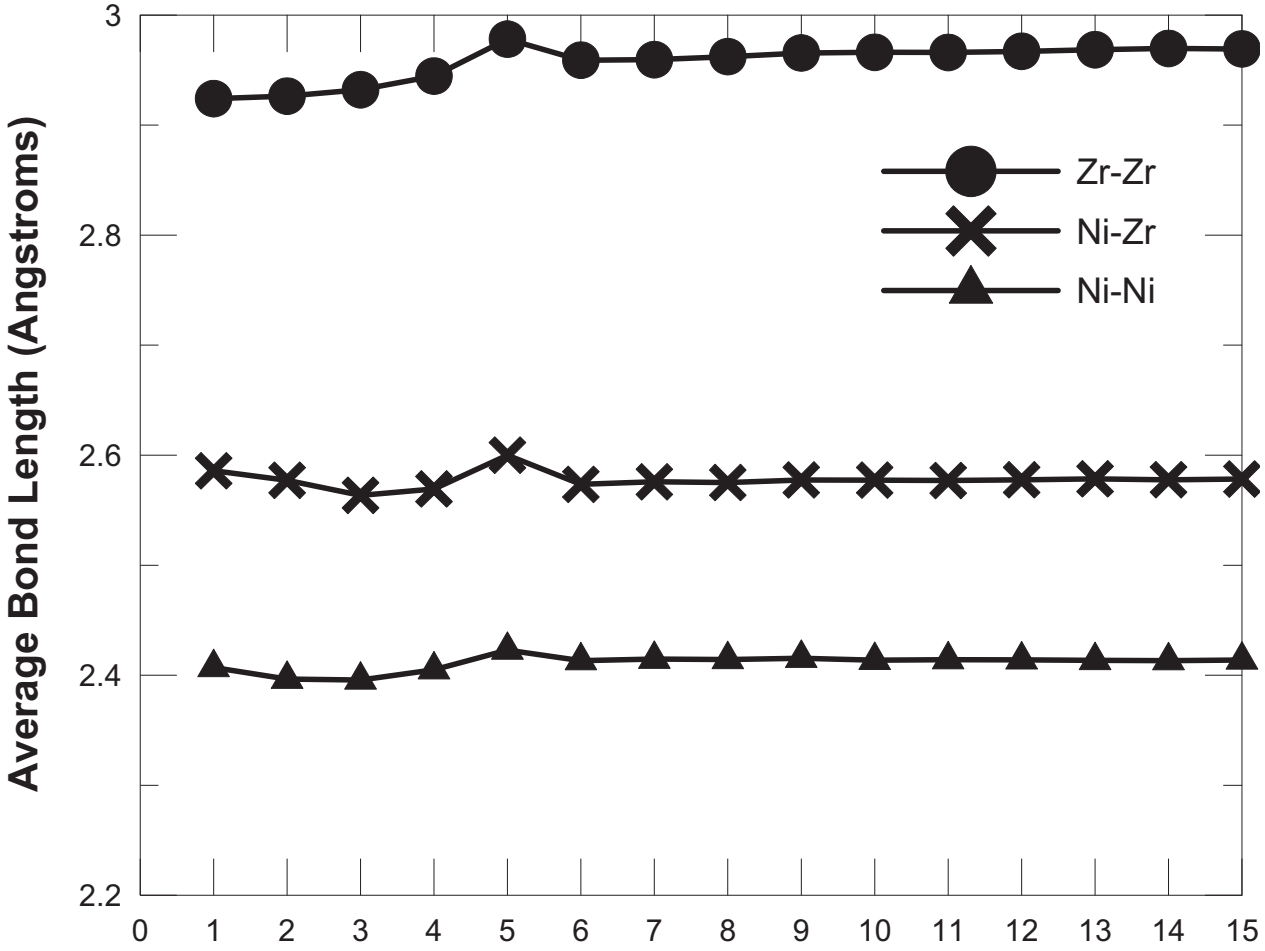

$d_{(cal)}$ (Å)	$g_{1\ (TEM)}$ ($Å^{-1}$)	$d_{(TEM)}$ (Å)	$d_{(MD)}$ (Å)	$d_{(TEM)}/d_{(cal)}$	$d_{(MD)}/d_{(cal)}$
2.84	**0.41**	**2.43**	**2.58**	**86%**	**91%**

• ***HA (Honeycutt & Anderson) pairs***

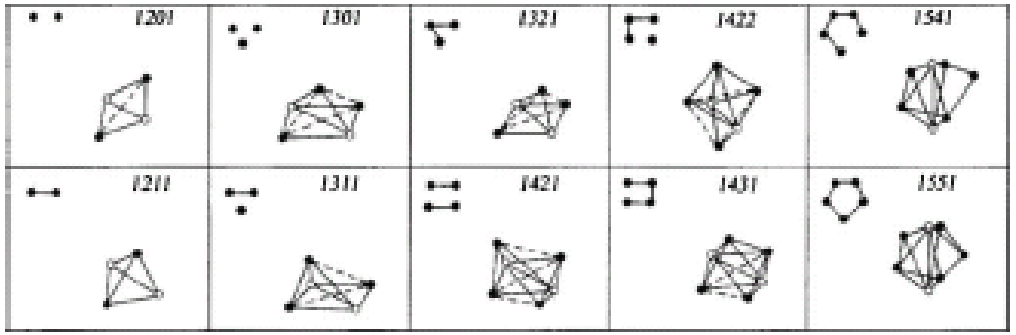

FIG. 1. The schematic drawing of the related HA pairs (Ref. 36).

• ***During different ARB cycles :*** Variation of HA index of Zr-Ni alloys

(a) HA index : 1421 and 1422

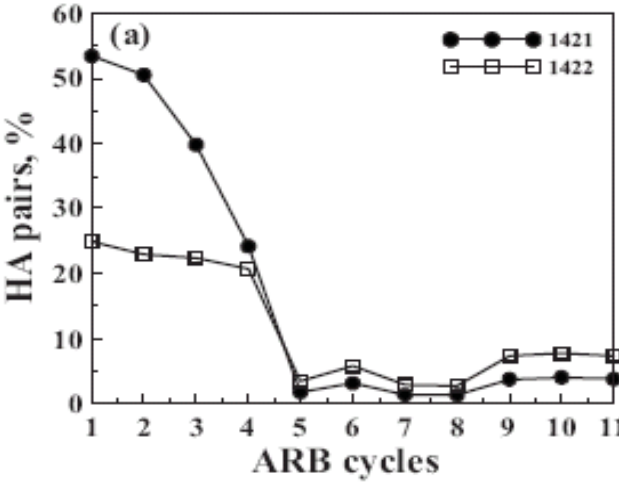

(b) HA index : 1431, 1541 and 1551

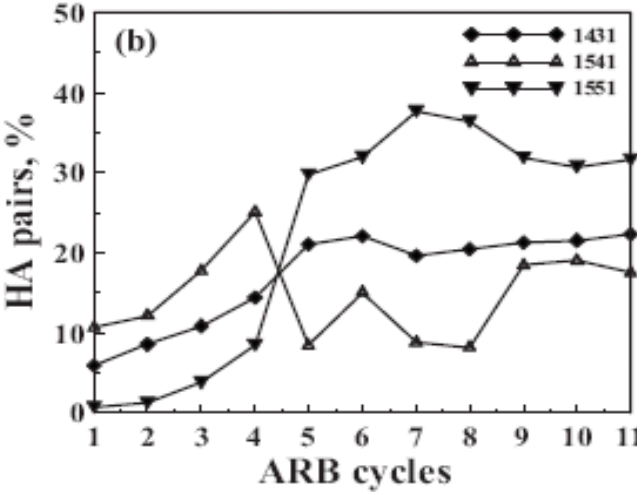

(c) HA index : 1441, 1661 and 1321

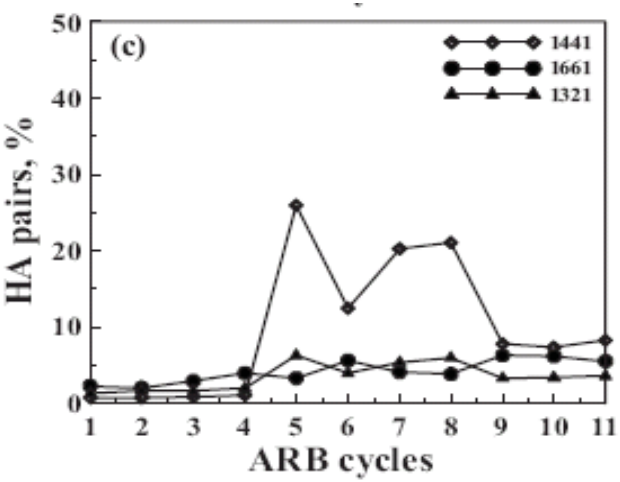

Motivation

The importance of the interface exists in materials

Multilayers、Bi-crystal1

Poly-crystal

- 界面處不同物質特性的存在導致其硬度受到影響。
- 多層材料具有優異的機械性質、磁性、電性。

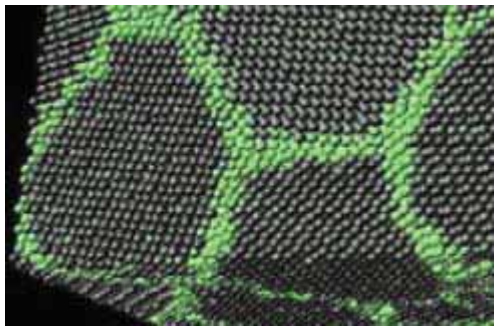

irregular boundary

tilt boundary

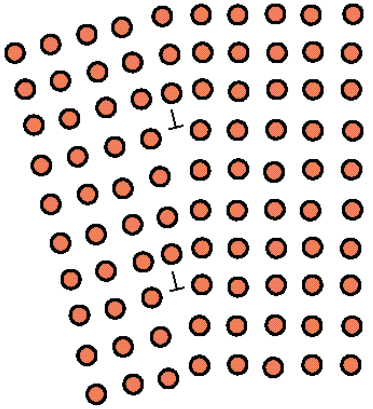

twin boundary

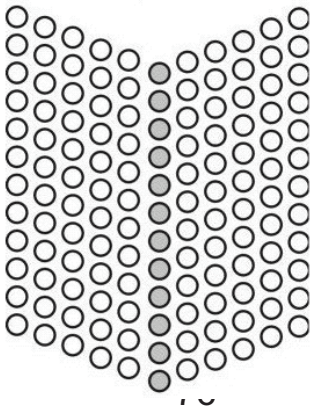

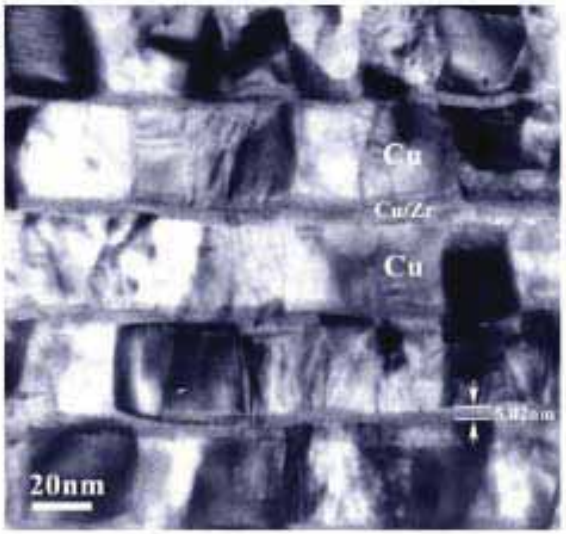

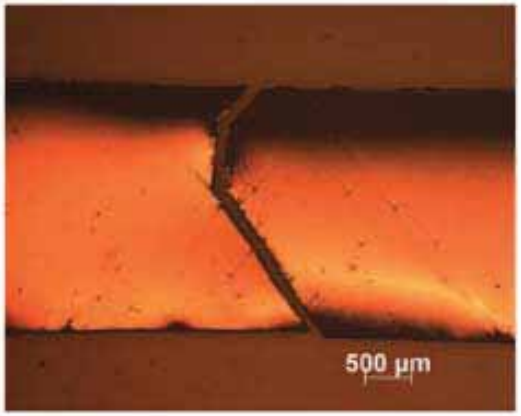

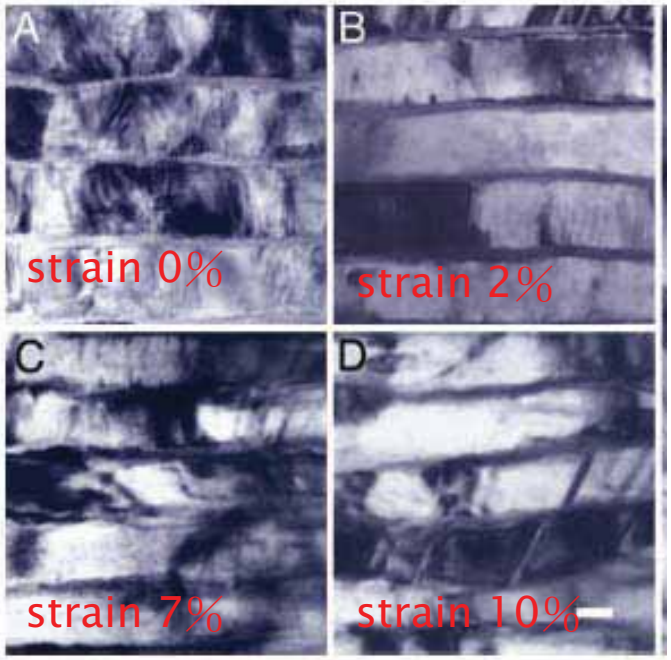

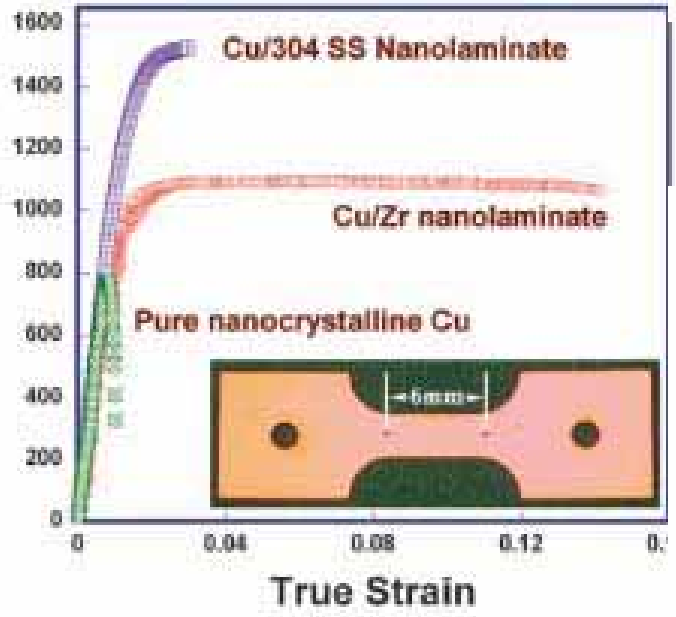

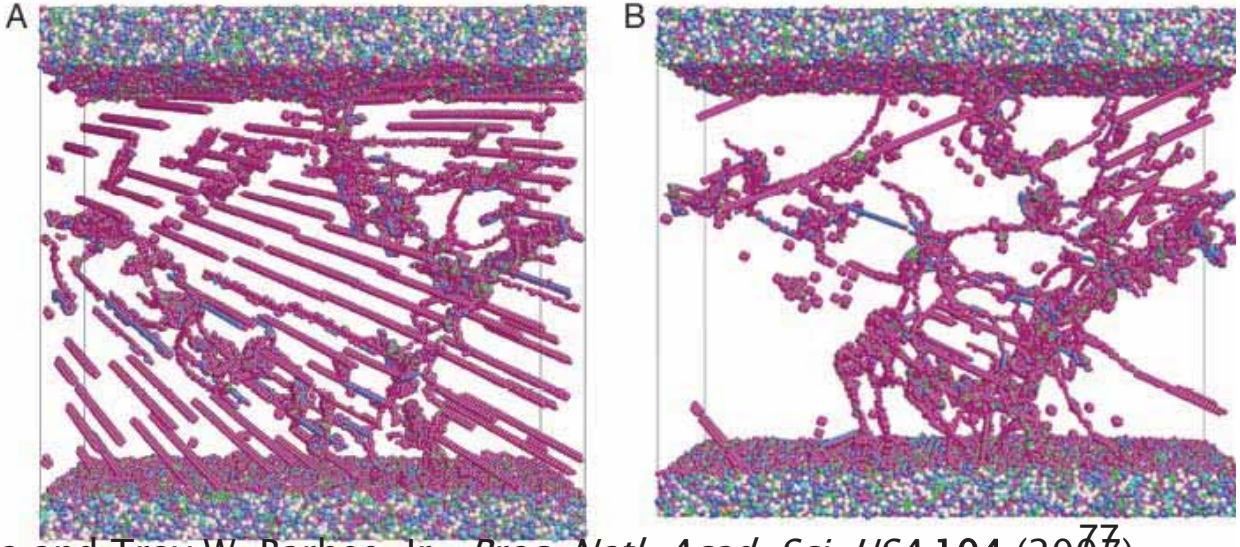

Yinmin Wang, Ju Li, Alex V. Hamza and Troy W. Barbee, Jr., *Proc. Natl. Acad. Sci. USA* **104** (2007) 11155–11160.

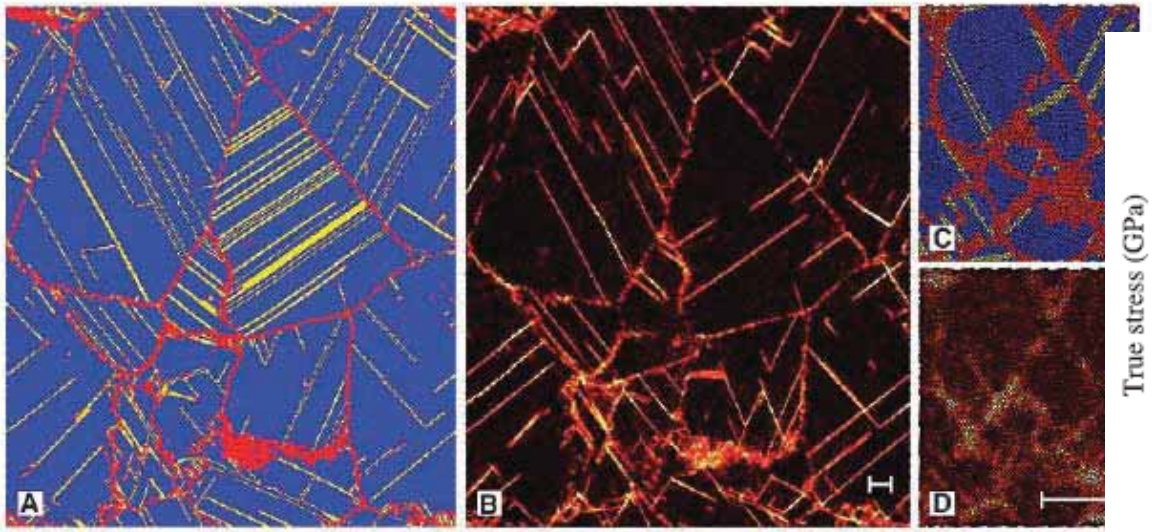

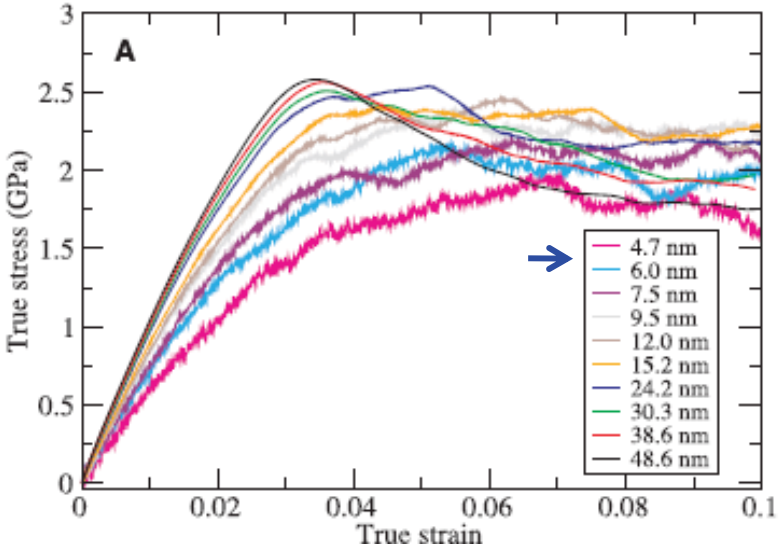

Schiotz, J. and Jacobsen, K.W., *Science,**301,1357-1359(2003)***

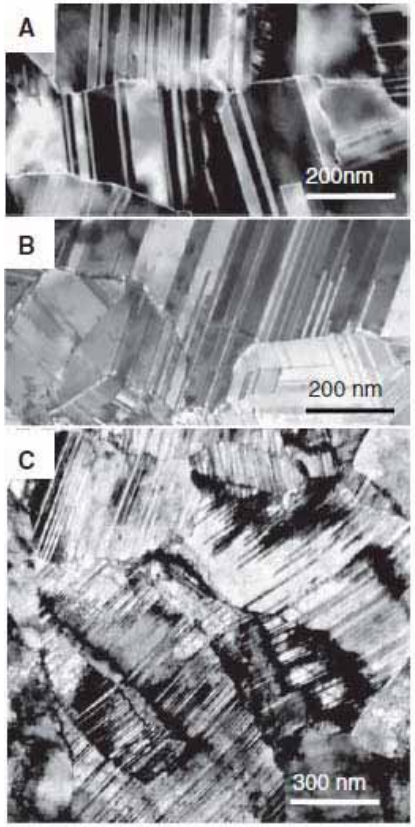

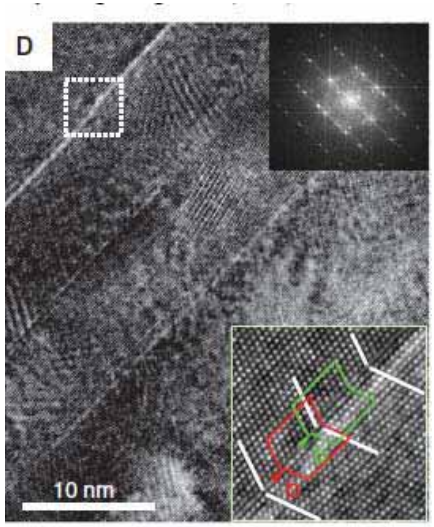

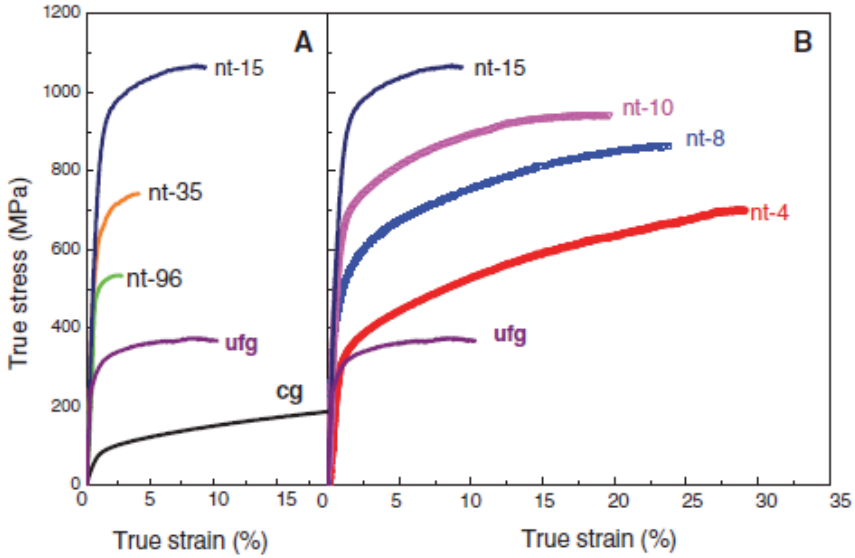

Lu, L., Chen, X., Huang, X., and Lu, K., *Science,**323,607-610(2009)***

奈米壓痕之簡介

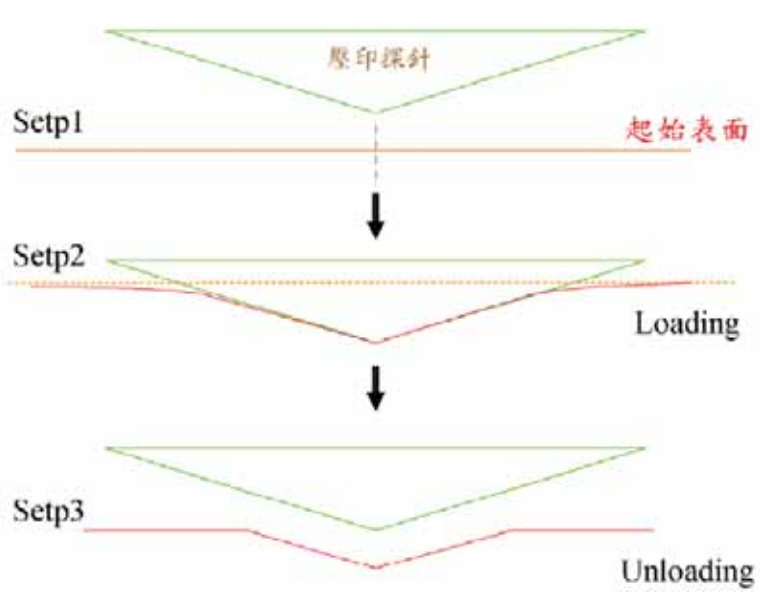

$$h_c \rightarrow A = f(h_c) \rightarrow H = \frac{P}{A}$$

$$S = \beta \frac{2}{\sqrt{\pi}} E_r \sqrt{A} \rightarrow E_r = \frac{S\sqrt{\pi}}{2\beta\sqrt{A}} \rightarrow \frac{1}{E_r} = \left(\frac{1-\nu_s^2}{E_s}\right) + \left(\frac{1-\nu_i^2}{E_i}\right)$$

Types	Cone	Sphere	Berkovich
β	1	1	1.034

◆壓痕的應用極為廣泛，除了被應用於薄膜機械性質的量測上，其亦被用於骨骼硬度與楊式模數的測量，藉此判斷成骨不全症的型態。

◆奈米壓痕為利用探針的下壓，使探針與所欲量測之材料產生接觸，並記錄探針之載重及探針的位移。

◆藉由壓痕過程中，所得到的負載-深度曲線圖，即可求出材料的彈性係數。

L-BFGS Algorithm

$$F(\vec{x}+\vec{h}) = F(\vec{x}) + \sum_{j=1}^{n} \partial_i F(\vec{x})\vec{h}_j + \frac{1}{2}\sum_{i,j=1}^{n} \partial_i \partial_j F(\vec{x})\vec{h}_i\vec{h}_j$$

$$= F(\vec{x}) + \sum_{j=1}^{n} \partial_i F(\vec{x})\vec{h}_j + \vec{h}^T \frac{1}{2} H\vec{h}$$

$\partial_i F(\vec{x})$ → 0

- 即可找出搜尋向量 $\vec{d}_n = -H_n \vec{g}_n$
- 由得到的 d_n，即可決定下一次的迭帶向量 $x_{n+1} = x_n + \alpha_n d_n$

（α 必須滿足 $F(x_{n+1}) < F(x_n)$ ）

- 更新Hessian matrix，重複此步驟，直到 $\frac{\|g\|}{\|\vec{x}\|} < \varepsilon$ 滿足所設收斂條件為止

Simulation Model

- Single Crystal Cu(100)
- Bicrystal Cu(100)/Cu(110)
- Sinlge Crystal Cu(110)
- Bicrystal Cu(110)/Cu(100)

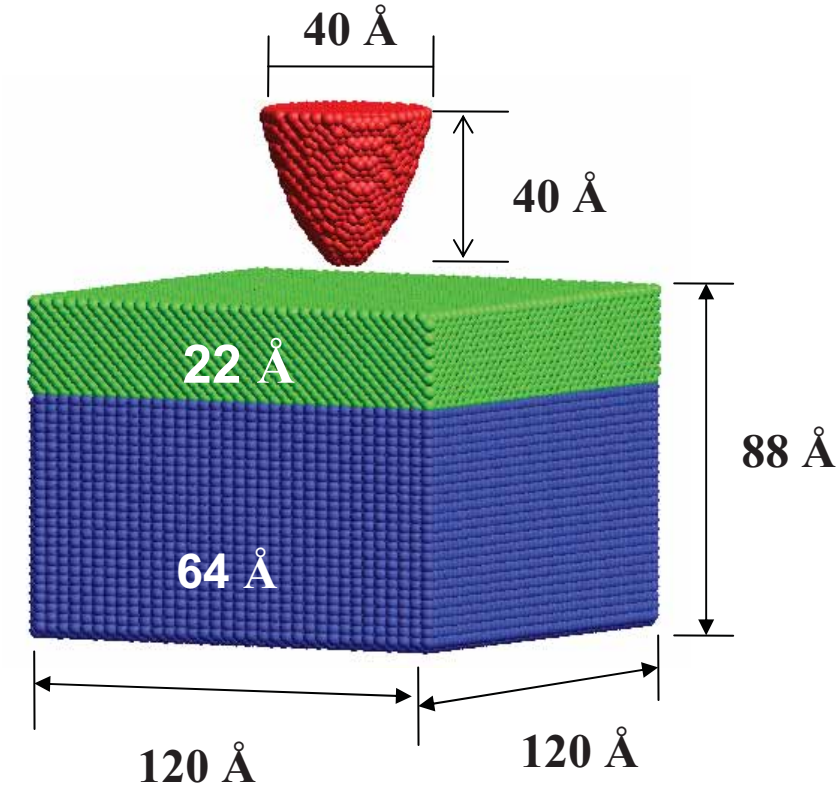

Average bond lengeth

$$\delta = \frac{\sqrt{\sum_{i=1}^{N} (\vec{R}_{ij} - \vec{R}_{ij}')^2}}{N}$$

N — The number of the first neighbor atoms of atom i

$\vec{R}_{ij}$ — The bond length between atoms i and j before the indentation

$\vec{R}_{ij}'$ — The bond length between atoms i and j before the indentation

Cu(100)

Cu(110)

Cu(100)/Cu(110)

Cu(110)/Cu(100)

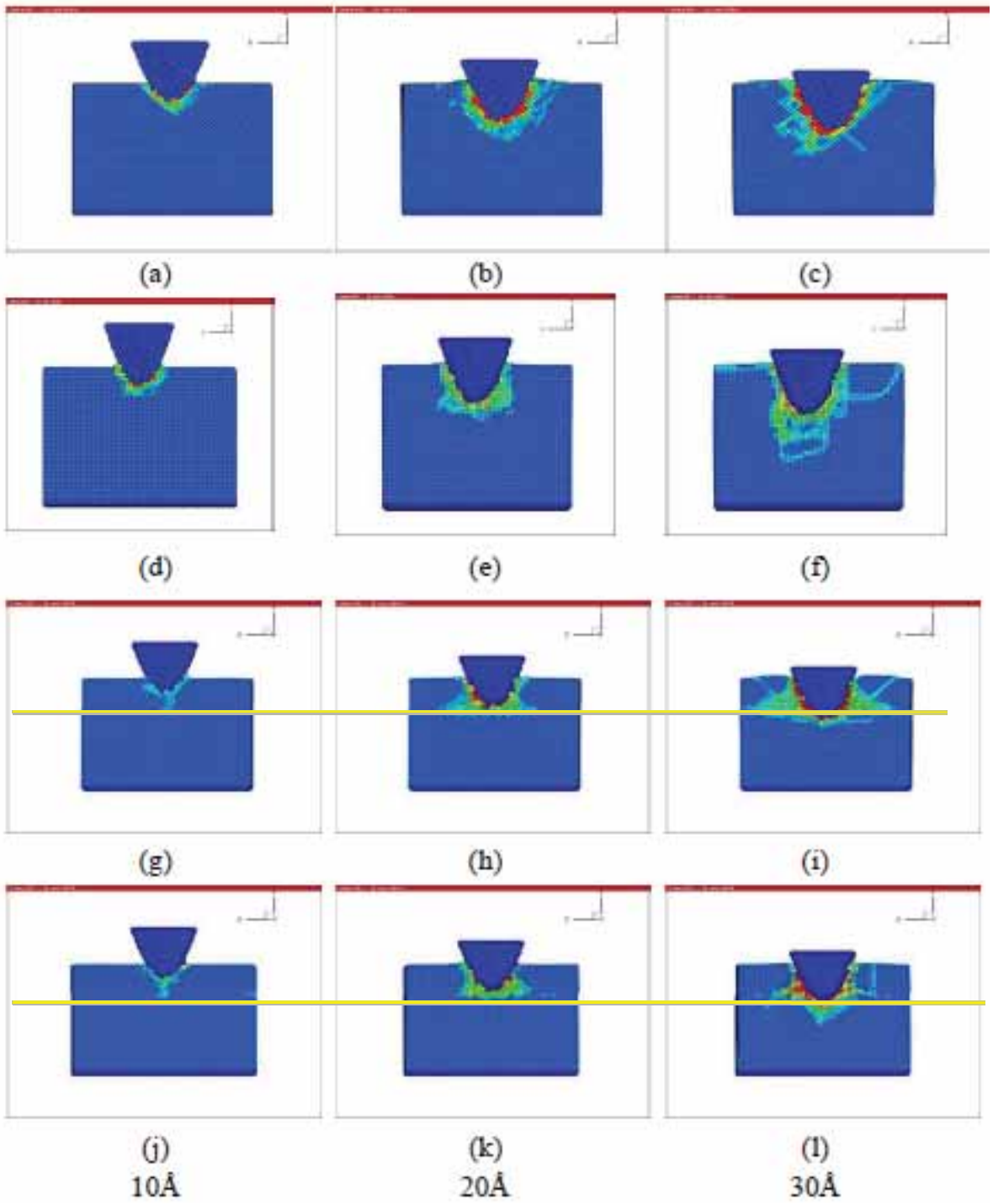

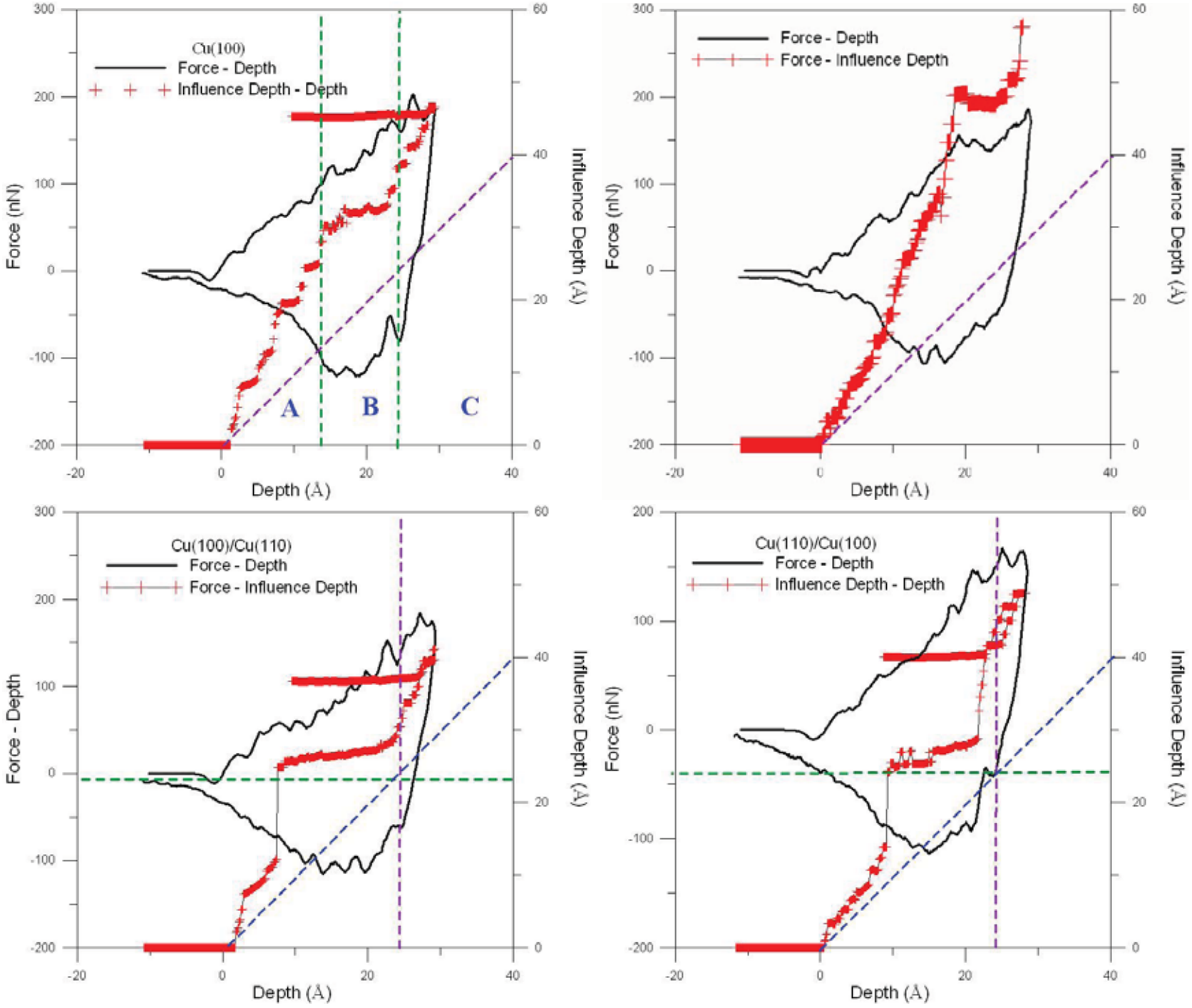
Cu(100)
Force - Depth
Influence Depth - Depth
A
B
C
Force (nN)
Influence Depth (Å)
Depth (Å)
Force - Depth
Force - Influence Depth
Cu(100)/Cu(110)
Force - Depth
Force - Influence Depth
Force - Depth
Influence Depth (Å)
Depth (Å)
Cu(110)/Cu(100)
Force - Depth
Influence Depth - Depth
Force (nN)
Influence Depth (Å)
Depth (Å)

Young's Modulus

Young's Modulus (GPa)					
	Simulation			Ref.	
	10 Å	20 Å	30 Å	I	II
Cu(100)	135.95	134.595	82.305	77.5	67.1
Cu(110)	196.051	135.001	137.939	137.0	163
Cu(100)/Cu(110)	166.390	154.679	142.667	--	--
Cu(110)/Cu(100)	162.529	161.944	151.017	--	--

I. Tsuru, T. and Shibutani, Y. *Physical Review B*,**75**(2007)

II. Liang, H.Y., et al., *Cmes-Computer Modeling in Engineering & Sciences*,**6**,105-114(2004)

IOP PUBLISHING JOURNAL OF PHYSICS: CONDENSED MATTER

J. Phys.: Condens. Matter 21 (2009) 185006 (8pp) doi:10.1088/0953-8984/21/18/185006

First principles studies of an Si tip on an Si(100)2 × 1 reconstructed surface

Dung Q Ly, Leonid Paramonov and Charalampos Makatsoris

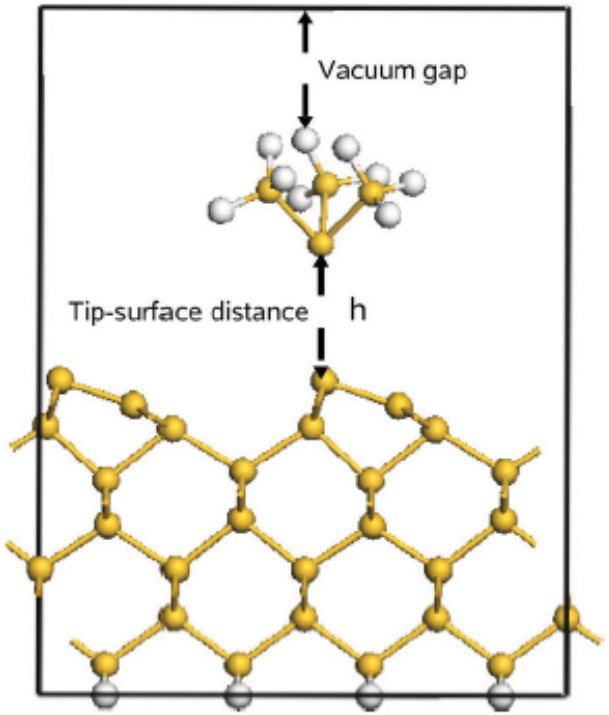

Figure 1. Side view of a supercell containing tip, slab and vacuum gap. A ball-and-stick model of our system with H atoms represented by the brighter coloured balls.

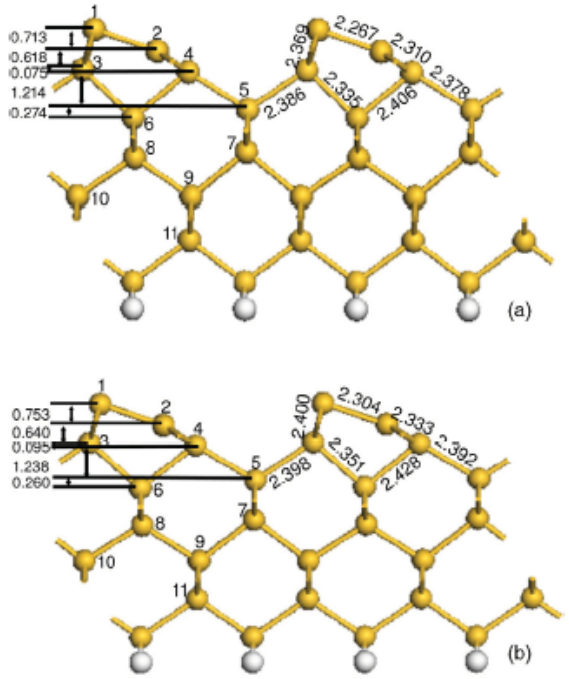

Figure 2. Bond lengths and buckling lengths for the reconstructed Si(100)2 × 1 surface obtained from LDA (a) and GGA (b) calculations.

Nanohelical Microstructure

R. M. Ho et al., J. Am. Chem. Soc., (2004)

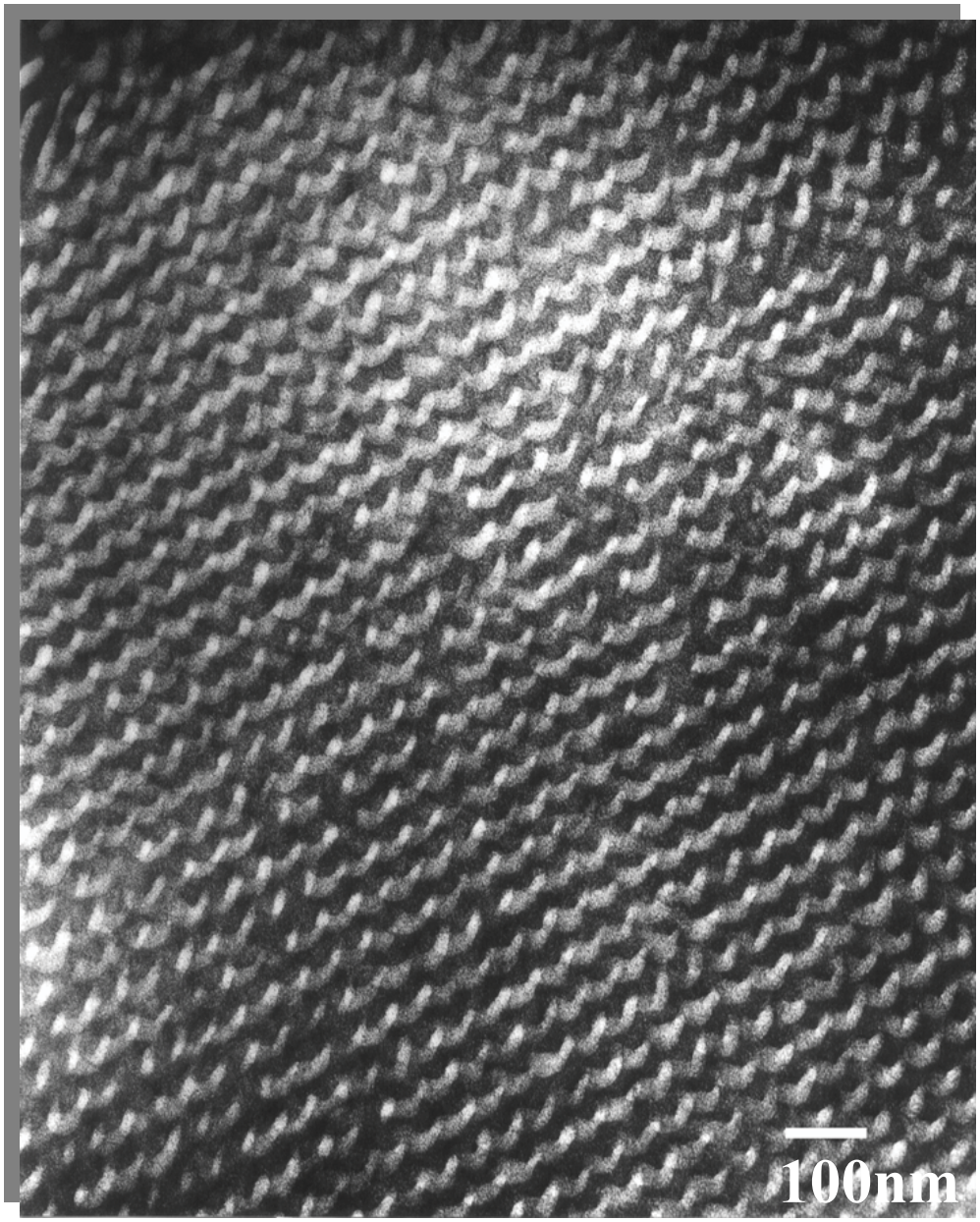

Left-handed helix (M-form)

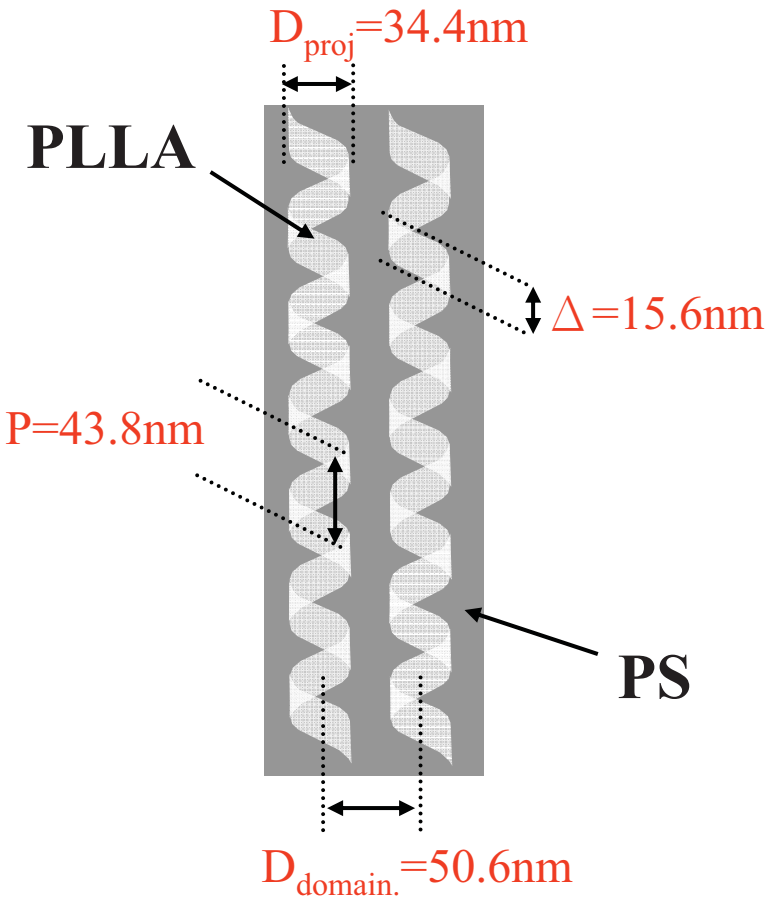

RuO_4 stained
PS: dark region
PLLA: bright region

Self assembly of PS-PLLA

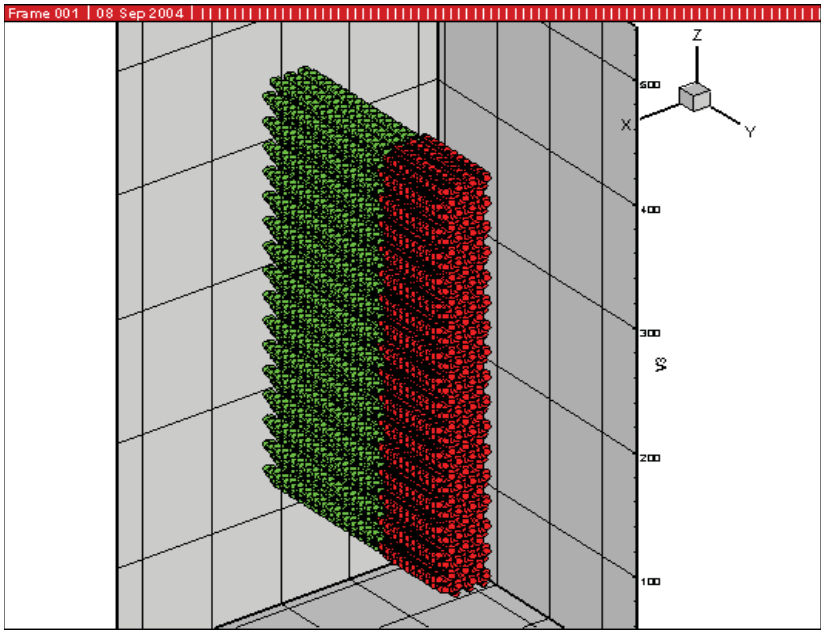

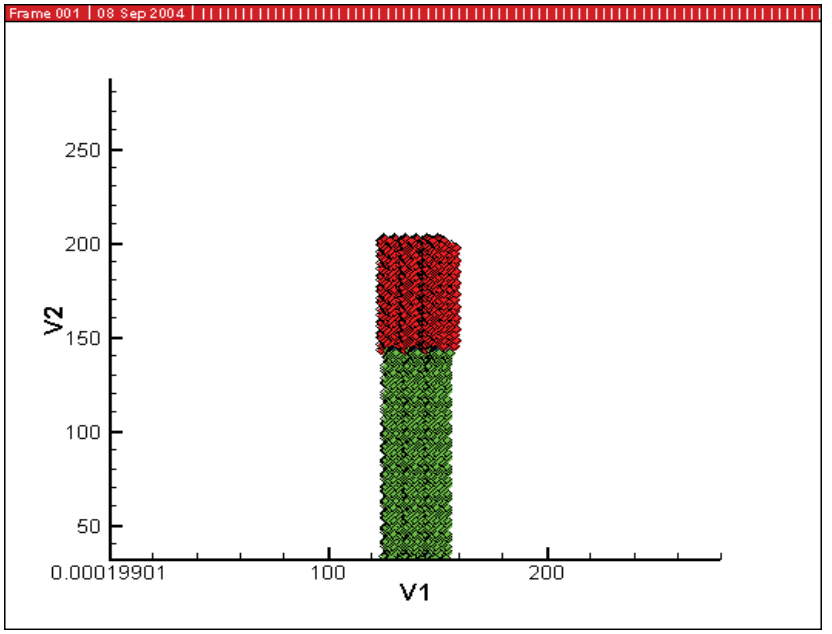

Require a more efficient method to find the equilibrium state for this system with such a large amount of degree of freedom !!!

Different levels for coarse-grained model

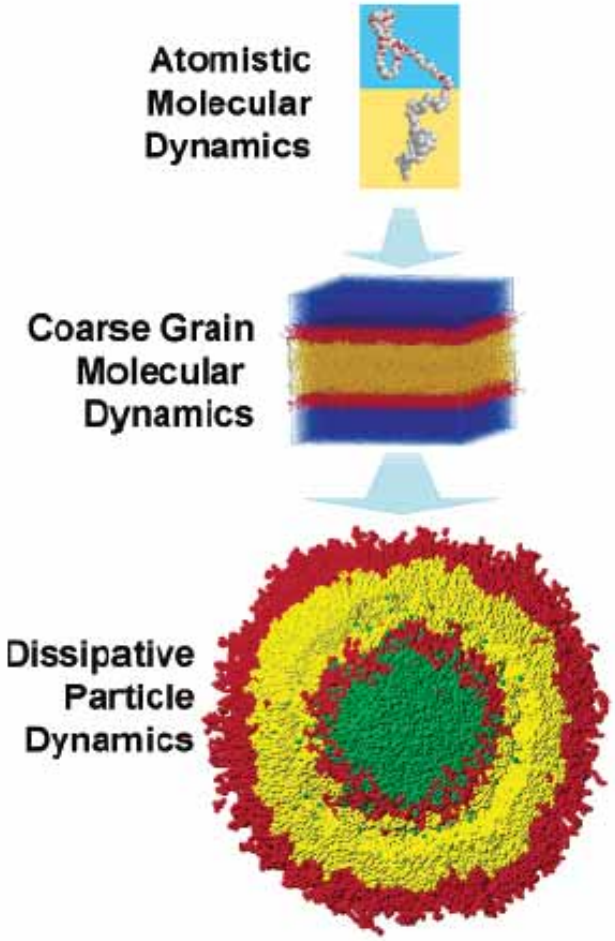

Dissipative Particle Dynamic (DPD)

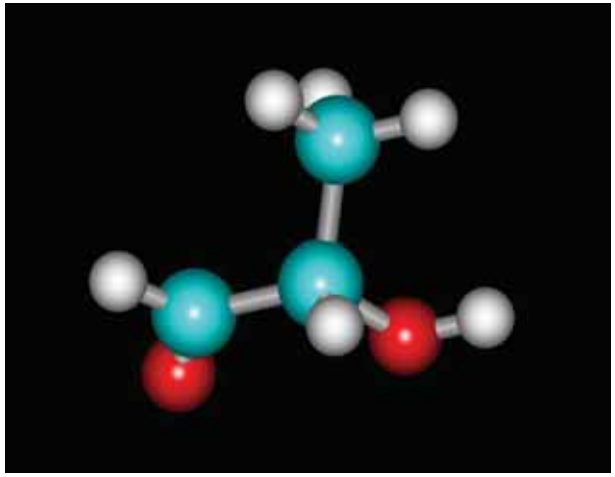

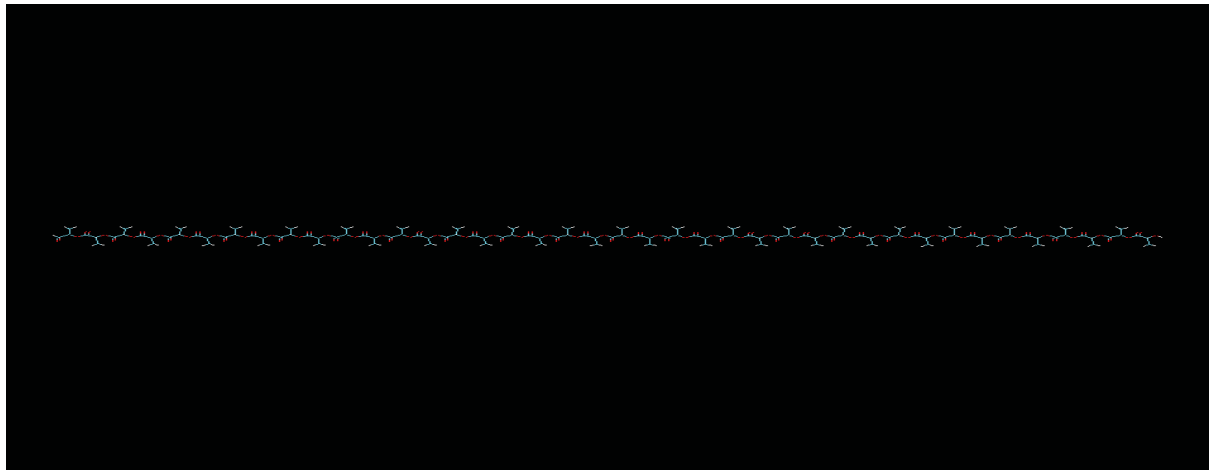

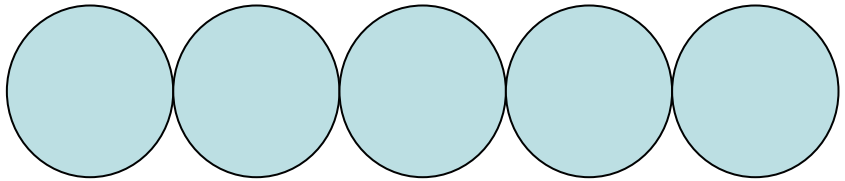

Using Box Length Search Algorithm to Predict Copolymer Structures

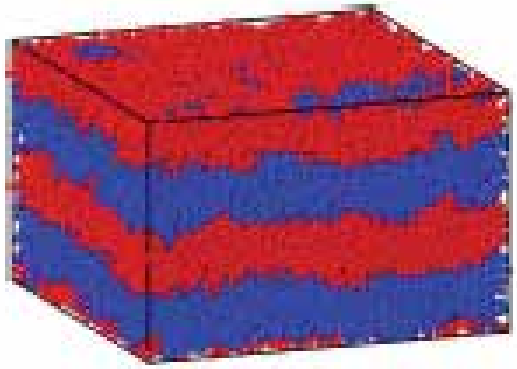

Lamellae

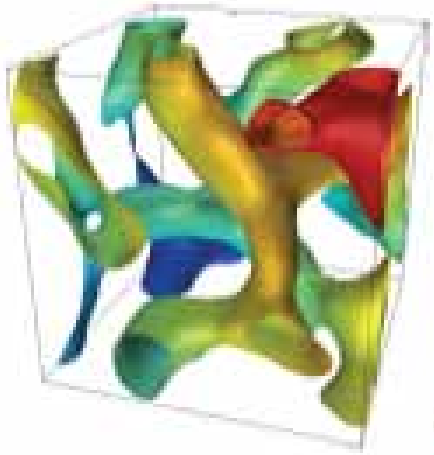

Gyroid

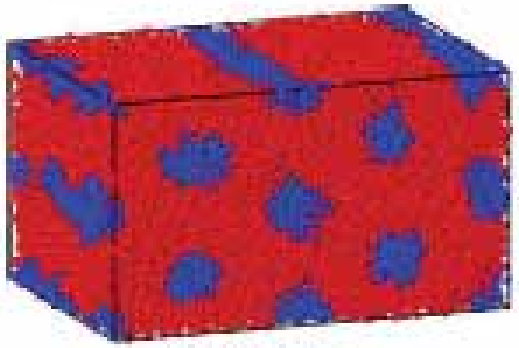

Cylinders

Perforated Lamellae

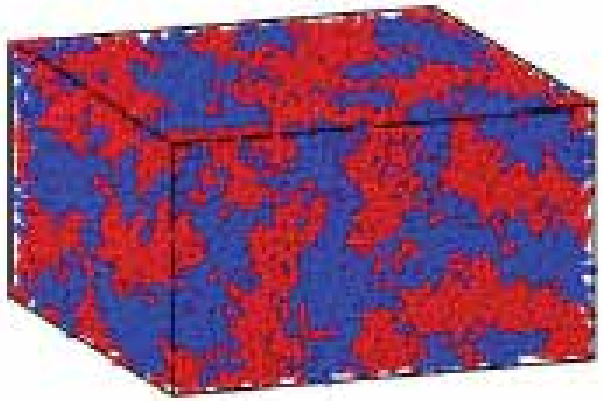

Disorder

Modeling of polyethylene and poly (L-lactide) polymer blends and diblock copolymer: Chain length and volume fraction effects on structural arrangement

TABLE III. Cohesive energy density, χ parameters, and a_{ij} for binary polymer blends of PE/PLLA at different volume fractions.

	PE(1)PLLA(9)	PE(3)PLLA(7)	PE(5)PLLA(5)	PE(7)PLLA(3)	PE(9)PLLA(1)
E (kcal/(mol A^3))	57.4	58.9	59.48	59.6	55.6
a_{ij}	34.43	53.18	64.68	88.74	47.91
χ	6.46	11.2	13.75	18.06	9.9

TABLE IV. Morphologies for PE/PLLA systems at different volume fractions, bead numbers, and mixing types (PE/PLLA diblock copolymer and PE/PLLA polymer blends), C and B standing for the PE-*b*-PLLA diblock copolymer, and the PE/PLLA polymer blends, respectively.

	PE(1)PLLA(9)		PE(3)PLLA(7)		PE(5)PLLA(5)	
Bead number	C	B	C	B	C	B
10	Disorder	Cluster	Gyroid	Perforated lamellae	Lamellae	Lamellae
20	Cluster	Cluster	Perforated lamellae	Cylinders	Lamellae	Lamellae
50	Cluster	Cluster	Perforated lamellae	Cylinders	Lamellae	Lamellae
60	Cluster	Cluster	Perforated lamellae	Cylinders	Lamellae	Lamellae
100	Cluster	Cluster	Perforated lamellae	Cylinders	Lamellae	Lamellae

Shin-Pon Ju ***et al., J. Chem. Phys*** **.127,** 064902 (2007)
Shin-Pon Ju ***et al.,*** Journal of Nanoscience and Nanotechnology (2008) (in press)
Shin-Pon Ju ***et al., J. Chem. Phys*** ., 2009 (in press)

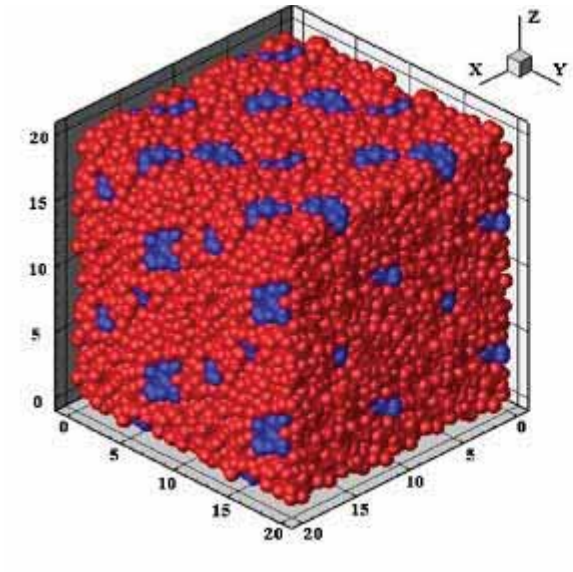

Disorder

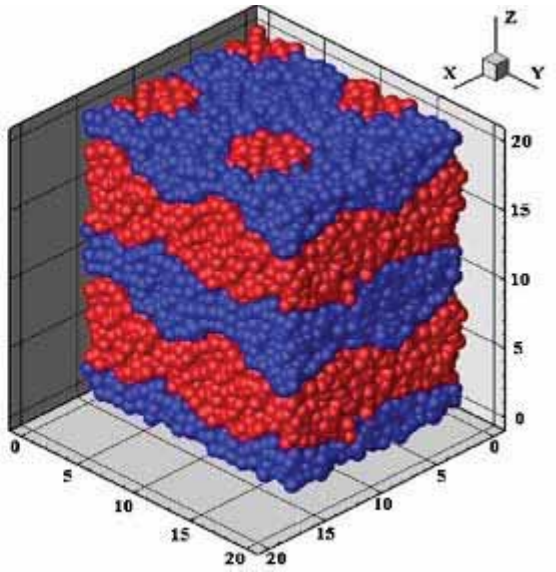

P. Lamellae

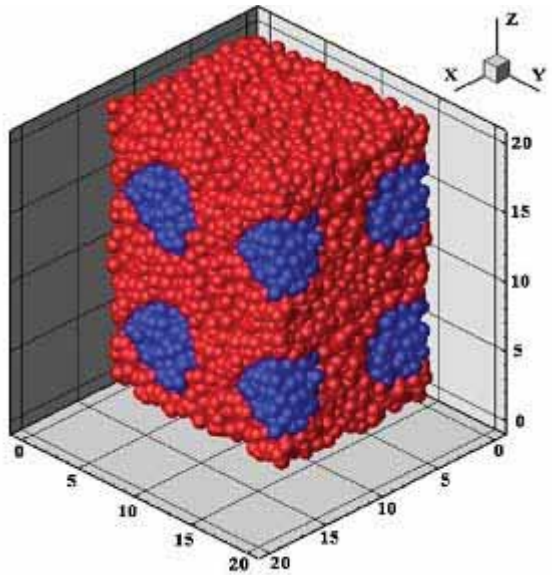

(b)

Cluster

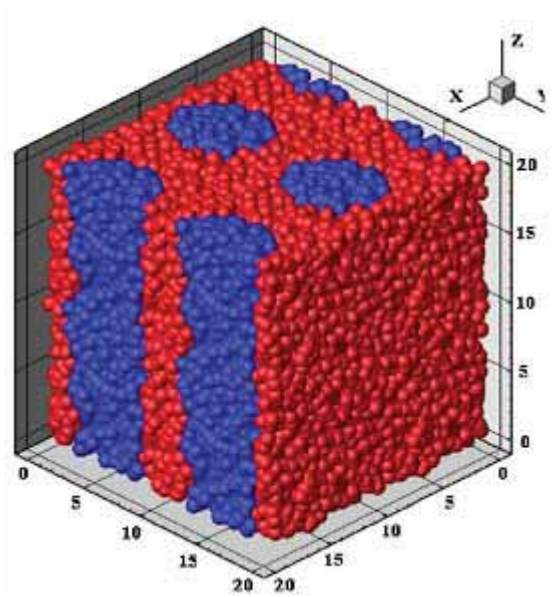

Cylinder

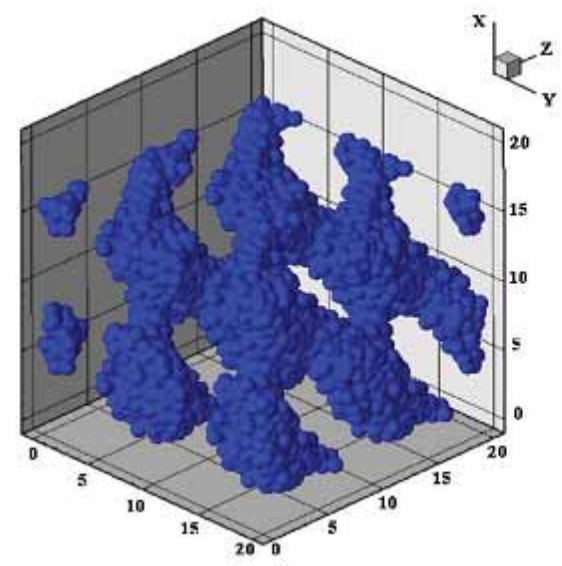

Gyroid

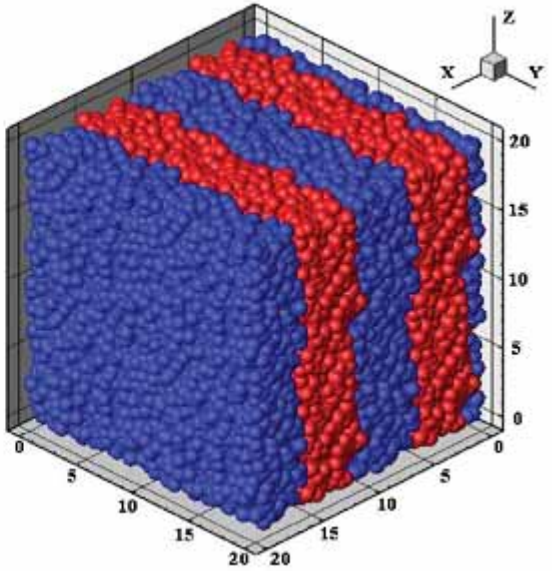

Lamellae

研究動機-奈米碳管應用

1. 場發射顯示器
2. 強化輪胎
3. 燃料電池
4. 儲氫材料
5. 奈米電晶體
6. 奈米整流二極體
7. 生醫感測器

隨著奈米碳管在rubber中含量的增加，其拉升強度與延展性上升

Table Physical properties of rubber composites

No.	Tensile strength σ/MPa	Extension at breat ε_b/%	Shore hardness *Hs*	Tear strength σ/kN·m^{-1}	Abrasion V_A/mL·(1.61 km)$^{-1}$	Volumic resistivity ρ_V/Ω·cm	Surface resistivity ρ_S/Ω·cm	Impact elasticity ε_I/%
MWNTs-10 *w*/%	4.8	253.1	58	25.9	0.22	1.2×10^{14}	6.0×10^{13}	47
MWNTs-20 *w*/%	5.1	288.1						
MWNTs-30 *w*/%	5.2	303.7						
N330-10 *w*/%	9.4	377.4	52	22.6	0.49	2.2×10^{14}	4.5×10^{13}	48

Chen, X. H.,Song, H. H., "Multi walled carbon nanotube filled SBR rubber composites" *New Carbon Mater.*, **19**, 214-218 (2004)

SWNT - bundles

•碳管與高分子間的介面連結(interfacial bonding)、碳管含量與溫度都會影響其奈米複材的機械性質

未添加SWNT 與 添加5% SWNT支

PAN高分子複合材料機械性質比較

TABLE I
Mechanical Properties of PAN and SWNT/PAN Composite Fibers[17]

SWNT (wt %)	Tensile modulus (GPa)	Tensile strength (GPa)
0	7.9 ± 0.4	0.23 ± 0.03
5	14.2 ± 0.6	0.36 ± 0.02

TABLE II
Mechanical Properties of PBO and SWNT/PBO Composite Fibers

SWNT (wt %)	Tensile modulus (GPa)	Tensile strength (GPa)
0	138 ± 20	2.6 ± 0.3
10	167 ± 15	4.2 ± 0.5
15	108 ± 10	2.0 ± 0.5

未添加SWNT 、 添加10% SWNT與15%SWNT之PBO高分子複合材料機械性質比較

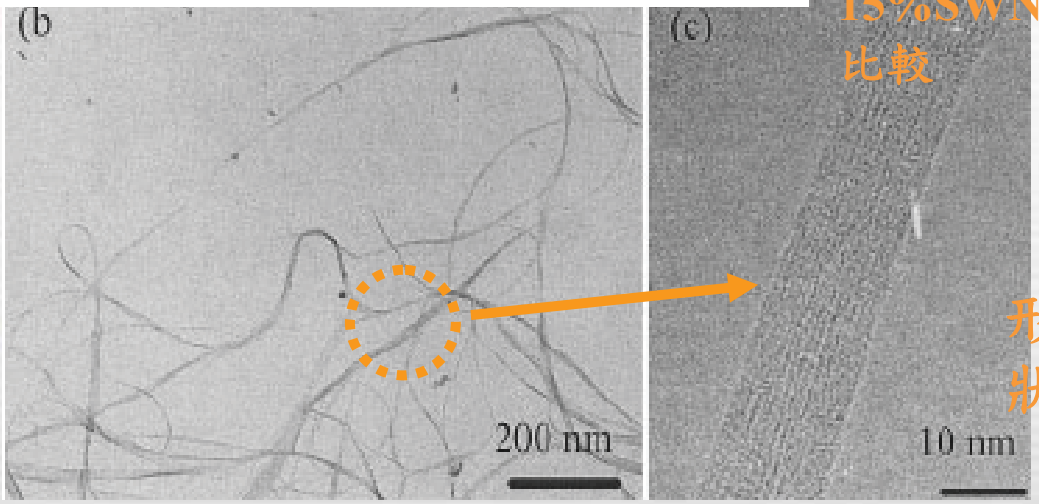

形成管束狀結構

Uchida, T.,Kumar, S., "Single wall carbon nanotube dispersion and exfoliation in polymers" *J. Appl. Polym. Sci.*, **98**, 985-989 (2005)

碳管表面官能化

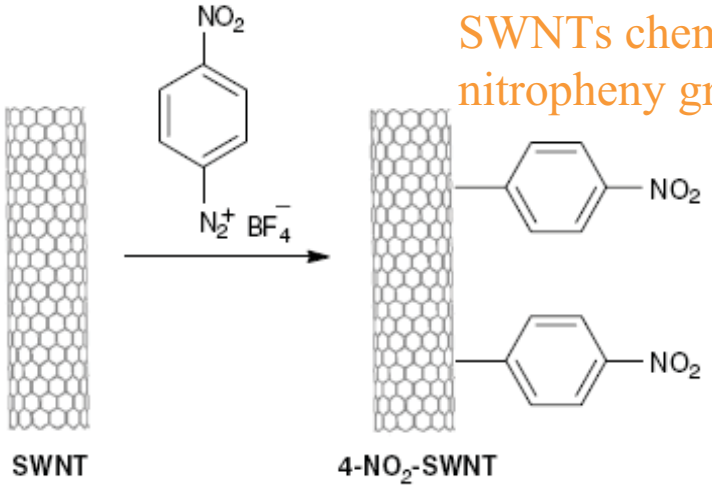

SWNTs chemically modified with 4-nitropheny groups, 4-NO_2-SWNT

Chakraborty, A. K.,Coleman, K. S.,Dhanak, V. R., "The electronic fine structure of 4-nitrophenyl functionalized single-walled carbon nanotubes" *Nanotechnology*, **20**, 6 (2009)

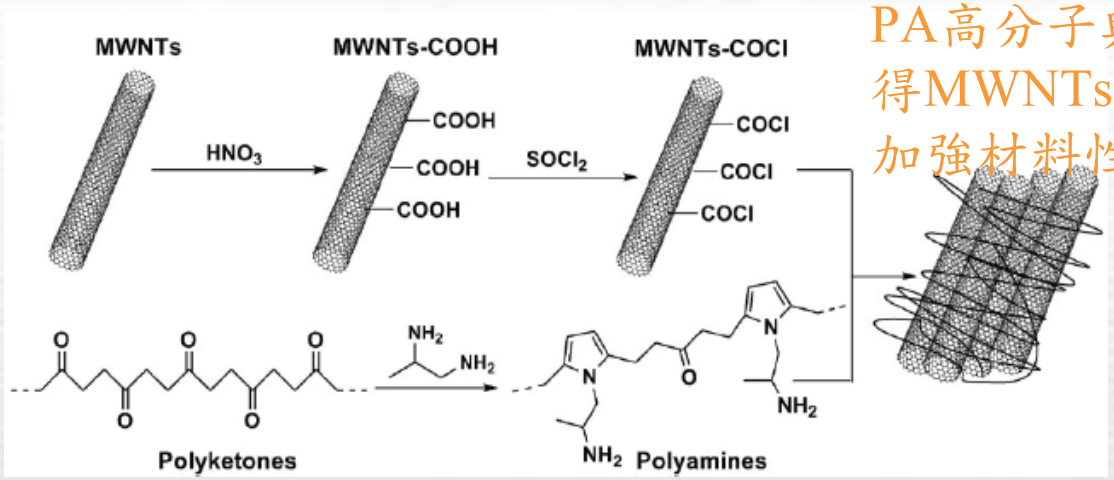

PA高分子與MWNTs表面鍵結　使得MWNTs分散於LDPE高分子中，加強材料性質

Zhang, Y. C.,Broekhuis, A. A.,Stuart, M. C. A.,Landaluce, T. F.,Fausti, D.,Rudolf, P.,Picchioni, F., "Cross-linking of multiwalled carbon nanotubes with polymeric amines" *Macromolecules*, **41**, 6141-6146 (2008)

碳管表面官能化 SWNTs - PE

Table 2. AFM height and length analysis data for the nanotubes.

Nanotube	Average tube length (nm)	Average tube height (nm)	Average aspect ratio of tubes	Average rope height (nm)	Average aspect ratio of ropes
HiPCO	418.1 ± 38.9	0.99 ± 0.04	444.7	7.8 ± 0.34	171.0
F-SWNTs	268.2 ± 16.0	0.97 ± 0.04	313.3	16.7 ± 0.98	40.3
F-SWNT-$C_{11}H_{23}$	265.7 ± 10.0	1.03 ± 0.02	283.5	9.3 ± 0.32	71.4
F-SWNT-$C_{11}F_xH_y$	294.0 ± 7.9	1.06 ± 0.01	296.0	5.4 ± 0.13	92.7

Table 5. Mechanical properties of MDPE and MDPE composites filled with 1 wt% nanotubes.

Properties	MDPE	SWNT	F-SWNT	F-SWNT-$C_{11}H_{23}$	F-SWNT-$C_{11}F_xH_y$
Tensile strength (MPa)	4.33 ± 0.28	4.82 ± 0.41	3.75 ± 0.23	5.01 ± 0.31	6.60 ± 0.48
Young's modulus (MPa)	638.6 ± 15.5	762.4 ± 20.5	590.7 ± 21.8	819.2 ± 13.1	740.1 ± 28.5
Elongation (%)	1.64 ± 0.19	1.05 ± 0.13	1.93 ± 0.27	1.11 ± 0.06	1.95 ± 0.19
Aspect ratio of ropes		171.0	40.3	71.4	92.7

未官能化碳管與官能化碳管在Medium density polyethylene (MDPE)高分子複合材料中所形成的管束狀結構size與機械性質比較

Pulikkathara, M. X., Kuznetsov, O.V, Peralta, I. R. G., Wei, X., Khabashesku, V. N., "Medium density polyethylene composites with functionalized carbon nanotubes " *Nanotechnology*, **20**, 195602 (2009)

研究動機-聚乙烯

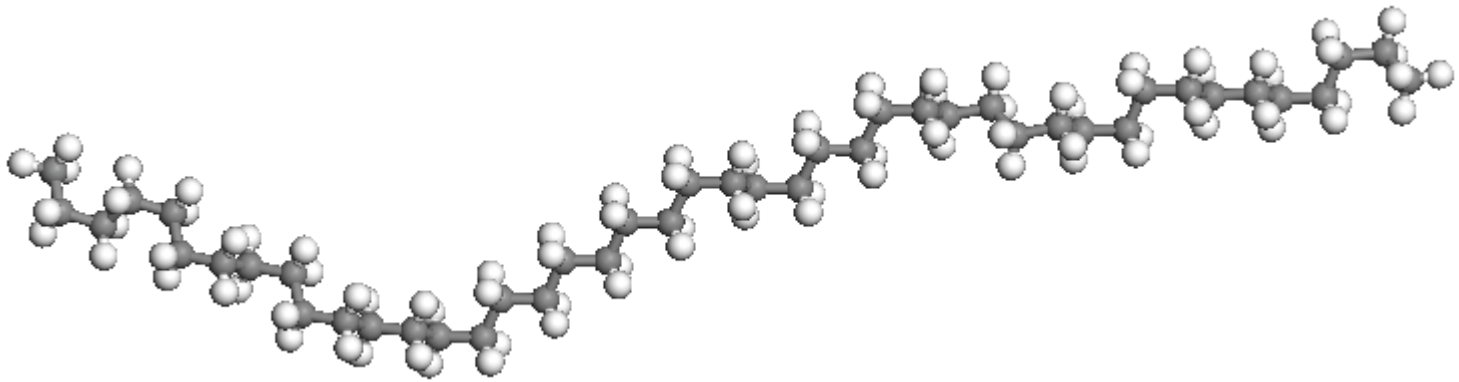

聚乙烯（PE）在世界塑膠總產量中約佔 20%，居首位。其組成的單體乙烯是從石油產品(直餾汽油、粗柴油或原油)熱裂解再經分離純化而得。聚乙烯適於製造瓶、罐、盆、桶、槽、管、箱和殼體結構等工業製品和生活用品，也可用於生產薄膜、板、帶、單絲和電纜覆蓋層。

polyethylene (PE)

MD模擬勢能 - COMPASS

$$E_{total} = \sum_{b}\left[k_2(b-b_0)^2 + k_3(b-b_0)^3 + k_4(b-b_0)^4\right] +$$ ← bonding

$$\sum_{\theta}\left[k_2(\theta-\theta_0)^2 + k_3(\theta-\theta_0)^3 + k_4(\theta-\theta_0)^4\right] +$$ ← bending

$$\sum_{\phi}\left[k_1(1-\cos\phi) + k_2(1-\cos 2\phi) + k_3(1-\cos 3\phi)\right] +$$ ← torsion

$$\sum_{x} k_2 x^2 +$$ ← x: out of plane angle

$$\sum_{b,b'} k(b-b_0)(b'-b_0') +$$ ← bond-bond

$$\sum_{b,\theta} k(b-b_0)(\theta-\theta_0) +$$ ← bond-bend

$$\sum_{b,\phi}(b-b_0)\left[k_1\cos\phi + k_2\cos 2\phi + k_3\cos 3\phi\right] +$$ ← bond-torsion

$$\sum_{\theta,\phi} k(\theta-\theta_0)\left[k_1\cos\phi + k_2\cos 2\phi + k_3\cos 3\phi\right] +$$ ← bend-torsion

$$\sum_{b,\theta} k(\theta'-\theta_0')(\theta-\theta_0) + \sum_{\theta,\theta',\phi} k(\theta-\theta_0)(\theta'-\theta_0')\cos\phi +$$ ← bend-bend

$$\sum_{i,j}\frac{q_i q_j}{r_{ij}} + \sum_{i,j}\varepsilon_{ij}\left[2\left(\frac{r_{ij}^0}{r_{ij}}\right)^9 - 3\left(\frac{r_{ij}^0}{r_{ij}}\right)^6\right]$$ ← Coulomb

Van der waals

壓縮係數(Compressibility parameter，κ^{-1})

• 先是執行溫度300K下的NVT系綜，平衡200ps

• 第二部份則是執行NPT系綜，在系統下我們給予我們所需的壓力，溫度為300K，模擬時間為400ps

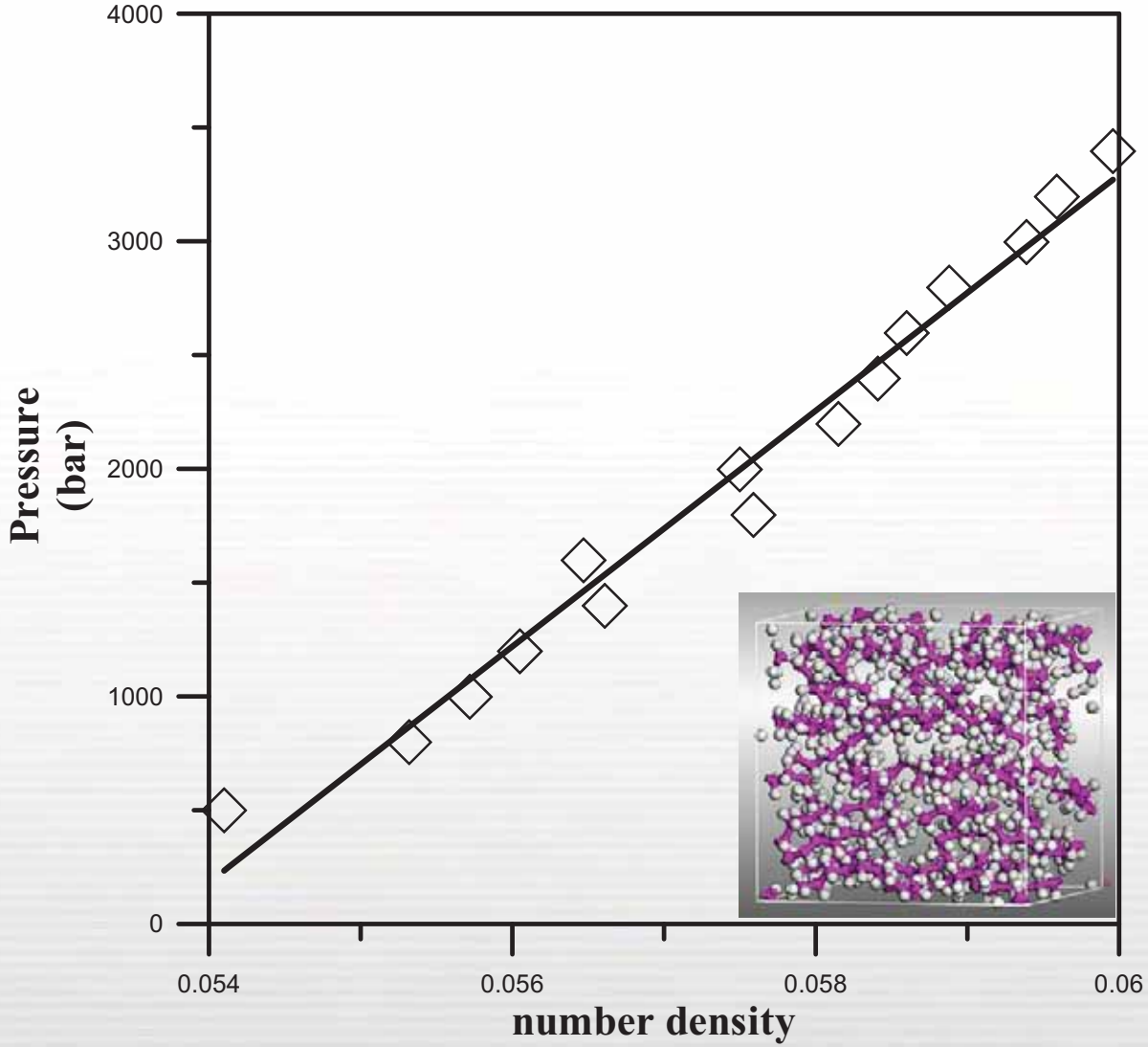

相同物質間之交互作用參數 a_{ii}

Groot, R. D.,Warren, P. B., "Dissipative particle dynamics: Bridging the gap between atomistic and mesoscopic simulation" *J. Chem. Phys.*, **107**, 4423-4435 (1997)

$$\begin{cases} p = \rho k_B T + \alpha a \rho^2 \\ k^{-1} = \dfrac{1}{k_B T}\left(\dfrac{\partial p}{\partial \rho}\right)_T \end{cases} \rightarrow k^{-1} = 1 + \frac{2\alpha a \rho}{k_B T} \rightarrow a_{ii} = \frac{\left(\kappa^{-1} - 1\right) k_B T}{2\alpha\rho}$$

p : Pressure

$$\rightarrow a_{ii} = 19.66$$

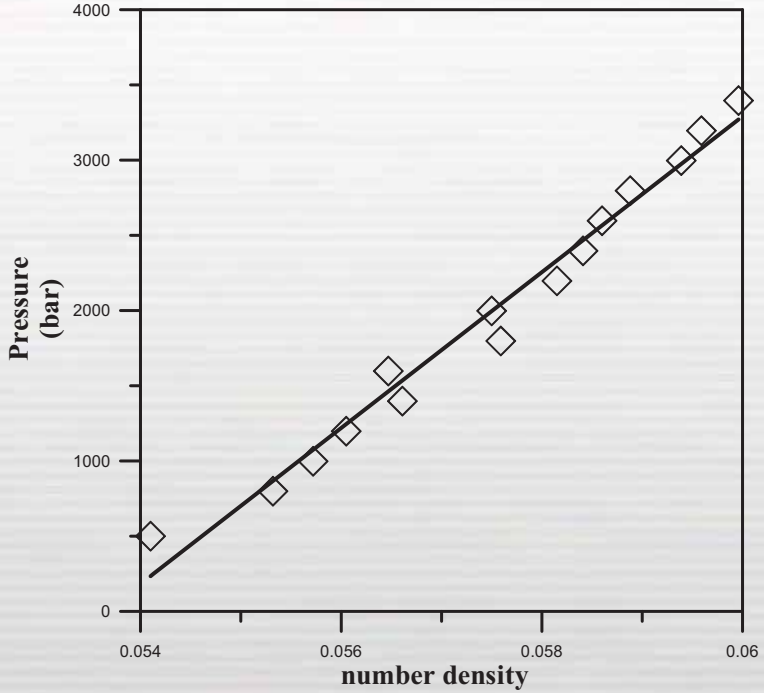

溶解度參數 (Solubility Parameter)

所謂的溶解度參數，即吸附能(cohesive energy)與體積比值的平方根，其中E_{coh}為分子間的吸附能，而V為模擬的系統體積。溶解度參數是一個常被使用來分辨兩種物質是否會互相溶混的指標

$$\delta = \sqrt{\frac{E_{nb}^{isolated} - E_{nb}^{periodic}}{V}} = \sqrt{\frac{E_{coh}}{V}}$$

PE　CNT　PE-CNT

$$\Delta E_{mix}(T) = \phi_A \left[\frac{E_{coh}}{V}\right]_{pureA} + \phi_B \left[\frac{E_{coh}}{V}\right]_{pureB} - \left[\frac{E_{coh}}{V}\right]_{blend}$$

Flory-Huggins parameter - χ

弗洛里-哈金斯參數廣泛被用於量化、描述polymer-solvent、 polymer-polymer間作用力

$$\chi_{FH} = V_{bead}\frac{\Delta E_{mix}(T)}{RT}$$

Polymer	Solvent	T, ℃	χ
Polystyrene	Toluene	25	0.37
Polystyrene	Cyclohexane	34	0.5
Polyisoprene	Benzene	25	0.4
Cellulose nitrate	Acetone	20	0.14
Cellulose nitrate	n-Propylacetate	20	-0.38
Poly(ethylene oxide)	Benzene	70	0.19
Poly(dimethyl siloxane)	Toluene	20	0.45
Polythylene	n-Heptane	109	0.29
Poly(butadiene-stat-styrene)	Toluene	25	0.39
Poly(ethylene oxide)	Water	25	0.4

Sperling, L. H., "Introduction to Physical Polymer Science, 4th Edition"; John Wiley & Sons: New York, (2006).

不同物質間交互作用參數a_{ij}

利用MD算出在不同體積分率下的混合能，經由下式可得福洛伊哈斯參數。

$$\chi_{FH} = V_{bead}\frac{\Delta E_{mix}(T)}{RT} \rightarrow \frac{100}{-0.1} = \frac{\Delta a - 15}{\chi_{FH}/\Delta a - 0.3} \rightarrow a_{ij} = a_{ii} + \Delta a$$

CNT:PE	1:1	1:4	1:6	1:14	1:20
$\Delta E_{mix}(T)$	34.69	30.83	22.284	30.542	29.478
χ_{FH}	2.47	2.195	1.587	2.175	2.099
a_{ij}	27.7	26.79	24.781	26.723	26.471

Coarse grain MD → DPD

Molecular Dynamics

Dissipative Particle Dynamics

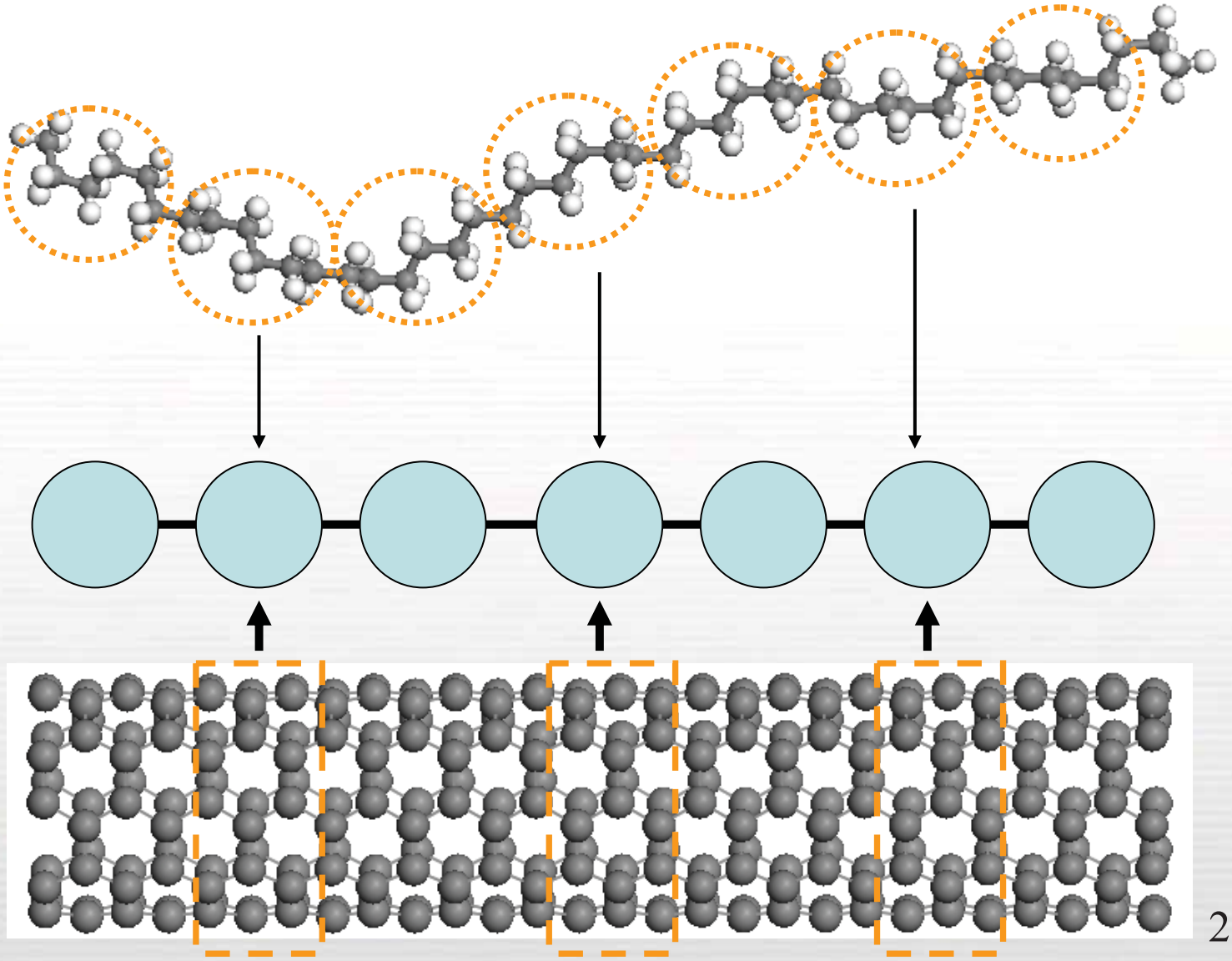

碳管的限制條件

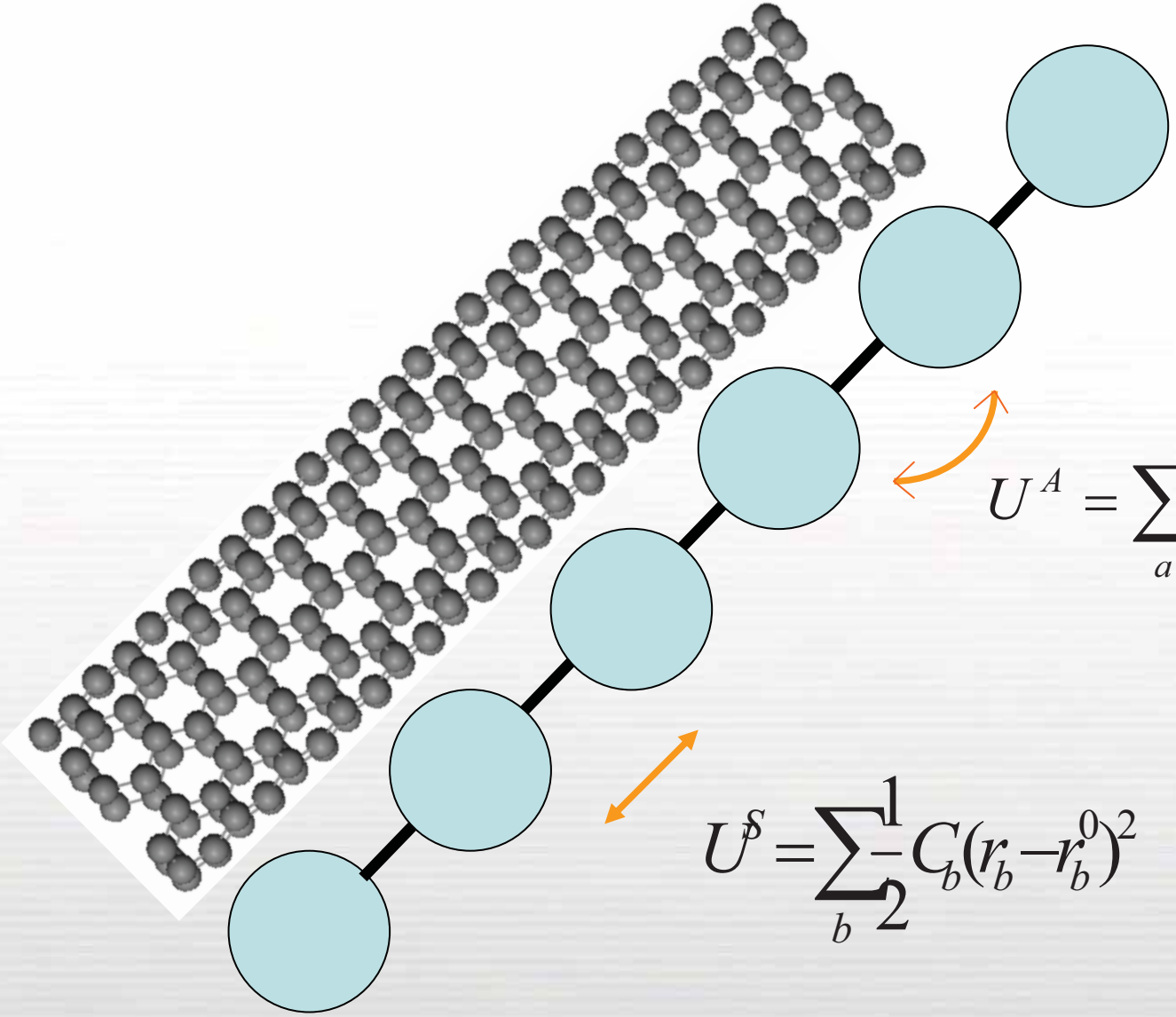

$$U^A = \sum_a \frac{1}{2} k_a \left(\theta_a - \theta_a^0\right)^2$$

$$U^S = \sum_b \frac{1}{2} C_b (r_b - r_b^0)^2$$

Simulation Model

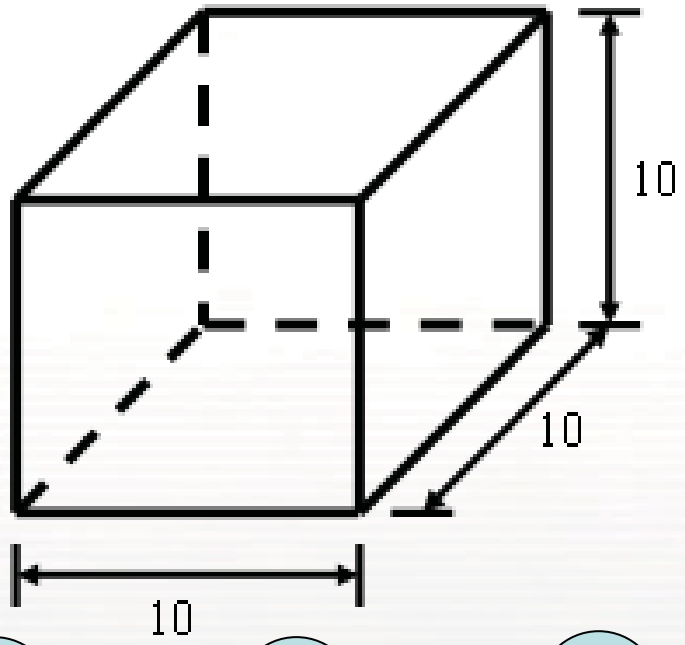

- 系統由3000 顆DPD珠子所組成
- 分別放入不同體積分率的PE與CNT
- PE與CNT的每一條鏈都由12顆DPD珠子所組成

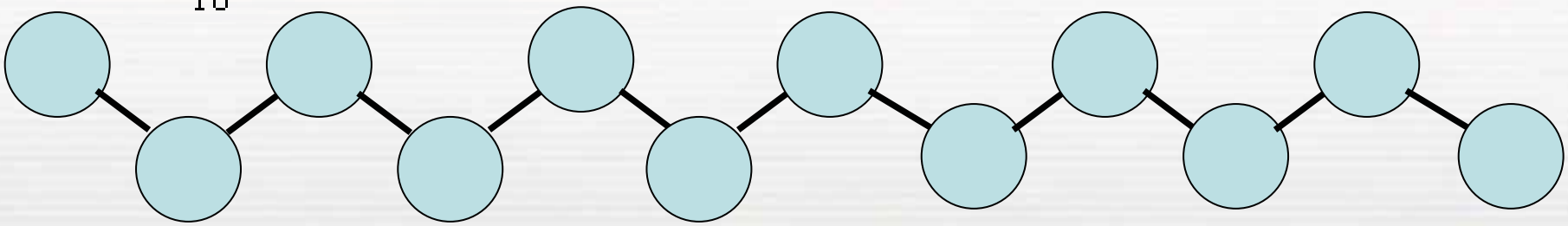

CNT:PE	1:1	1:4	1:6	1:14	1:20

體積分率與平衡結構的關係

CNT:PE	1:1	1:4	1:6	1:14	1:20
a_{ij}	27.7	26.79	24.781	26.723	26.471
equilibrium phase	Lamellae	Cylinder	Cylinder	Cylinder	Cylinder

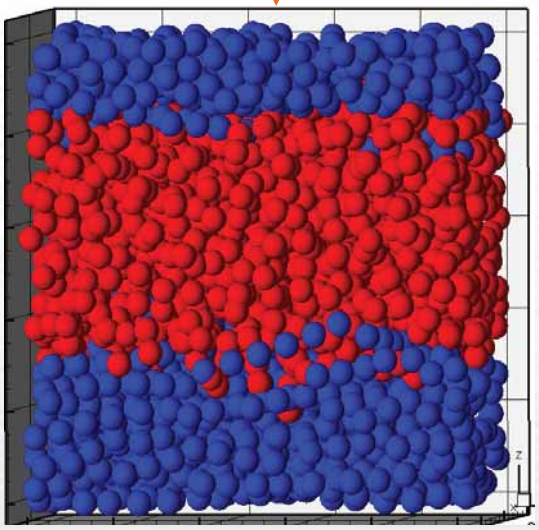

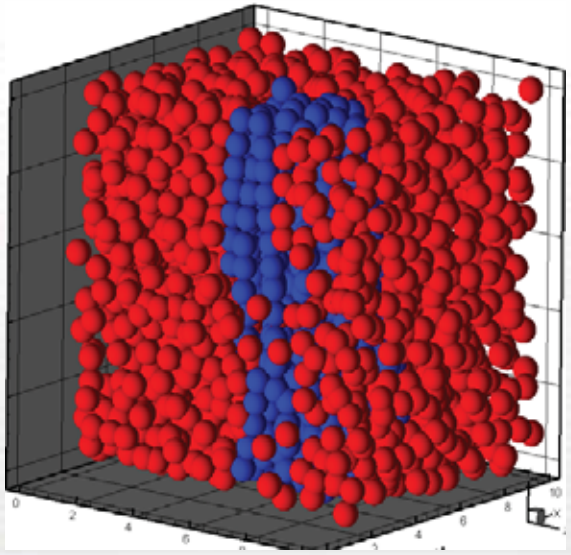

blue : 碳管

red : 聚乙烯

藉由表面官能化探討碳管之方向秩序參數

u: 系統中個別碳管的指向

n: 系統中全部碳管的平均指向

$$\overline{P_2} = \frac{3\overline{\cos^2\theta} - 1}{2} \quad (\cos\theta = u \cdot n)$$

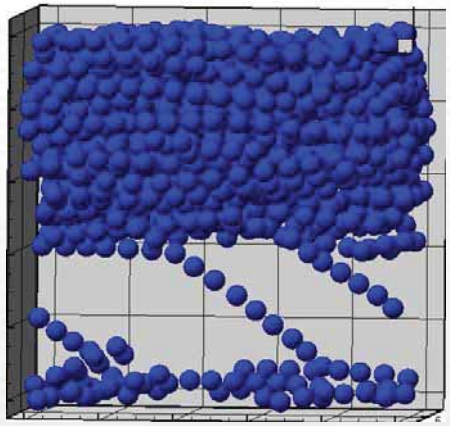

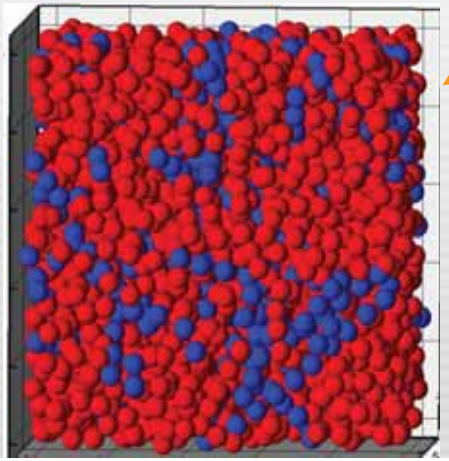

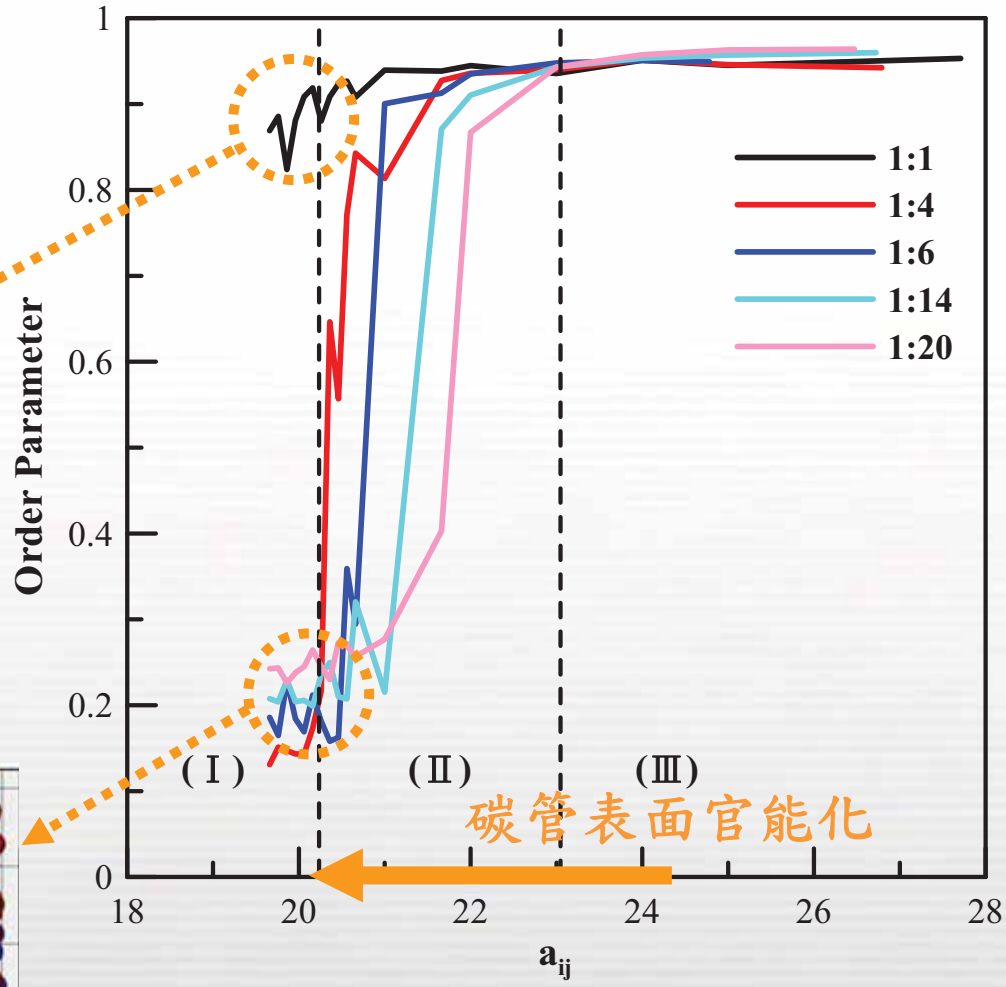

藉由表面官能化探討碳管之方向秩序參數

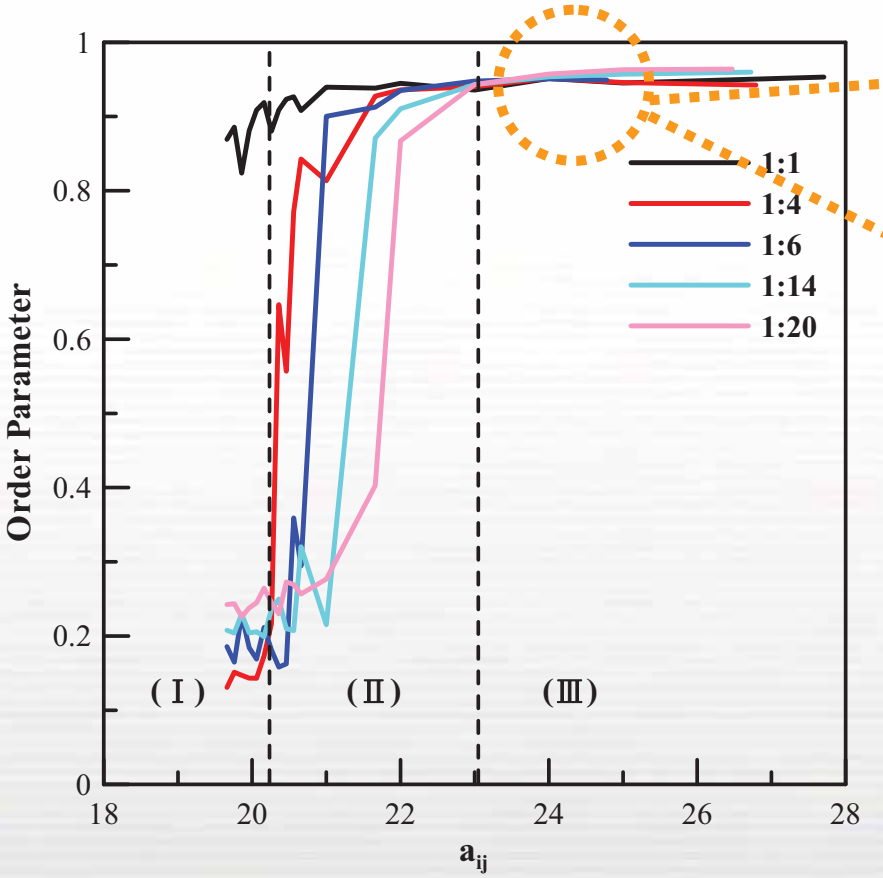

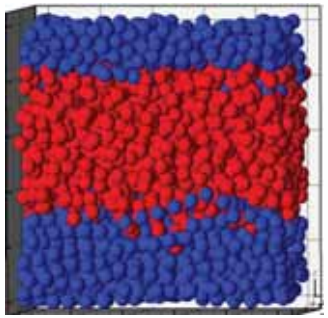

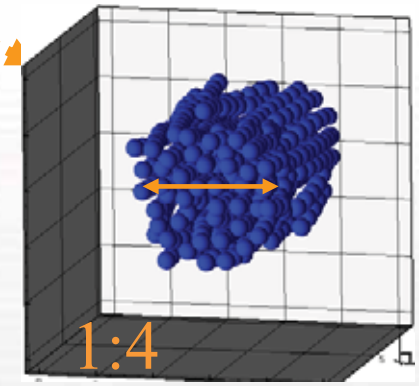

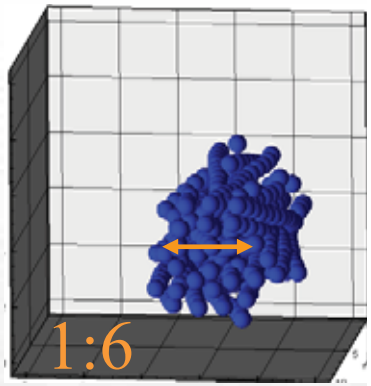

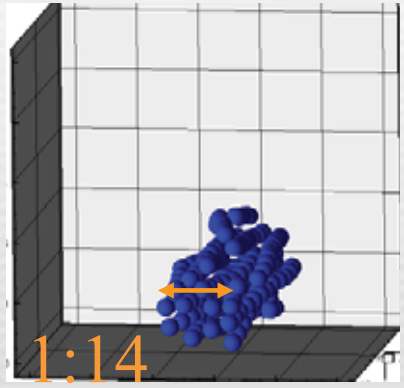

Conclusion : current study

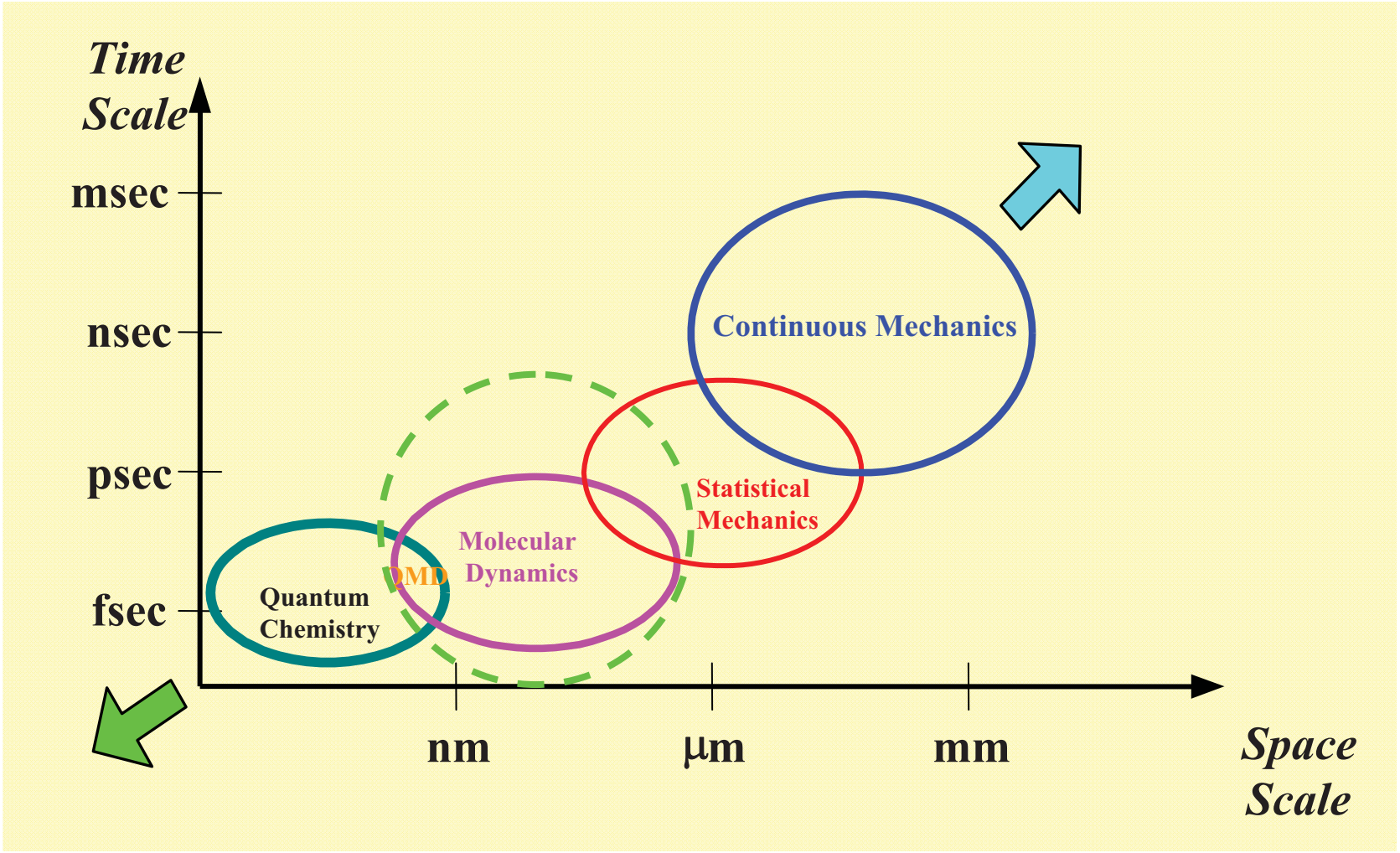

Thank you for your attention